

University of Windsor

Scholarship at UWindor

Electronic Theses and Dissertations

Theses, Dissertations, and Major Papers

9-20-2019

Phosphine Supported Mono-and Polynuclear Ni Complexes for Inert Bond Activation: Mechanisms and Isolation of Reactive Intermediates

Sha Zhu

University of Windsor

Follow this and additional works at: <https://scholar.uwindsor.ca/etd>

Recommended Citation

Zhu, Sha, "Phosphine Supported Mono-and Polynuclear Ni Complexes for Inert Bond Activation: Mechanisms and Isolation of Reactive Intermediates" (2019). *Electronic Theses and Dissertations*. 7858. <https://scholar.uwindsor.ca/etd/7858>

This online database contains the full-text of PhD dissertations and Masters' theses of University of Windsor students from 1954 forward. These documents are made available for personal study and research purposes only, in accordance with the Canadian Copyright Act and the Creative Commons license—CC BY-NC-ND (Attribution, Non-Commercial, No Derivative Works). Under this license, works must always be attributed to the copyright holder (original author), cannot be used for any commercial purposes, and may not be altered. Any other use would require the permission of the copyright holder. Students may inquire about withdrawing their dissertation and/or thesis from this database. For additional inquiries, please contact the repository administrator via email (scholarship@uwindsor.ca) or by telephone at 519-253-3000ext. 3208.

**Phosphine Supported Mono- and Polynuclear Ni
Complexes for Inert Bond Activation: Mechanisms
and Isolation of Reactive Intermediates**

By

Sha Zhu

A Dissertation

Submitted to the Faculty of Graduate Studies
through the Department of Chemistry and Biochemistry
in Partial Fulfillment of the Requirements for
the Degree of Doctor of Philosophy
at the University of Windsor

Windsor, Ontario, Canada

2019

© 2019 Sha Zhu

Phosphine supported mono-and polynuclear Ni complexes for inert
bond activation: Mechanism and isolation of reactive intermediates

by

Sha Zhu

APPROVED BY:

S. Groysman, External Examiner
Wayne State University

S. Rehse
Department of Physics

J. Rawson
Department of Chemistry and Biochemistry

C. Macdonald
Department of Chemistry and Biochemistry

S. Johnson, Advisor
Department of Chemistry and Biochemistry

September 20, 2019

DECLARATION OF CO-AUTHORSHIP/PREVIOUS PUBLICATION

I. Declaration of Co-Authorship

I hereby declare that this thesis incorporates material that is the result of joint research, as follows: this thesis contains five chapters, out of which one chapter has been previously published. Chapter two contains results published in the communication “Versatile (η^6 -arene)Ni(PCy₃) Nickel Monophosphine Precursors” Zhu, S.; Shoshani, M.; Johnson, S. A. *Chemical Communications*, 2017, **53**, 13176-13179. I acknowledge my supervisor as a co-author in this work as he made significant contribution to the editing and preparation of these manuscripts. I acknowledge that other listed authors on the manuscripts contributed through proposed methodology. I have obtained written permission to use work from other listed authors.

I am aware of the University of Windsor Senate Policy on Authorship and I certify that I have properly acknowledged the contribution of other researchers to my thesis, and have obtained written permission from each of the co-author(s) to include the above material(s) in my thesis.

I certify that, with the above qualification, this thesis, and the research to which it refers, is the product of my own work.

II. Declaration of Previous Publication

I certify that I have obtained a written permission from the copyright owner(s) to include the above published material(s) in my thesis. I certify that the above material describes work completed during my registration as a graduate student at the University of Windsor.

I declare that, to the best of my knowledge, my thesis does not infringe upon anyone's copyright nor violate any proprietary rights and that any ideas, techniques, quotations, or any other material from the work of other people included in my thesis, published or otherwise, are fully acknowledged in accordance with the standard referencing practices. Furthermore, to the extent that I have included copyrighted material that surpasses the bounds of fair dealing within the meaning of the Canada Copyright Act, I certify that I have obtained a written permission from the copyright owner(s) to include such material(s) in my thesis.

I declare that this is a true copy of my thesis, including any final revisions, as approved by my thesis committee and the Graduate Studies office, and that this thesis has not been submitted for a higher degree to any other University or Institution.

ABSTRACT

Inert C–O bond activation has been an important research area because ethers have the potential to replace organohalides as relatively economic and less toxic building blocks. Phosphine supported Ni complexes have been found to be reactive towards C–O bonds. A number of cross-coupling reactions using Ni catalysts for C–O activation have been developed. However, mechanistic understanding lags behind current application. Multiple mechanisms have been proposed based on DFT studies, while few intermediates have been isolated or observed experimentally. This dissertation focuses on the mechanistic details of Ni mediated C(sp²)–O activation.

The number of ligand coordinated to Ni in the critical bond cleavage step remains unclear, and previous DFT studies have suggested that both L₂Ni and LNi species might be the active species, where L is a neutral phosphine donor. The lack of easily accessible LNi(0) sources has been an obstacle to examining the ability of the LNi moiety to facilitate C–O bond cleavage. This work provides a synthesis to a series of (Cy₃P)Ni(η⁶-arene) complexes that provide a source of the (Cy₃P)Ni(0) moiety. We compared the stability of (Cy₃P)Ni(η⁶-arene) complexes with different substituents. Arenes with electron-withdrawing substituents form the most thermodynamically stable adducts. More fluorinated arenes form less stable adducts. This trend is opposite to the adducts of L₂Ni(0) species where more fluorinated substituents form more stable adducts. In the preparation of (Cy₃P)Ni(η⁶-arene) complexes we also correct a longstanding error in the nature of the starting material [(Cy₃P)₂Ni]₂(μ-N₂) in solution.

In our mechanistic studies of C(sp²)-O activation, (Cy₃P)Ni(η⁶-arene) and [(Cy₃P)₂Ni]₂(μ-N₂) were used as the LNi(0) and L₂Ni(0) sources. The reactions of naphthyl substrates with LNi(0) or L₂Ni(0) produce different products. However, the isolation of these adducts proved impossible, so other substrates were examined. The reactions of alkenyl ethers with LNi(0) or L₂Ni(0) at room temperature provided (Cy₃P)₂Ni(η²-alkenylether). The reactions of vinyl ethers (RH₂COCH=CH₂, R is aliphatic groups) with [(Cy₃P)₂Ni]₂(μ-N₂) produces esters through nickel mediated homocoupling of ethers. [(Cy₃P)₂Ni]₂(μ-N₂) can also mediate the coupling of acetaldehyde and vinyl ethers. A mechanism of the ether-acetaldehyde coupling was proposed based on the experimental and computational studies.

Apart from the traditional mononuclear complexes, electron-deficient transition metal clusters are emerging as powerful catalysts to inert bond activations. They are able to cooperatively activate bonds under mild conditions. Our previous work reported the synthesis of a pentanuclear nickel clusters, [(ⁱPr₃P)Ni]₅H₆, which shows high reactivities with inert C-O bonds. This thesis examines the role of the supporting phosphine donor in cluster formation and reactivity. A series of phosphines were investigated; P^tBuMe₂ provided [(^tBu₂MeP)Ni]₅H₆, which is even more reactive than the PⁱPr₃ analogue. PCy₂Me is able to form a dinuclear complex [(Cy₂MeP)₂Ni]₂(μ-H)₂. In the case of PCy₃ and PCyp₃, P-C bond cleavage occurred and led to the production of a dinuclear Ni complex [(R₃P)HNi]₂(μ-H)(μ-PR₂). We also proposed mechanisms of the production of these nickel hydride complexes based on the experimental studies.

ACKNOWLEDGEMENTS

First and most of all, I would like to express my deepest appreciation to my supervisor Dr. Sam Johnson. Without his expertise, consistent guidance and infinite patience this dissertation would not have been possible. I would like to thank my committee members Dr. Jeremy Rawson, Dr. Charles MacDonald and Dr. Steven Rehse for their help and advice over the years. I would also like to thank Dr. Stanislav Groysman for being my external reader.

Many thanks to present and past Johnson group members: Meghan, Manar, Jacob, Adam, Tina, Drake, Matt, Aaron, Vova, Jun and Galen. My lab life was enjoyable with their assistance and encouragement.

I would also like to extend my acknowledgement to my precious family for always supporting me over the past few years. Special thanks to my cousin Feifei and Aunt Lan for your encouragement even when you were in a really hard time.

Last but not the least, I'm deeply indebted to my parents for their endless encouragement and love.

TABLE OF CONTENTS

DECLARATION OF CO-AUTHORSHIP/PREVIOUS PUBLICATION.....	III
ABSTRACT.....	V
ACKNOWLEDGEMENTS	VII
LIST OF TABLES	XIII
LIST OF FIGURES	XIV
LIST OF SCHEMES	XVII
LIST OF ABBREVIATIONS/SYMBOLS.....	XXIII
Chapter 1 Transition Metal Complexes in Catalysis: from Mononuclear Complexes to Metal Clusters.....	1
1.1 General Introduction	1
1.2 Overview of Organometallic Nickel Complexes	6
1.3 Inert Bond Activation.....	7
1.3.1 C(sp ²)-O Activation.....	7
1.3.1.1 Cross-coupling Reactions through Nickel Catalyzed C(sp ²)-O Activation .	7
1.3.1.2 Mechanistic Studies in C-O activation by Nickel Complexes	11
1.3.1.3 The “Naphthalene Problem”	15
1.3.2 C(sp ³)-O Activation.....	18

1.4 Transition Metal Clusters	20
1.4.1 General Introduction	20
1.4.2 Geometry and Electron Counting of Transition Metal Clusters	21
1.4.3 Electron Deficient Transition Metal Clusters in Cooperative Catalysis	24
1.5 Dissertation Scope.....	30
1.6 References	31
Chapter 2 Versatile (Cy₃P)Ni(η⁶-arene) Nickel Monophosphine Precursor	38
2.1 Introduction	38
2.2 Results and Discussion.....	40
2.3 Summary and Conclusions.....	48
2.4 Experimental Section	49
2.4.1 General Procedures	49
2.4.2 Synthesis and Characterization of Complexes	50
2.4.3 Equilibrium Studies of 1 and 1-PⁱPr₃	53
2.5 X-ray Crystallography.....	54
2.6 References	56
Chapter 3 Nickel C(sp²)-O Bond Cleavage by Oxidative Addition and β-Oxygen Elimination to give Esters from Coupling of Vinyl Ethers or Cross Coupling of Vinyl Ethers and Aldehydes	61
3.1 Introduction	61

3.2 Results and Discussion.....	63
3.3 Conclusions and Future Work.....	77
3.4 Experimental section.....	79
3.4.1 General Procedure	79
3.4.2 Synthesis and Characterization of Complexes	80
3.4.3 Equilibrium Study	81
3.4.4 The Synthesis and Characterization of Organic Products from Vinyl Ethers and $[(\text{Cy}_3\text{P})_2\text{Ni}]_2(\mu\text{-N}_2)$ (1)	82
3.5 X-ray Crystallography.....	84
3.6 References	85
Chapter 4 The Formation of Nickel Hydride Clusters: Influence of Phosphines and Intermediates.....	88
4.1 Introduction	88
4.2 Results and Discussion.....	91
4.2.1 Phosphine Scope	91
4.2.1.1 Hydrogenation of Tricyclohexylphosphine Supported Ni(0).....	93
4.2.1.2 Hydrogenation of Tricyclopentylphosphine Supported Ni(0).....	96
4.2.1.3 The Preparation of Pentanuclear Cluster from Di-tert-butylmethylphosphine Supported Dinitrogen Complex	97
4.2.1.4 Dicyclohexylmethylphosphine	104

4.2.1.5 The Reduction of Di-tert-butylethylphosphine and Diisopropylethyl phosphine Supported Ni(II) Complexes	107
4.2.1.6 The Reactions of Triethylphosphine or Triphenylphosphine Supported Ni(0) species with H ₂ gas.....	108
4.2.2 Mechanistic Study of the Formation of Polynuclear Nickel Hydride Phosphine Complexes	110
4.3 Conclusions and Future Work.....	113
4.4 Experimental Section	116
4.4.1 General Procedures	116
4.4.2 Synthesis and Characterization of Complexes	116
4.4.3 The Decomposition of Complex 3d in Pentane, Benzene and Toluene.....	121
4.4.4 NMR Spectroscopically Characterization of [(Cy ₂ Me) ₂ Ni] ₂ (μ-H) ₂ (5e).....	121
4.4.5 NMR Spectroscopically Characterization of L ₂ NiH ₂ (4a-c).....	122
4.5 X-ray Crystallography.....	123
4.6 References	125
Chapter 5 Summary and Future Work	127
5.1 Summary	127
5.1 Preliminary Results and Future Work.....	130
5.3 Experimental Section	139
5.4 References	142
APPENDIX	144

VITA AUCTORIS145

LIST OF TABLES

Table 1.1 Bonding Capabilities of Clusters according to Lauher's Rule.....	23
Table 2.1 Selective Bond Lengths of (Cy ₃ P)Ni(η ⁶ -arene) Complexes	48
Table 2.2 Crystallographic Data for Complexes 2a-2f	54
Table 3.1 Crystallographic Data for Complex 2a	84
Table 4.1 Key Physical Parameters of Phosphines	92
Table 4.2 Crystallographic Data for Complex 2d, 3d, 6 and 7	123
Table 5.1 Kumada-type Coupling Catalyzed by (Cy ₃ P)Ni(η ⁶ -PhMe) (1).....	136

LIST OF FIGURES

Figure 1.1 Comparison of nickel and other Group 10 metals.....	6
Figure 1.2 Selective fully characterized $L_2Ni(0)$ complexes and $LNi(0)$ complexes.	14
Figure 1.3 The structures of <i>closo</i> polyhedra with 6-8 vertices and their corresponding <i>nido</i> and <i>arachno</i> fragments.....	21
Figure 2.1 An example of $(NHC)Ni(\eta^6\text{-arene})$, where arene is C_6H_6 , NHC is IPr (1,3-bis(2,6-diisopropylphenyl)imidazol-2-ylidene); b) The structure of $(tBu_2PCH_2P^tBu_2)Ni(\eta^6-C_6H_6)$	39
Figure 2.2 $^{31}P\{^1H\}$ NMR of a) Complex 1 in pentane and b) Complex 1 in toluene.....	41
Figure 2.3 VT- $^{31}P\{^1H\}$ NMR of complex 1 in toluene. The integral of 1 increases as the temperature decreases. * is $O=PCy_3$	42
Figure 2.4 $^{31}P\{^1H\}$ NMR of a) Complex 1 in THF under N_2 atmosphere and b) Complex 1 in THF under vacuum.	42
Figure 2.5 ORTEP depiction of 2a	45
Figure 3.1 Solid state structure of 2a . Hydrogen atoms were omitted for clarity. Selected bond length (unit: Å): Ni–C(1) = 1.968(2); Ni–C(2) = 1.978(2); Ni–P(1) = 2.1971(5); Ni–P(2) = 2.1854(6); C(1)–C(2) = 1.402(3); C(2)–O(1) = 1.413(2). Selected bond angles (unit: °): C(1)–Ni–C(2) = 41.63(7); Ni–C(1)–C(2) = 69.6(1); Ni–C(2)–C(1) = 68.8(1); P(1)–Ni–P(2) = 117.98(2).....	71
Figure 3.2 The variable-temperature $^{31}P\{^1H\}$ of 2a in HMDSO.....	72
Figure 4.1 The structure of $L_2Ni(\mu-H)_2$ synthesized by Barnett and co-workers in 1977.	91

Figure 4.2 ORTEP depiction of **6**. The cyclohexyl groups are omitted for clarity. Selected bond distances (unit: Å): Ni(1)-H(1) = 1.52(2); Ni(1)-H(3) = 1.67; Ni(2)-H(2) = 1.47; Ni(2)-H(3) = 1.59(2); Ni(1)-P(1) = 2.1689(5); Ni(1)-P(3) = 2.0960(4); Ni(2)-P(2) = 2.1709(6); Ni(2)-P(3) = 2.1039(6). Selected bond angles (unit: °): P(3)-Ni(1)-H(3) = 88.2(7)°; P(3)-Ni(2)-H(3) = 90.0(8)°; Ni(1)-P(3)-Ni(2) = 76.22(2)°; Ni(1)-H(3)-Ni(2) = 106(1)°; H(1)-Ni(1)-P(3) = 76.8(8)°; H(2)-Ni(2)-P(3) = 82.1(8)°; H(3)-Ni(1)-P(1) = 96.6(7)°; H(3)-Ni(2)-P(2) = 94.1(8)°..... 94

Figure 4.3 The experimental (red) and modeled (blue) hydride ligands peaks in ¹H NMR spectrum of **6**. The modelling software is Bruker TopSpin 4.0.6. 95

Figure 4.4 Solid state molecular structure of cluster **3d** was determined by single crystal X-ray diffraction. Both side view (left) and top view (right) are shown here. *Tert*-butyl and methyl groups are omitted for clarity. Selected bond distances (unit: Å): Ni(1)-N(2) = 2.4279(6); Ni(1)-Ni(3) = 2.4621(6); Ni(1)-Ni(4) = 2.4167(8); Ni(1)-Ni(5) = 2.4477(7); Ni(2)-Ni(3) = 2.6353(6); Ni(2)-Ni(5) = 2.4021(8); Ni(3)-Ni(4) = 2.3936(8); Ni(4)-Ni(5) = 2.6656(6); Ni(1)-P(1) = 2.218(2); Ni(2)-P(2) = 2.199(2); Ni(3)-P(3) = 2.189(1); Ni(4)-P(4) = 2.175(1). Selective bond angles (unit: °): Ni(2)-Ni(3)-Ni(4) = 90.43(2)°; Ni(3)-Ni(4)-Ni(5) = 89.72(2)°; Ni(4)-Ni(5)-Ni(2) = 89.52(2)°; Ni(5)-Ni(2)-Ni(3) = 90.25(2)°; Ni(2)-Ni(1)-Ni(4) = 95.05(2)°; Ni(3)-Ni(1)-Ni(5) = 93.41(2)°; Ni(2)-Ni(1)-Ni(3) = 65.21(2)°; Ni(3)-Ni(1)-Ni(4) = 58.75(2)°; Ni(4)-Ni(1)-Ni(5) = 66.45(2)°; Ni(5)-Ni(1)-Ni(2) = 59.03(2)° 98

Figure 4.5 Nickel framework of **3d** with selected approximate bond lengths and bond angles..... 99

Figure 4.6 The H/D exchange of **3d** and C₆D₆ at 8 °C over a period of 44 minutes monitored by ¹H NMR spectroscopy. 101

Figure 4.7 Plot of peak half height width in ³¹P{¹H} NMR versus temperature for **3d**. The peak width is largely affected by temperature above -10 °C 102

Figure 4.8 Plot of $^{31}\text{P}\{^1\text{H}\}$ NMR chemical shift versus temperature for **3d**. The red solid line is a fitted curve based on a model assuming that **3d** is a ground state singlet ($S = 0$) with a triplet state ($S = 1$) that is thermally accessible. According to the Boltzmann function, $2|J|$ from the Hamiltonian $H = -2JS_1S_2$ represents the energy difference between singlet ground state and triplet excited state. The chemical shift is influenced by a temperature-dependent magnetization $m(T)$ and follows the equation $\delta(T) = \delta_0 + \delta_p \cdot m(T)$, where δ_0 is the chemical shift for the diamagnetic ground state sample, which is δ 35 in this case, δ_p is a coefficient for the paramagnetic excited state. $m(T)$ is proportional to population difference of m_s and can be approximated by the equation $m(T) = \text{const} \cdot p(T)/T$, where $p(T)$ is the Boltzmann population at temperature T, $p(T) = e^{2J/KT}/(1 + 3e^{2J/KT})$. K is the Boltzmann constant 8.314 J/(K•mol). 103

Figure 4.9 Solid state molecular structure of complex **7** was determined by single crystal X-ray diffraction. H atoms are omitted for clarity. Selected bond distances (unit: Å): Ni-N(1) = 1.718(2); Ni-P(1) = 2.1362(6); Ni-P(2) = 2.1432(7); Ni-P(3) = 2.1505(7); N(1)-N(2) = 1.17(2). Selective bond angles: N(2)-N(1)-Ni = 177.10(2) $^\circ$; P(1)-Ni-P(2) = 119.34(3) $^\circ$; P(1)-Ni-P(3) = 120.12(3) $^\circ$; P(2)-Ni-P(3) = 119.34(3) $^\circ$ 105

Figure 5.1 Variable-temperature $^{31}\text{P}\{^1\text{H}\}$ NMR of $(\text{Cy}_3\text{P})_2\text{Ni}(\eta^2\text{-2-methoxynaphthalene})$ (**4**) in pentane. The singlet peak at δ 33.8 decoalesces into two broad singlets at 253 K. * is a trace unidentified byproduct. 133

LIST OF SCHEMES

- Scheme 1.1** Generic potential energy diagram showing the effect of a catalyst in an exothermic reaction. The catalyst triggers a different reaction pathway (shown in red) with a lower activation energy. The activation energy is decided by the transition state with the higher/highest energy. 2
- Scheme 1.2** Suzuki coupling of organoboron species and halide species is an example of heavy metal catalyzed reaction. This reaction is now widely applied in chemical industry. 3
- Scheme 1.3** Nickel catalysed cross-coupling of aromatic ethers and nucleophiles. 3
- Scheme 1.4** Milestones in the area of nickel catalyzed C–O bond activation cross couplings. a) Kumada-Corriu cross-coupling of aryl ether and Grignard reagent; b) Suzuki-Miyaura cross-coupling of aryl ether and boronic ester; c) Suzuki-Miyaura cross-coupling of aryl pivalates and boronic acid; d) Suzuki-Miyaura cross-coupling of alkenyl ether and boronic ester. 9
- Scheme 1.5** Mechanism of cross-coupling reaction through Ni catalyzed C(sp²)–O activation. 11
- Scheme 1.6** a) Oxidative addition product of naphthyl pivalate to Ni(0) centre supported by a bidentate phosphine ligand; b) Oxidative addition product of naphthyl pivalate to Ni(0) centre supported by PCy₃. 12
- Scheme 1.7** Ni(0)-ate pathway of cross coupling of aryl ether and Grignard reagent. Adapted from Ref 61. 13
- Scheme 1.8** Important breakthroughs in phenyl ether C(sp²)–O activation. a) NiCl₂(PCy₃) can efficiently catalyze Kumada-Corriu-type cross-coupling of aryl ether and *p*-tolMgBr; b) The scope of substrate was extended to electron-rich anisole

derivatives; c) Suzuki-Miyaura-type and Kumada-Corriu-type cross-coupling of phenyl ether catalyzed by Ni ⁰ /NHC ligand; d) Bidentate phosphine ligand can help catalyze Kumada-Corriu-type cross-coupling of phenyl ether and Grignard reagent containing β-H.....	17
Scheme 1.9 Selective examples of benzylic C(sp ³)-O activations. a) Kumada-Corriu-type cross-coupling of benzylic ethers. b) Kumada-Corriu-type cross-coupling of benzylic alcohols. c) Stereospecific Suzuki-Miyaura-type cross-coupling of benzyl pivalates, need no ancillary ligand. d) Stereospecific Kumada-Miyaura-type cross-coupling of benzylic ethers.	19
Scheme 1.10 Cooperative C-C, C-H, C-Si and C-S activation by a Ru ₃ cluster.	25
Scheme 1.11 Reversible H ₂ gas absorption and release on the [(R ₃ P)Rh] ₆ H ₁₂ ²⁺ cluster. Exact hydride locations in [(R ₃ P)Rh] ₆ H ₁₆ ²⁺ are not known.	26
Scheme 1.12 Ni mediated C-S bond cleavage. Equilibrium between mononuclear nickel sulfide and dinuclear nickel sulfide proves the cooperative action of substrate on the both nickel centres.	27
Scheme 1.13 Ligand steric effects on single-site vs cooperative activation of azide by a Cr ₃ cluster.	28
Scheme 1.14 Cooperative C-C, C-O, C-S bond activation and H/D exchange on a Ni ₅ cluster.....	29
Scheme 2.1 Equilibrium reaction of complex 1 with toluene.	40
Scheme 2.2 Isolation of toluene (2a), benzene (2b) and mesitylene (2c) complexes from 1 by oxidation of unbound PCy ₃ with NMO.....	44
Scheme 2.3 Use of 2a as a (Cy ₃ P)Ni transfer reagent in the synthesis of complexes of α,α,α-trifluorotoluene (2d), 1,3-bis(trifluoromethyl)benzene (2e) and anisole (2f).....	45

- Scheme 2.4** Determination of Gibbs free energy change (ΔG) for equilibrium $(\text{Cy}_3\text{P})\text{Ni}$ transfer from **2a** to arenes..... 47
- Scheme 3.1** Examples of Ni catalyzed cross-coupling reactions of alkenyl ethers and nucleophiles through $\text{C}(\text{sp}^2)\text{-O}$ bond activation. a) Negishi-style cross-coupling of alkenyl pivalate and organic zinc reagent catalyzed by $\text{NiCl}_2(\text{PCy}_3)_2$. b) Suzuki-Miyaura-style cross-coupling of alkenyl ethers and boronic ester catalyzed by $\text{Ni}(\text{COD})_2/\text{PCy}_3$. c) Kumada-type cross-coupling of alkenyl ethers and aromatic Grignard reagent catalyzed by nickel phosphine complex..... 63
- Scheme 3.2** Reactions of $\text{H}_2\text{C}=\text{CHOEt}$, $\text{H}_2\text{C}=\text{CHO}^i\text{Pr}$ and $\text{H}_2\text{C}=\text{CHO}^i\text{Bu}$ with $[(\text{Cy}_3\text{P})_2\text{Ni}]_2(\mu\text{-N}_2)$ (**1**) in benzene to give esters upon heating. 64
- Scheme 3.3** Precedented mechanism for the production of aldehydes from C–O bond oxidative addition and $\beta\text{-H}$ elimination as applied to system under study.. 64
- Scheme 3.4** a) Aluminum or sodium alkoxide catalyzed aldehyde condensation (typical Tishchenko reaction without selectivity to cross-coupling of two aldehydes). b) Nickel catalyzed Tishchenko reaction with the assistance of NHC or PCy_3 ligand. The substrates include at least one aryl ester. SIPr = 1,3-(2,6-bis(isopropyl)phenyl)imidazolidine. c) Reaction of aldehydes with stoichiometric amount of $[(\text{Cy}_3\text{P})_2\text{Ni}]_2(\mu\text{-N}_2)$ (**1**) does not produce an ester. 66
- Scheme 3.5** The reaction of $[(\text{Cy}_3\text{P})_2\text{Ni}]_2(\mu\text{-N}_2)$ (**1**) and $\text{CyOCH}=\text{CH}_2$ at $80\text{ }^\circ\text{C}$ produces cyclohexanone and $(\text{Cy}_3\text{P})_2\text{Ni}(\eta^2\text{-C}_2\text{H}_4)$ 67
- Scheme 3.6** a) The cross-coupling of $^i\text{BuOCH}=\text{CH}_2$ and acetaldehyde mediated by $[(\text{Cy}_3\text{P})_2\text{Ni}]_2(\mu\text{-N}_2)$ (**1**). MeCOO^iBu and $(\text{Cy}_3\text{P})_2\text{Ni}(\eta^2\text{-C}_2\text{H}_4)$ are produced. b) The cross-coupling of $\text{CyOCH}=\text{CH}_2$ and acetaldehyde mediated by $[(\text{Cy}_3\text{P})_2\text{Ni}]_2(\mu\text{-N}_2)$ (**1**). MeCOOCy and $(\text{Cy}_3\text{P})_2\text{Ni}(\eta^2\text{-C}_2\text{H}_4)$ are produced. 68

- Scheme 3.7** a) The reaction of ROCH=CH₂ and [(Cy₃P)₂Ni]2(μ-N₂) (**1**) produces (Cy₃P)₂Ni(η²-H₂C=CHOR) (**2a-c**). b) The reaction of (Cy₃P)Ni(η⁶-PhMe) with ^tBuOCH=CH₂ also produces **2a**. c) The equilibrium of **2a** and (Cy₃P)Ni(η⁶-PhMe) in THF. 69
- Scheme 3.8** The ³¹P{¹H} NMR spectrum showing the equilibrium formation of (Cy₃P)Ni(η⁶-PhMe) and PCy₃ upon addition of toluene to a THF solution of **2a**, as shown in **Scheme 3.7 c**. * is O=PCy₃. 70
- Scheme 3.9** The ³¹P{¹H} NMR spectrum of the reaction of **2a** with acetaldehyde at room temperature to give (Cy₃P)₂Ni(η²-O=CHMe) (**3**). 73
- Scheme 3.10** a) The reaction of (Cy₃P)Ni(η⁶-PhMe) with stoichiometric amount of ^tBuOCH=CH₂ and O=CHMe. Both complex **4** and **5** were generated. b) The reaction of (Cy₃P)Ni(η⁶-PhMe) with 2 equivalent of O=CHMe. Only Complex **3** was produced, which rules out the possibility of (Cy₃P)Ni(η²-O=CHMe)₂. * are unidentified products. 74
- Scheme 3.11** Two mechanisms of Ni mediated production of ester from vinyl ether and acetaldehyde, differing by mechanism of the C–O bond cleavage step. **Mechanism 1** features a β-OR elimination step, whereas **Mechanism 2** operates by a more classical C–O bond oxidative addition. 75
- Scheme 3.12** DFT calculations of intermediates in the 2 plausible mechanisms. Mechanism 2 is in red. Mechanism 1 is shown in black and the blue one is an off-cycle reaction pathway considered in Mechanism 1. 76
- Scheme 4.1** Synthesis and selected reactivity of the pentanuclear nickel hydride cluster [(ⁱPr₃P)₂Ni]2(μ-N₂) (**2a**). 89
- Scheme 4.2** Plausible mechanism of the formation of complex **3a** from **2a** under 4 atm H₂ atmosphere. 90
- Scheme 4.3** The synthesis of **6** from **2b** under 4 atm H₂ atmosphere. 93

Scheme 4.4 a) The reaction of $(\text{Cy}_3\text{P})\text{Ni}(\eta^6\text{-PhMe})$ with 4 atm H_2 gas does not produce polynuclear nickel hydride complexes. b) The reaction of 2b with 4 atm H_2 gas in toluene only produces $(\text{Cy}_3\text{P})\text{Ni}(\eta^6\text{-PhMe})$	96
Scheme 4.5 The synthesis of 7 from 2c under 4 atm H_2 atmosphere.	96
Scheme 4.6 The synthesis of the pentanuclear nickel cluster 3d under from 2d under 4 atm H_2 atmosphere.	97
Scheme 4.7 The $^{31}\text{P}\{^1\text{H}\}$ NMR of the decomposition product of complex 3d in benzene, toluene or pentane.	100
Scheme 4.8 H/D exchange between C_6D_6 and complex 3a or 3d	100
Scheme 4.9 The synthesis of $(\text{Cy}_2\text{Me})_3\text{P}(\mu\text{-N}_2)$ (8) from 1e under 4 atm N_2 and the production of $[(\text{Cy}_2\text{MeP})_2\text{Ni}](\mu\text{-H})_2$ (5e) under 4 atm H_2 atmosphere.	104
Scheme 4.10 The characterization of 5e by NMR spectroscopy.	106
Scheme 4.11 The reduction of 1f and 1g led to the decomposition of the starting materials and produced Ni particles and the corresponding tertiary phosphines.	107
Scheme 4.12 No reaction observed by NMR spectroscopy when complex 8 and 9 were exposed to 4 atm of H_2 gas.	108
Scheme 4.13 NMR spectroscopically characterization of complex 4a . The coupling constants of the triplets in ^1H and ^{31}P NMR spectra are both 52.5 Hz. The peak at δ 43.9 was proposed to be a Ni_5H_8 species.	110
Scheme 4.14 The reaction of $(\text{L}_2\text{Ni})(\mu\text{-N}_2)$ (2a-d) or 2e and H_2 gas. The Ni(II) intermediate L_2NiH_2 (4a-e) was observed and characterized by NMR spectroscopy. ...	112
Scheme 5.1 The $^{31}\text{P}\{^1\text{H}\}$ NMR spectra of: a) 1 reacted with 2-methoxynaphthalene to give predominantly a product tentatively assigned as $(\text{Cy}_3\text{P})\text{Ni}(\eta^6\text{-2-methoxynaphthalene})$ (3); b) 2 reacted with two equivalents of 2-	

methoxynaphthalene to give a product tentatively assigned as $(\text{Cy}_3\text{P})_2\text{Ni}(\eta^2\text{-2-methoxynaphthalene})$ (**4**). * is a trace unknown byproduct. 132

Scheme 5.2 The $^{31}\text{P}\{^1\text{H}\}$ NMR spectra of: a) **1** reacted with 2-naphthyl acetate in a ratio of 1:3, producing a product at δ 25.2. b) **2** reacts with 2-methoxynaphthalene in a ratio of 1:2, producing multiple products. * represents unknown species. 134

LIST OF ABBREVIATIONS/SYMBOLS

Å	Angström
acac	acetylacetonate
Anal.	analysis
Ar	aryl group
atm.	atmosphere
BDE	bond dissociation energy
Bn	benzyl
br	broad
ⁿ Bu	butyl group, -CH ₂ CH ₂ CH ₂ CH ₃
ⁱ Bu	<i>iso</i> -butyl group, -CH(CH ₃)CH ₂ CH ₃
^t Bu	<i>tert</i> -butyl group, -C(CH ₃) ₃
cal	calorie
calcd	calculated
¹³ C	carbon-13
cm	centimeter
COD	1,5-cyclooctadiene group, C ₈ H ₁₂
cryst	crystal
CVE	cluster valence electron
CVMO	cluster valence molecular orbitals
Cy	cyclohexyl group, -C ₆ H ₁₁
Cyp	cyclopentyl group, -C ₅ H ₉

d	doublet
°C	degrees Celsius
D	deuterium
DFT	density functional theory
e ⁻	electron
EA	elemental analysis
eq.	equation
equiv	equivalents
Et	ethyl group, -CH ₂ CH ₃
¹⁹ F	fluorine-19
FW	formula weight
G	Gauss
ΔG	Gibb's free energy
g	gram(s)
h	hour(s)
¹ H	proton
{ ¹ H}	proton decoupled
HDS	hydrodesulfurization
HLAO	high-lying atomic orbitals
HMDSO	hexamethyldisiloxane
Hz	hertz
IPr	1,3-Bis(2,6-diisopropylphenyl)imidazol-2-ylidene
J	Joules

${}^nJ_{AB}$	n-bond scalar coupling constant between nuclei A and B
K	Kelvin
kcal	kilocalories
kJ	kilojoules
L	neutral two electron donor
ln	natural logarithm
M	central metal atom
<i>m</i>	meta
m	multiplet
Me	methyl group, -CH ₃
4,6-Me ₂ DBT	4,6-dimethyldibenzothiophene
Mes	mesityl group, -2,4,6-Me ₃ C ₆ H ₂
mg	milligrams(s)
MHz	megahertz
min	minutes(s)
mL	milliliter
mmol	millimole
MO	molecular orbital
mol	mole
MW	molecular weight
NMR	nuclear magnetic resonance
<i>o</i>	ortho

ORTEP	Oakridge Thermal Ellipsoid Plotting program
<i>p</i>	<i>para</i>
p	pentet
³¹ P	phosphorus-31
%	percent
Ph	phenyl group, -C ₆ H ₅
ppm	parts per million
<i>i</i> Pr	<i>isopropyl</i> group, -CH(CH ₃) ₂
R	alkyl or aryl substituent
<i>R</i>	reliability factor (X-ray crystallography)
R ²	coefficient of determination for a linear regression
Reflns	reflections (X-ray crystallography)
s	singlet
t	triplet
T	temperature in K or °C
THF	tetrahydrofuran
<i>V</i>	unit cell volume
<i>W</i> _{1/2}	width at half height
X	halide substituent
Z	asymmetric units per unit cell (X-ray crystallography)

α	atom in the alpha position or angle label (X-ray crystallography)
β	atom in the beta position or angle label (X-ray crystallography)
γ	angle label (X-ray crystallography)
δ	chemical shift in ppm
θ	detector angle (X-ray crystallography)
λ	wavelength
μ	bridging or absorption coefficient (X-ray crystallography)
π	pi-bonding
σ	estimated standard deviation (X-ray crystallography) or sigma-bonding

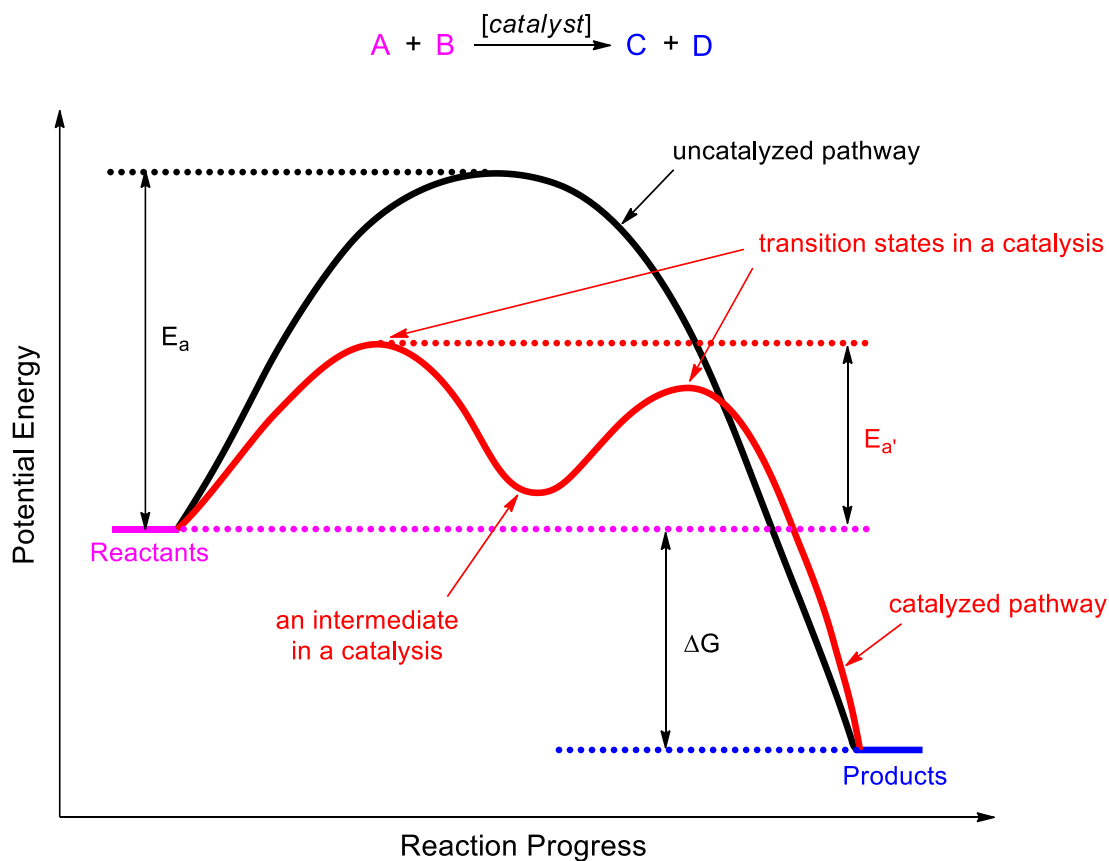
Chapter 1 Transition Metal Complexes in Catalysis: from Mononuclear Complexes to Metal Clusters

1.1 General Introduction

Many catalytic chemical reactions proceed via steps that involve bond cleavage and new bond formation. The most thermodynamically viable reaction steps feature either i) steps where the bonds being broken are weak, or ii) the concomitant formation of new strong bonds in a concerted manner that offsets the energy cost of breaking strong bonds. The same principles that apply to the thermodynamic viability of reaction steps also apply to the transition states between intermediates, which determines if reactions, whether favourable or not, occur at an appreciable rate.

The breaking of bonds with high barriers to dissociation, often described as inert bond activation, provides a challenge for chemists. But with this challenge comes rewards, as chemical reactions of traditionally unreactive bonds like $\text{N}\equiv\text{N}^{1-5}$, C-H^{6-10} , C-F^{11-16} and C-O^{17-22} could open new avenues to important value-added products both in small scale and large scale chemical industry, particular if utilized in a catalytic manner. The high reaction barriers associated with the activation of inert bonds are often associated with the strength of these bonds, where their cleavage is strongly thermodynamically disfavoured, and thus feature late transition states that resemble the high energy products of these steps; however, some bonds can also be inert solely due to kinetic factors, where the cleavage of

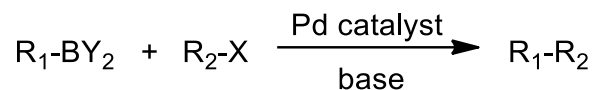
bonds can be thermodynamically favourable, but the barrier to cleavage is insurmountable under available reaction conditions. Catalysts can accelerate reaction rates by providing lower energy transition states without being consumed in the net reaction. Such catalysts also commonly provide reaction pathways with intermediates that have relatively low energy²³ (**Scheme 1.1**). Nowadays, the production of more than 90 % of commercial chemicals in modern industry includes catalytic steps.²⁴



Scheme 1.1 Generic potential energy diagram showing the effect of a catalyst in an exothermic reaction. The catalyst triggers a different reaction pathway (shown in red) with a lower activation energy. The activation energy is decided by the transition state with the higher/highest energy.

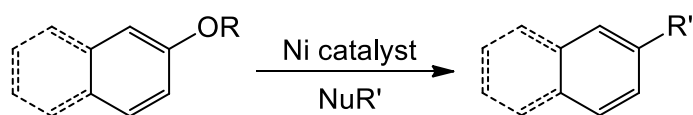
Historically second- and third-row transition metal complexes have been the most utilized in the development of catalytic processes. An example of palladium catalyzed

cross-coupling is shown in **Scheme 1.2**.²⁵⁻²⁷ This is particularly true for systems capable of the functionalization of traditionally inert C–H⁶⁻¹⁰, C–C²⁸⁻³¹ and C–heteroatom³²⁻³⁵ bonds. Stronger bonds to elements like carbon and hydrogen provide extra thermodynamic driving force in the difficult bond activation steps.



Scheme 1.2 Suzuki coupling of organoboron species and halide species is an example of heavy metal catalyzed reaction. This reaction is now widely applied in chemical industry.

However, these heavy metals have drawbacks, such as a low abundance that results in high cost and long-term resource shortages. As well, many pose long-term problems as environmental contaminants. These shortcomings provide the impetus to seek methods that utilize more abundant and less harmful metals starting for catalytic applications in any synthetic application that involves the breaking of strong bonds for the formation value added chemicals. Many first-row metals would be attractive replacements, but generally form weaker bonds than the heavier elements, which gives them a thermodynamic disadvantage in key bond-activation steps.



R = alkyl groups, R' = alkyl or aryl groups, Nu = nucleophiles

Scheme 1.3 Nickel catalyzed cross-coupling of aromatic ethers and nucleophiles.

Nickel has demonstrated the ability to compete with and even outperform the heavier elements in some bond-activation reactions of current interest (as shown in **Scheme 1.3**). The replacement of aromatic halide substrates with aromatic ethers in bond-coupling reactions is one example. Aromatic ethers are abundant in nature and much less toxic than

synthetically derived aryl halides that are the easiest substrates for coupling reactions like Suzuki couplings. Research done over the past decade has shown that complexes of the earth-abundant first-row metal Ni³⁶ are able to cleave the relatively unreactive C–O bonds in aromatic ethers in catalytic processes that give new C–C bonds, which is fundamental to the majority of synthetic chemistry.¹⁷⁻²² The development of nickel catalysts has the potential to reduce cost and improve sustainability compared to metals like Pd that provide the most popular and traditional catalysts for coupling chemistry. Numerous research groups from all around the world have developed Ni complexes for difficult bond activation and catalytic functionalization reactions over the past decade; however, in many cases the development has not always been rational, and often a fundamental understanding of the reaction mechanisms and key intermediates is lacking, particularly in terms of experimental rather than computational studies. Detailed insight into the mechanism of these reactions could provide a new avenue for the development of nickel catalyzed inert bond activation and its practical application in both large scale industrial chemistry and fine-chemical synthesis.

Several approaches have been taken to adapt the chemistry of first-row metals to achieve catalysis. Despite the similarities in the chemistry of Ni and the heavier elements like Pd, ubiquitous in coupling chemistry and catalysis, the differences prevent immediate replacement of Ni supported by similar ligands in most processes. It is well known that Ni is more disposed to single-electron transfer chemistry in coupling reactions. Although these alternate reaction pathways hinder the direct replacement of Ni in Pd catalysis, it also provides the opportunity for new catalytic processes and pathways.

Nature provides inspiration in the way first-row metals are utilized for enzymatic catalysis. In Nature, there are numerous examples of cooperative catalysis with 1st-row transition metals in close proximity. Remarkable small molecule transformations are catalyzed by earth-abundant metal enzymes under mild conditions with high efficiency and selectivity. For example, even substrates as unreactive as dinitrogen can be converted to useful nitrogen containing products at the polymetallic reaction sites in nitrogenase.^{37, 38} Cooperative catalysis has also been proved to be a promising method for the activation and

functionalization of unreactive bonds, such as C–O and C–C bonds.³⁹⁻⁴² Early transition metal clusters are potential catalysts to facilitate difficult bond transformations efficiently and economically.

Transition metal clusters featuring cooperative reactivity also play an important role as the bridge between homogeneous catalysis and heterogeneous catalysis. Heterogeneous catalysts play a vital role in large scale industrial applications, but active site identification, mechanistic insight and catalytic tuneability are all more easily achieved with homogeneous catalysts. Heterogeneous catalysts are typically cheaper and more easily adapted to the constant flow processes typical of large scale chemical production. But they are not as readily tuneable as homogeneous catalysts and the reaction mechanisms are more difficult to ascertain. Mechanistic studies are paramount to the optimization of difficult transformations and the development of new transformations. Transition metal nanomaterial is a major type of heterogeneous catalysts. According to the Eley-Rideal model and the Langmuir-Hinshelwood model^{43, 44}, reactants are physically or chemically absorbed to active sites on transition metal surfaces during reaction progress and products are desorbed when reactions finish. The interactions between substrates and metal-metal bonds in large clusters give semblance to the reactions that happen on metal surface of heterogeneous catalysts and the possibility of cooperativity, while the discrete molecular nature of clusters simplifies mechanistic investigations and often enhances solubility so that a range of solution techniques can be used in characterization and mechanistic study. The design of reactive new clusters is a target goal, as the majority of first-row metal clusters simply lack reactivity in difficult bond transformations. Further goals include the identification of inert bond activation with these clusters, and in-depth mechanistic studies with the final goal of new first-row transition metal cluster catalysis with applications in chemical industry or synthesis.

This dissertation features research with a variety of related goals in inert bond activation with Ni complexes, both mononuclear and polynuclear. One area of intense interest is C(sp²)–O bond activation. Computational studies have supported LNi or L₂Ni as the active species in the C(sp²)–O bond cleavage step, where L is a neutral donor ligand

and in particular often a phosphine such as tricyclohexylphosphine in this work. The lack of synthetically available LNi(0) sources has hindered the prospects for experimental mechanistic studies to support or refute theoretical predictions, so the initial goal was to develop easily prepared LNi(0) sources and use them to probe C(sp²)-O cleavage mechanisms, as well as to compare to related L₂Ni(0) precursors in these reactions. Out of the interest in transition metal cluster catalyzed bond activation, this thesis also examined the role of phosphine choice in the preparation and stability of clusters of the type (LNi)₅H₆ because these clusters show remarkable inert bond activation potential while retaining tolerance to commonly reactive substrate functional groups.

1.2 Overview of Organometallic Nickel Complexes



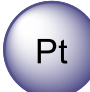
 Ni	 Pd	 Pt
smaller atomic radius	about 10% larger atomic radius	
less toxic	more toxic	
higher abundance in nature	lower abundance in nature	
more available oxidation states -1, 0, +1, +2, +3, +4	0, +1, +2, +3, +4	
higher electropositivity	higher electronegativity	

Figure 1.1 Comparison of nickel and other Group 10 metals.

Nickel is a first-row Group 10 transition metal. As noted previously, it is more abundant³⁶, cheaper and less toxic than its heavier counterparts in the same group, which makes it an economical replacement of palladium or platinum in a variety of reactions. The higher electropositivity and smaller size of nickel also give nickel unique reactivities.⁴⁵ The

oxidation states of 0 and +2 are common for Pd and the oxidation states of 0, +2 and +4 are common for Pt. Most of the reactions catalyzed by Pd and Pt often have non-radical mechanisms; compared to Pd and Pt, the Ni(I) and Ni(III) oxidation states are far more common than Pd(I) or Pt(III), which means it allows different reactivities and radical mechanisms in nickel mediated reactions.

Among all of the possible oxidation states, Ni(0) and Ni(II) complexes are the most common ones. Ni(0)/Ni(II) catalytic cycles are observed in a wide range of reactions.⁴⁵ Ni(I) also appears in some catalysis,⁴⁶ while Ni(III) and particularly Ni(IV) are less common. Ni(0) complexes are often stabilized by tertiary phosphines, *N*-heterocyclic carbenes (NHC) or π -complexes through σ and π interaction. Ni(0) undergoes oxidative addition with an extensive range of substrates, breaking C–heteroatom bonds and prompting the formation of new bonds, though unlike the heavier elements these reactions are not always concerted, but rather occur via radicals obtained by single-electron transfer chemistry.⁴⁷⁻⁵¹ The applicability of Ni(0) in synthetic processes is limited due to its air sensitivity. It is more common for air-stable Ni(II) precatalysts to be used, which decreases the cost of storage and makes reactions more amenable, but oftentimes in these processes the true nature of the catalyst formed from the Ni(II) precatalyst is not known experimentally.

1.3 Inert Bond Activation

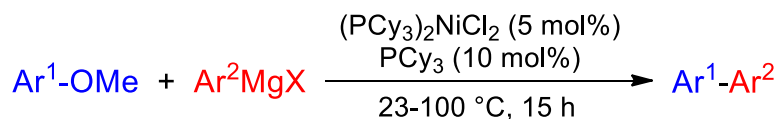
1.3.1 C(sp²)-O Activation

1.3.1.1 Cross-coupling Reactions through Nickel Catalyzed C(sp²)-O Activation

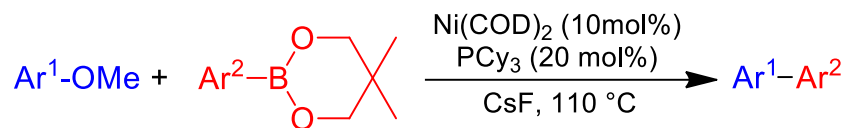
The activation and functionalization of aromatic C–O bonds has attracted considerable interest across a wide range of fields, including organic synthesis and green fuels.^{17, 19, 45, 52-54} In the past few decades, the application of aryl halides as building blocks in organic and pharmaceutical syntheses was developed rapidly; the 2010 Nobel Prize in

chemistry was awarded for work on palladium catalyzed cross-coupling of aryl halides and nucleophiles. However, halogenated chemicals are usually highly toxic and improper disposal or treatment cause severe environmental contamination and health impairment or even DNA damage. In contrast, aryl ethers have a potential to be utilized as the ideal environmentally friendly alternative to aryl halides in organic synthesis because of their low toxicity, large variety of derivatives, and easy access from natural products that offers sustainability and low cost. The replacement of aryl halides by aryl ethers in chemistry has long term future benefits for our environment. Aryl ether is the major component in plant lignin, so the aromatic C–O bond cleavage could be used to produce green fuels from plants.⁵⁵⁻⁵⁸ For the past two decades, chemists have been developing various methodologies to realize aromatic C–O activation and extending the scope of aryl ether substrates and their nucleophilic coupling partners.

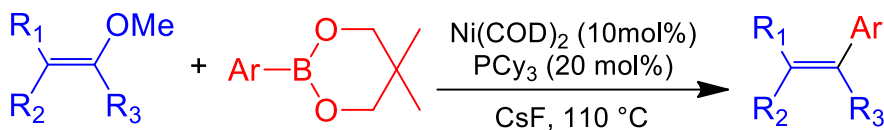
a) Dankwardt, 2004



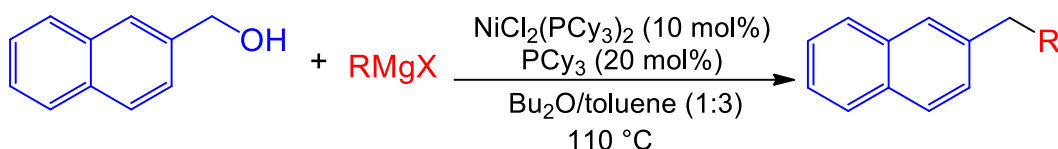
b) Chatani, 2008



c) Chatani, 2009



d) Shi, 2012



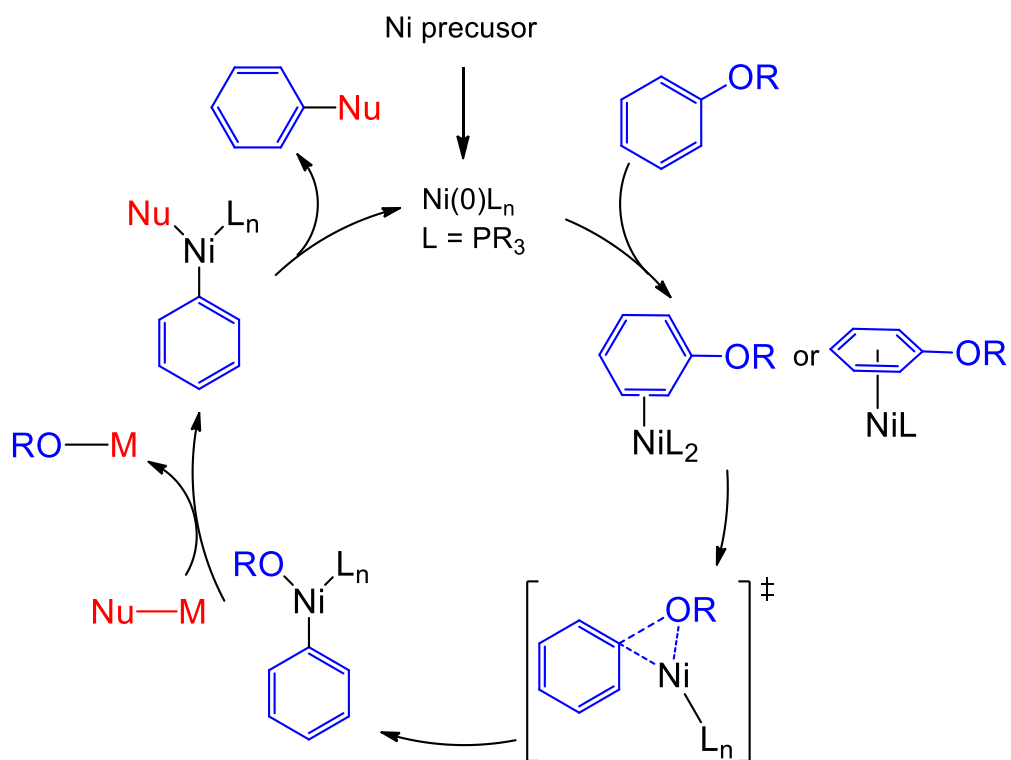
Scheme 1.4 Milestones in the area of nickel catalyzed C–O bond activation cross couplings.

a) Kumada-Corriue cross-coupling of aryl ether and Grignard reagent; b) Suzuki-Miyaura cross-coupling of aryl ether and boronic ester; c) Suzuki-Miyaura cross-coupling of aryl pivalates and boronic acid; d) Suzuki-Miyaura cross-coupling of alkenyl ether and boronic ester.

The aromatic C–O bond is particularly inert in traditional chemistry compared to other kinds of C–O bonds. It can tolerate a large variety of metal compounds. The Density Functional Theory (DFT) calculations of Houk⁵³ show that the bond dissociation enthalpy of C–O in anisole can be as high as 95.7 kcal/mol. It has been found that Ni complexes can efficiently selectively catalyze the activation of aromatic C–O with the assistance of a bulky, strong σ -donating ligand, such as PCy₃ (Cy =cyclohexyl) and IPr, where IPr is the carbene donor 1,3-bis-2,6-di(*isopropylphenyl*)imidazolium.⁵⁵⁻⁵⁸ The first example of Ni-catalyzed aromatic C–O bond activation was reported by Wenkert⁵⁹ as early as 1979. In that work (Ph₃P)₂NiCl₂ (Ph = phenyl) was used as a precatalyst in the cross-coupling

reaction of phenylmagnesium bromide and C(sp²)-O substrates, including aryl ether and enol ether. The conversions of these cross-coupling reactions were low, especially those of aryl ethers, and this methodology was not synthetic useful in chemical industry, which was maybe the reason why this paper did not get significant attention. It was not until 2004, when Dankwardt⁶⁰ reported a (Cy₃P)₂NiCl₂ catalyzed cross-coupling reaction of aryl ether and *p*-tolylmagnesium bromide (shown in **Scheme 1.4a**), that chemists started to turn their attention to catalyzed aromatic C-O bond activation. Dankwardt optimized the reaction conditions on the basis of Wenkert's study. He investigated the catalytic behaviour of phosphines with different cone angles and found that phosphines with cone angles around 160° (PCy₃, PhPCy₂ and P^{*i*}Pr₃) provided the highest conversion. Phosphines with smaller or larger cone angles performed poorly. This pioneering study aroused people's interest in the potential of Ni complexes for catalytic C-O bond activation and offered a starting point to the rapid development in this field for the following decades. As shown in **Scheme 1.4b**, in 2008, Chatani and his co-worker⁶¹ reported the first Suzuki-Miyaura-type nickel catalyzed C-O activation. Boronic ester serves as the nucleophile and CsF was used as the halide-trap base. Before Chatani, only organometallic nucleophiles were used in the catalysis. Although the substrates in this paper were restricted to naphthyl ether and its derivatives, the application of boronic nucleophiles, which are relatively more compatible with a wide range of functional groups, will help considerably extends the scope of the substrates. Another breakthrough was shown as **Scheme 1.4c**, which was made by Garg and his co-workers in 2008,⁶² who published the Suzuki-Miyaura-type cross-coupling of naphthyl pivalates and boronic acid for the first time. The catalytic system, showed highly selectivity to the C(aryl)-O bond instead of C(acyl)-O and offered good to excellent isolated yield. In 2009, Chatani and his co-workers for the first time published the Suzuki-Miyaura-type cross-coupling of alkenyl ether and boronic ester, adopting the same catalytic system as the aryl ether one (**Scheme 1.4d**).⁶³ It was shown that alkenyl ether group was exclusively converted prior to the activation of aryl ether moiety when a molecule had both functional groups in their catalytic system, offering a method for orthogonal functionalization of conjugated molecules.

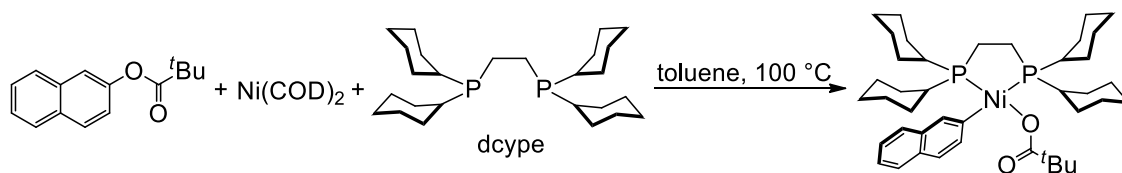
1.3.1.2 Mechanistic Studies in C–O activation by Nickel Complexes



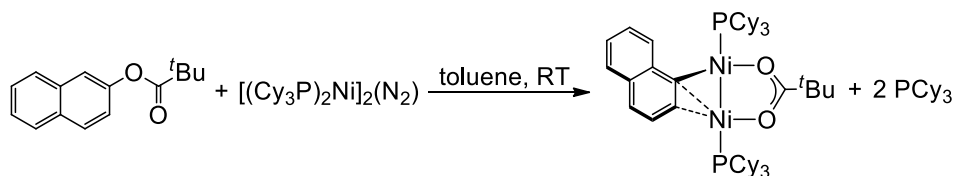
Scheme 1.5 Mechanism of cross-coupling reaction through Ni catalyzed C(sp²)-O activation.

Although a large body of work has emerged since the first example of nickel catalyzed aromatic C–O activation was reported, experimental evidence regarding the mechanism of the bond cleavage step is minimal. As shown in **Scheme 1.5**, it is believed that catalysis occurs via a conventional pathway: oxidative addition to a Ni(0) complex to give Ni(II), followed by transmetalation and reductive elimination to form a new C–C bond and reform the Ni(0) catalyst. It is assumed that the very first step of this cycle is the formation of a coordinatively unsaturated L_nNi(0) species,^{46, 53, 64-67} followed by the oxidative addition step.

a) Itami, 2013

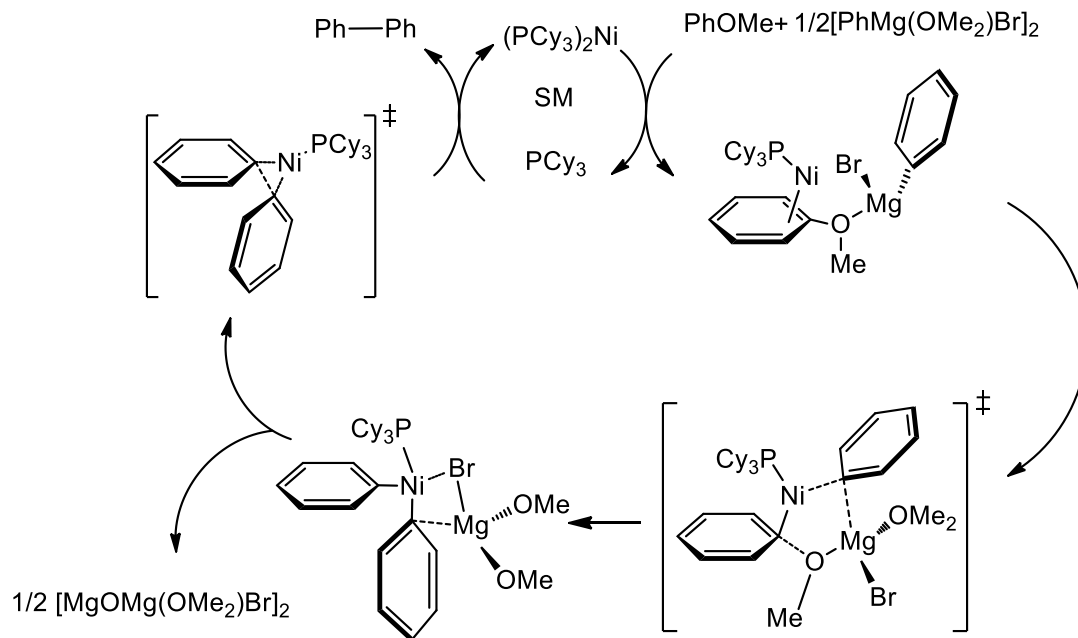


b) Martin, 2018



Scheme 1.6 a) Oxidative addition product of naphthyl pivalate to Ni(0) centre supported by a bidentate phosphine ligand; b) Oxidative addition product of naphthyl pivalate to Ni(0) centre supported by PCy₃.

Current mechanistic understanding regarding the C–O activation step has mostly been gleaned from theoretical studies using DFT calculations, but to date lack any experimental support. To the best of our knowledge, no oxidation complexes of aryl ether to Ni⁰ have ever been isolated *in situ* from a nickel catalyzed reaction involving C–O activation. Itami and co-workers⁶⁸ isolated and fully characterized the first *in situ* oxidation product of aryl ester to Ni catalyst (**Scheme 1.6a**). The supporting ligand they used was a bidentate phosphine. It is noteworthy because in these cross-coupling reactions monodentate phosphine are ubiquitous, whereas bidentate phosphines are not, perhaps rendering the mechanism of this C–O oxidative addition unrelated to those observed under catalytic conditions. More recently, as shown in **Scheme 1.6b**, Martin and co-workers⁶⁹ isolated the first oxidative addition complex of aryl ester to Ni centre supported by PCy₃. This complex is not a square planar Ni(II) complex as expected, but a dinuclear complex with one PCy₃ supporting each Ni centre.



Scheme 1.7 Ni(0)-ate pathway of cross coupling of aryl ether and Grignard reagent. Adapted from Ref 61.

Although the conventional mechanism can explain most of the experimental results observed in Ni catalyzed C(sp²)-O activation, there are still unsolved problems. For example, the substrate scope coupling with boronic nucleophiles is still restricted to naphthyl ether and aryl ester, while only more reactive Grignard reagent allow the functionalization of phenyl ethers. Some chemists have suggested that the Grignard reagent may also play an important role in the critical oxidation step. For example, Martin's proposed mechanism for a nickel catalyzed alkenyl C-O functionalization invoked an oxidative addition step that was assisted by the Grignard reagent behaving as a Lewis acid.⁷⁰ As shown in **Scheme 1.7**, Uchiyama and co-workers proposed a Ni(0)-ate complex, which is formed from the addition of Grignard reagent to Ni(0) complex, as a key intermediate on the catalytic pathway.⁶⁴ They found that the energy barrier would be much lower if the pathway did not include the conventional oxidative addition to Ni centre but the oxidative addition to Mg centre. However, effort to promote the coupling of phenyl ethers and boronic nucleophiles with added Lewis acids failed. Obviously, more in depth

mechanistic studies are necessary, and the details of the key bond activation step may be more complex than the traditional mechanism.

The number of phosphine ligands coordinated to Ni in each step of the catalytic C–O cross coupling pathway is also unclear. Both monophosphine and diphosphine pathways have been proposed as active species in the key C–O bond oxidative addition process in different DFT studies; that is, are complexes such as $(\text{Cy}_3\text{P})\text{Ni}$ or $(\text{Cy}_3\text{P})_2\text{Ni}$ the relevant species in these difficult bond activations? As mentioned above (see **Scheme 1.6a**), in Itami's work, the oxidative addition of naphthyl pivalate to $\text{Ni}(\text{COD})_2$ produces a Ni(II) complex supported by a bidentate phosphine ligand; while Martin's work shows that the oxidative addition of naphthyl pivalate to $[(\text{Cy}_3\text{P})_2\text{Ni}]_2(\mu\text{-N}_2)$ produces a dinuclear Ni complex, with each Ni centre associated to a PCy_3 ligand. These only two experimentally characterized oxidative addition step intermediates gave out two different results.

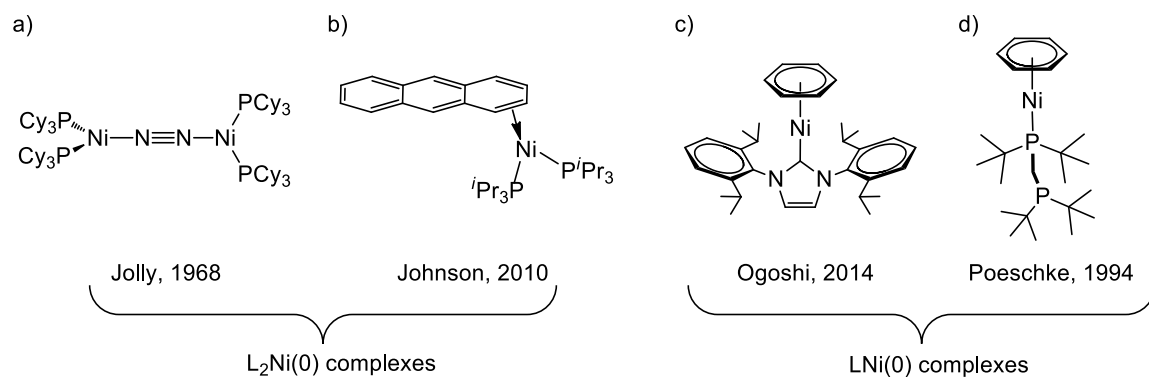


Figure 1.2 Selective fully characterized $\text{L}_2\text{Ni}(0)$ complexes and $\text{LNi}(0)$ complexes.

In order to further study the mechanism experimentally, Ni(0) monophosphine and diphosphine sources are needed. The dinuclear nickel phosphine complex, $[(\text{Cy}_3\text{P})_2\text{Ni}]_2(\mu\text{-N}_2)$ as shown in **Figure 1.2a** often serves as a source of the diphosphine moiety $(\text{Cy}_3\text{P})_2\text{Ni}$.⁷¹ In 2010, Johnson and co-workers synthesized and characterized a mononuclear complex, $(\eta^2\text{-naphthalene})\text{Ni}(\text{PCy}_3)_2$, which is also a versatile $(\text{Cy}_3\text{P})_2\text{Ni}(0)$ source, and easily prepared (**Figure 1.2b**).⁷² However, no Ni(0) complex that is a versatile source of $(\text{Cy}_3\text{P})\text{Ni}(0)$ is available. A related (NHC)Ni(0) source was isolated and

characterized by Ogoshi and co-workers in 2014 (**Figure 1.2c**).⁷³ As shown in **Figure 1.2d**, the only phosphine analogue was prepared by Poeschke in 1994,⁷⁴ but the phosphine was a bidentate phosphine and this complex decomposed in solution about $-30\text{ }^{\circ}\text{C}$, which is not synthetically useful. The goal of preparing a synthetically useful $(\text{Cy}_3\text{P})_2\text{Ni}(0)$ source will be discussed in detail in Chapter 2.

Apart from the conventional oxidative addition reaction pathway, Martin and co-workers offered a totally different mechanism of C–O activation.⁴⁶ In their mechanistic study of Ni catalyzed reductive cleavage of naphthyl ethers by hydrosilane, it is predicted that the formation of $(\text{R}_3\text{Si})\text{Ni}(\text{I})$ species was a key step of bond activation. This work suggests that the oxidative addition may not be the only pathway of C–O bond activation.

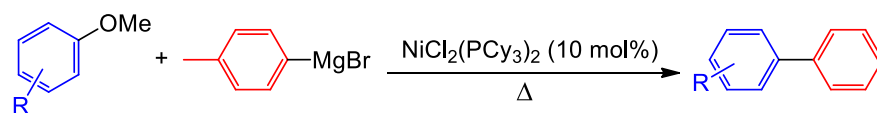
All of the problems and various mechanistic studies based almost exclusively on computational studies potentially hinders progress in Ni catalyzed $\text{C}(\text{sp}^2)\text{--O}$ activation, particularly if aspects of the mechanism are incorrect and fueling poor catalyst design principles. On the other hand, the diversity in mechanistic proposals, if correct, suggest the potential for more new reactions and catalytic systems based on these unexpected mechanisms.

1.3.1.3 The “Naphthalene Problem”

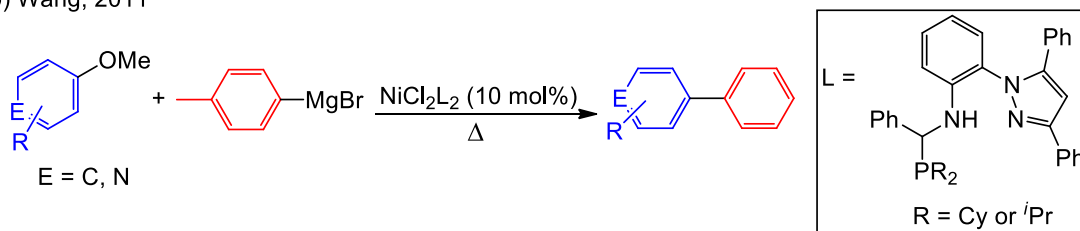
The famous “naphthalene problem”, is used to describe the much lower reactivity of phenyl ethers with nickel catalysts than π -extended substrate such as naphthalene and anthracene. It has been shown that the formation of a π -arene $\text{Ni}(0)$ complexes occurs prior to the intramolecular oxidative additions that activate $\text{C}(\text{sp}^2)\text{--O}$ bonds.⁷⁵⁻⁷⁸ The $\text{Ni}(0)$ centre accepts electrons from arene and back-donates electron to π anti-bonding orbitals of the arene.⁷⁹ It is easier for π -extended substrate to associate with nickel species⁵⁶, leading to their higher reactivity than phenyl ethers. This problematic limitation of substrate scope prevents the synthetic application of nickel catalyzed $\text{C}(\text{sp}^2)\text{--O}$ activation from being fully adopted.

To overcome this problem, efforts have been made to modify the catalytic systems by screening ancillary ligands. Dankwardt reported the first cross-coupling of phenyl ether and an aromatic Grignard reagent in 2004,⁶⁰ and Wang and co-workers extended the substrate scope to heterocycle derivatives such as 2-methoxypyridine.⁸⁰ The Chatani group developed the method to catalyze the cross-coupling with a series of aliphatic Grignard reagents⁸¹⁻⁸³ and organoboron reagents⁸⁴. These limited examples are shown in **Scheme 1.8**. However, electron-rich anisole derivatives are not reactive with their catalysts. To date there are also no examples of C(sp²)-O cross-coupling with organozinc, amine and hydrosilane moieties that provide useful yields. In conclusion, there is still a considerable room for the development of Ni catalysts for C-O coupling systems that could find wide application in industry.

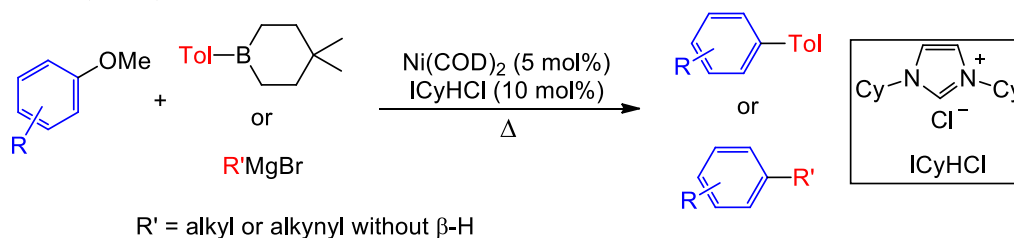
a) Dankwardt, 2004



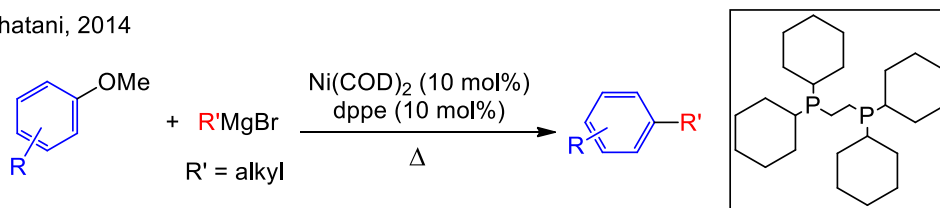
b) Wang, 2011



c) Chatani, 2015, 2016



d) Chatani, 2014

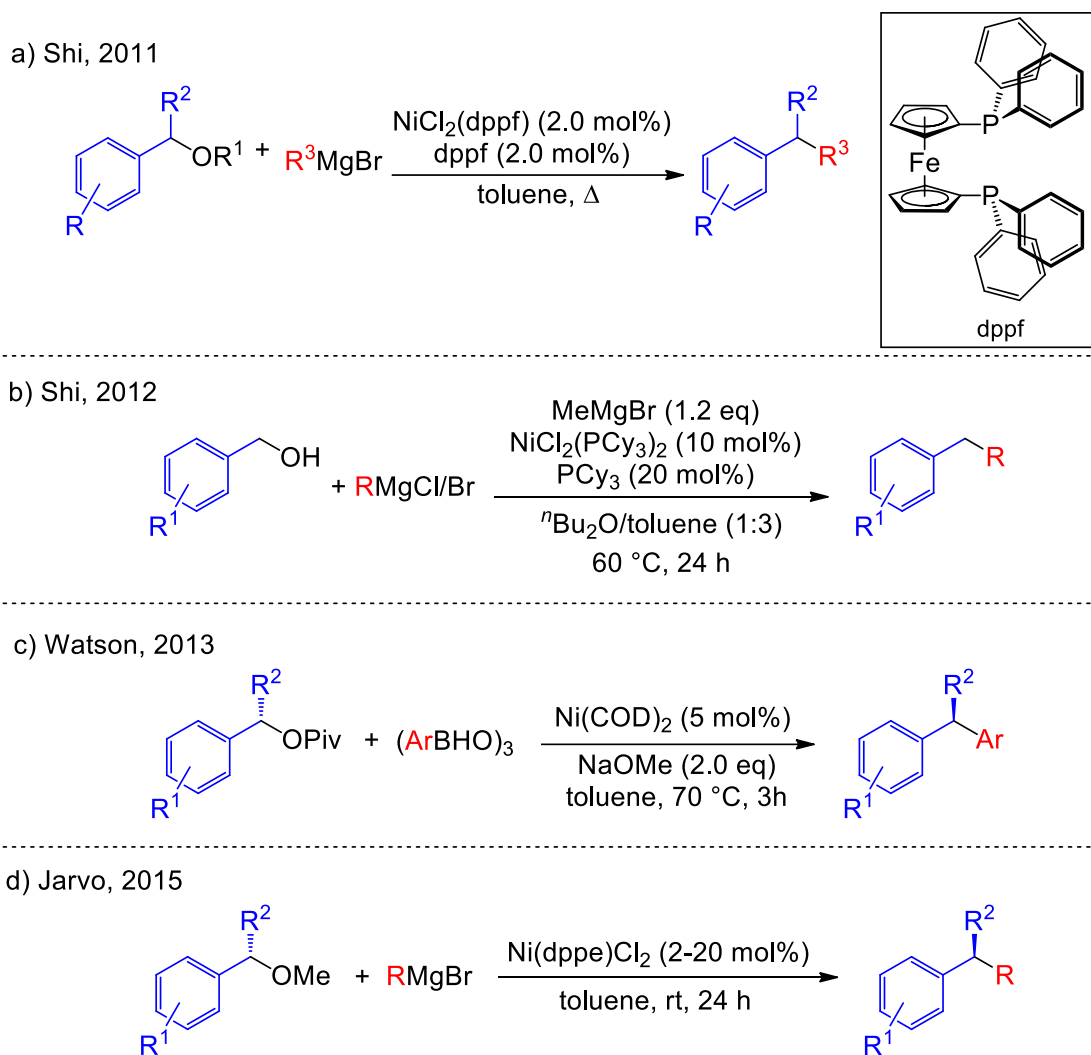


Scheme 1.8 Important breakthroughs in phenyl ether C(sp²)-O activation. a) NiCl₂(PCy₃)₂ can efficiently catalyze Kumada-Corriu-type cross-coupling of aryl ether and *p*-tolMgBr; b) The scope of substrate was extended to electron-rich anisole derivatives; c) Suzuki-Miyaura-type and Kumada-Corriu-type cross-coupling of phenyl ether catalyzed by Ni⁰/NHC ligand; d) Bidentate phosphine ligand can help catalyze Kumada-Corriu-type cross-coupling of phenyl ether and Grignard reagent containing β -H.

1.3.2 C(sp³)-O Activation

Aromatic halides are important building block in synthetic chemistry. They serve as the electrophiles in Suzuki-Miyaura- or Kumada-Corriu-type cross-coupling reactions that form C(sp²)-C bond. Aromatic ethers are ideal alternatives to aromatic halides and research on C(sp²)-O bond activation has seen significant progression. More recently, benzylic halides have also been used in cross-coupling reactions to form C(sp³)-C bonds.⁸⁵⁻⁹⁰ Enantioenriched benzylic compounds plays an important role in organic and pharmaceutical chemistry as the starting material to prepare chiral compounds. However, research concerning more general C(sp³)-O activation has developed slowly compared to C(sp²)-O bond activation. One reason that has hampered the development of C(sp³)-O activation is that the higher bond dissociation energy comparing to the related C-Cl and C-Br bonds.^{91, 92}

Selective examples of benzylic C(sp³)-O are shown in **Scheme 1.9**. In 2008, Shi and co-workers described the nickel catalyzed Kumada-Corriu-type cross-coupling of benzylic ether and its derivatives.⁹³ The introduction of dppf as the supporting ligand enabled the chemoselective C(sp³)-O bond activation. This method can be used to functionalize sp³ methoxy group in the presence of sp² methoxy group and allows orthogonal C-O activation of different type of group in one molecule. While using PCy₃ as the supporting ligand, both sp³ and sp² methoxy group are functionalized, which allows the one-pot cross-coupling of more than one methoxy group in one molecule. Shi's group also published the Ni catalyzed C(sp³)-O activation of α -pivaloxyl ketones⁹⁴ and benzylic alcohols⁹⁵. In 2013, Watson and co-workers described the stereospecific Suzuki-Miyaura-type reaction of chiral benzylic pivalates⁹⁶ and paved the way to apply enantioenriched benzylic ethers in synthetic and pharmaceutical industry. It is also noteworthy that Watson's method use only Ni(COD)₂ as the catalyst. This atom economical method may help functionalize other kinds of C-O activation in the future. In 2015, Jarvo and co-workers published the stereospecific Kumada-Corriu-type cross-coupling of benzylic ether, further extending the scope of substrate and nucleophile.⁹⁷



Scheme 1.9 Selective examples of benzylic $\text{C}(\text{sp}^3)\text{-O}$ activations. a) Kumada-Corriu-type cross-coupling of benzylic ethers. b) Kumada-Corriu-type cross-coupling of benzylic alcohols. c) Stereospecific Suzuki-Miyaura-type cross-coupling of benzyl pivalates, need no ancillary ligand. d) Stereospecific Kumada-Miyaura-type cross-coupling of benzylic ethers.

1.4 Transition Metal Clusters

1.4.1 General Introduction

Transition metal clusters is a term used for molecules containing more than two metal centers bound to each other. The first preparation of a transition metal clusters was reported about a century ago, although at the time the geometric and electronic properties were not understood.^{98,99} It was only after the application of single crystal X-ray diffraction in structure determination that breakthroughs in understanding the properties of such metal compounds were made. Although “naked” metal clusters are known, more often clusters are enveloped and stabilized by ligands. The ligands can be as simple as a hydrogen atom or common neutral molecules such as carbon monoxide and tertiary phosphines such as PPh₃. Transition metal clusters have often been studied in the hopes of discovering high reactivity due to cooperativity between metals in bond breaking and making processes. It has also been realized that clusters offer an opportunity to better understand reactivity at heterogeneous surface sites, bridging the gap between homogeneous and heterogeneous chemistry.

1.4.2 Geometry and Electron Counting of Transition Metal Clusters

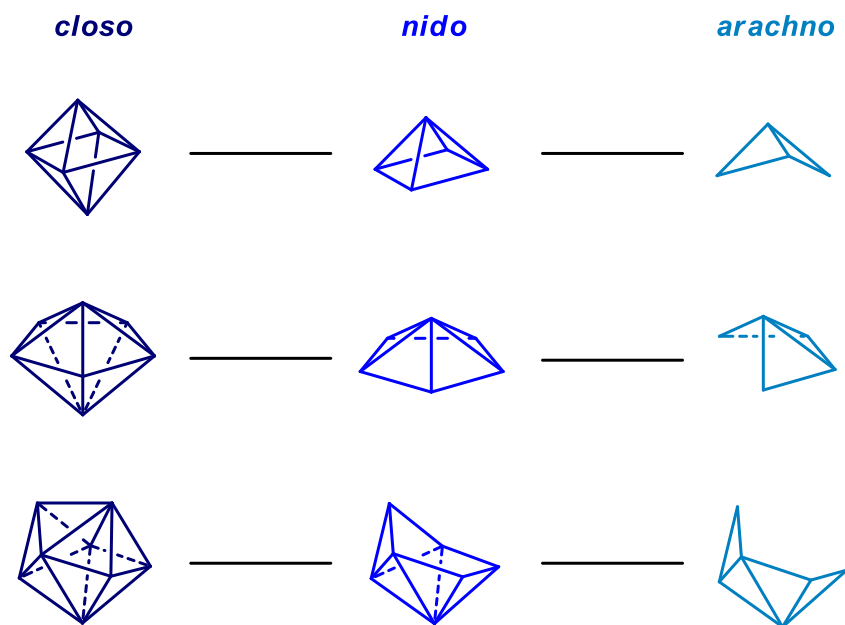


Figure 1.3 The structures of *closo* polyhedra with 6-8 vertices and their corresponding *nido* and *arachno* fragments.

In 1962, Lipscomb reported a LCAO-MO computational study on boron clusters.¹⁰⁰ The structure of boron clusters were rationalized by “localized bond” method in this paper. This principle also successfully predicted the structure and charge distribution of new boron clusters. However, electron-deficient boron clusters with higher symmetry such as octahedral ones do not follow this principle. In 1971, Wade published a landmark paper solving the problem by introducing a method of counting the number of skeletal electron pairs and bonding molecular orbitals.¹⁰¹ In this paper, clusters were sorted into three types, *closo*, *nido* and *arachno*, according to the number of vertex skeletal atoms. As shown in **Figure 1.3**, if a parent *closo* cluster has n vertices, then *nido* and *arachno* clusters are the $n-1$ and $n-2$ vertex fragments, and they all share the same number of skeletal bonding number, $n+1$. Wade also extended this straightforward principle to transition metal carbonyl clusters. Wade’s rule not only rationalized the structures of electron-deficient clusters, but also suggested that the skeletal electron count may influence the structure and

reactivity of a cluster more than its chemical nature. For example, both $\{\text{BH}\}_c$ and $\{\text{Ru}(\text{CO})_3\}$ offer 2 skeletal electrons. They have similar bond capability and lead to *closo* octahedral structure of $[\text{B}_6\text{H}_6]^{2-}$ and $[\text{Ru}_6(\text{CO})_{18}]^{2-}$.¹⁰²

Table 1.1 Bonding Capabilities of Clusters according to Lauher's Rule.

Geometry	Number of Skeletal Atoms	Number of CVMO	Number of Saturated CVE
dimer	2	17	34
trimer	3	24	48
tetrahedron	4	30	60
square plane	4	32	64
trigonal bipyramid	5	36	72
square pyramid	5	37	74
bicapped tetrahedron	6	42	84
octahedron	6	43	86
capped square pyramid	6	43	86
pentagonal pyramid	6	44	88
trigonal prism	6	45	90
capped octahedron	7	49	98
pentagonal bipyramid	7	49	98
capped trigonal prism	7	51	102
bicapped octahedron	8	55	110
triangular dodecahedron	8	56	112
square antiprism	8	57	114
cube	8	60	120

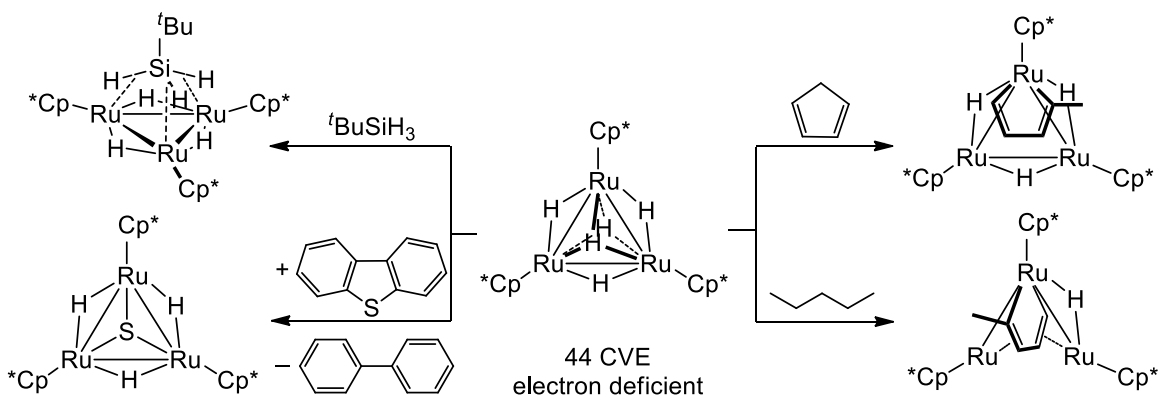
Based on semi-empirical works on main group clusters and bare metal clusters, Lauher introduced the concept of *cluster valence molecular orbital* (CVMO) to rationalize

the structure and ligand bonding capability of transition metal clusters.¹⁰³ Although typical transition metals have 9 frontier atomic orbitals from their valence s, p and d atomic orbitals, clusters with different symmetry have different number of CVMOs because of the various number of high lying anti-bonding orbitals (HLAO). Lauher rationalized the stable electron counts observed by noting that the energy of HLAOs is too high to be occupied by electrons. Each CVMO has a pair of electrons, thus the number of cluster valence electrons (CVE) can be calculated easily. The calculated CVMO and CVE counts of different geometries are shown in table above. Lauher believed that electron count of multinuclear transition metal clusters prefer to follow the CVMO rule, which resembles the 18 electron rule for mononuclear transition metal complexes. But he also mentioned that there are examples of stable mononuclear transition metal complex with less than 18 electrons. Similarly, a cluster with CVE count less than twice of CVMO count may be stable. He predicted that platinum and Group 1B metals may be stable even with unsaturated CVEs and those transition metal clusters with unsaturated CVE will show unusual reactivity because they can readily interact with ligands or other metal complexes. Lauher's theoretical approach has in general proven to be true, with exceptions being readily rationalized based on the energies on the relative energies of the clusters molecular orbitals; in general the most stable clusters has a large energy difference between the highest-occupied molecular orbitals (HOMOs) and lowest-unoccupied molecular orbitals (LUMOs). Unsaturated clusters where there is not a large HOMO-LUMO gap offer an interesting opportunity for future catalysis because of their unique potential for reactivity and similarity to the most reactive heterogeneous catalysts reactive sites.

1.4.3 Electron Deficient Transition Metal Clusters in Cooperative Catalysis

As noted previously, small molecule transformations catalyzed by metallo-enzyme systems are a perfect example of cooperative catalysis under mild conditions in Nature.¹⁰⁴ Metal and protein scaffold offer one active site to facilitate difficult chemical reactions with high efficiency. Transition metal clusters can mimic natural cooperative system through not only metal-ligand but also metal-metal cooperative effects. A number of

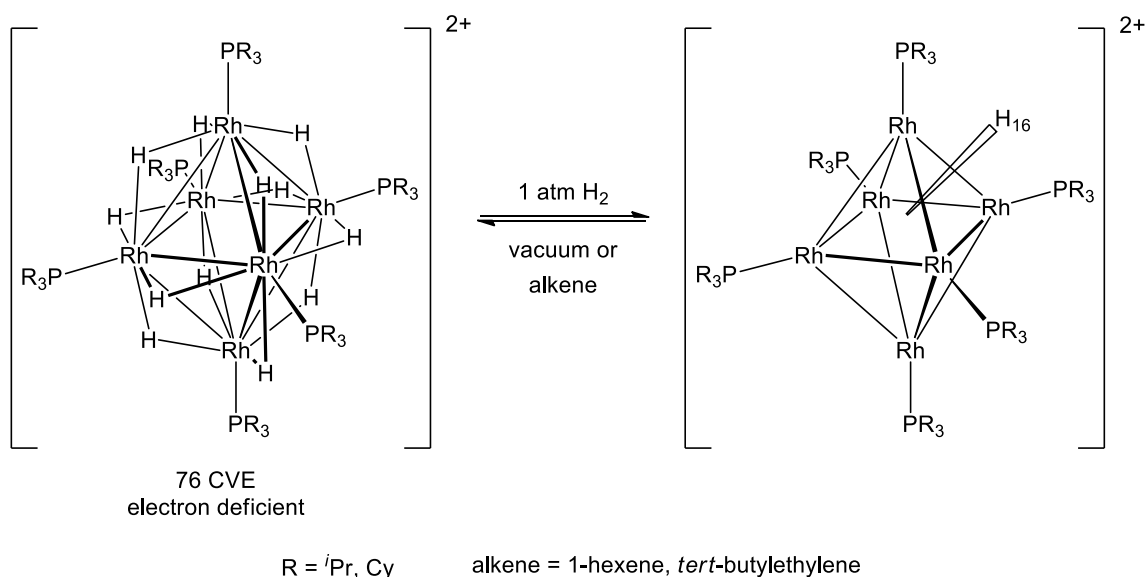
electron deficient transition metal clusters have been synthesized and their unique reactivities, distinct from monomeric catalysts and electron-saturated clusters, has been verified. The ubiquitous and classic transition metal carbonyl clusters usually follow Lauher's rules, while the more recently synthesized clusters supported by hydride, cyclopentadienyl or other main group ligands are often electron deficient. Their available CVMOs endows them abilities to undergo facile activation of exceptionally inert chemical bonds.



Scheme 1.10 Cooperative C–C, C–H, C–Si and C–S activation by a Ru₃ cluster.

An example of such a reactive transition metal cluster is a trinuclear Ru complex reported by Suzuki and co-workers, as shown in **Scheme 1.10**. Each Ru is bound to a cyclopentadienyl ligand, each skeletal edge of the cluster was bridged by a hydride ligand and the trigonal plane is capped by a hydride ligand on both sides. This cluster has 44 cluster valence electrons (CVE), which is 4 electrons less than predicted by traditional electron counting rules. The cluster undergoes selective C(sp²)–C(sp³) bond activation when reacted with cyclopentadiene.¹⁰⁵ This is the first example of inert C–C activation through cooperative action with 3 metal centres. Additionally, C–H bond activation in linear alkanes and alkenes proceed smoothly at room temperature through cooperative

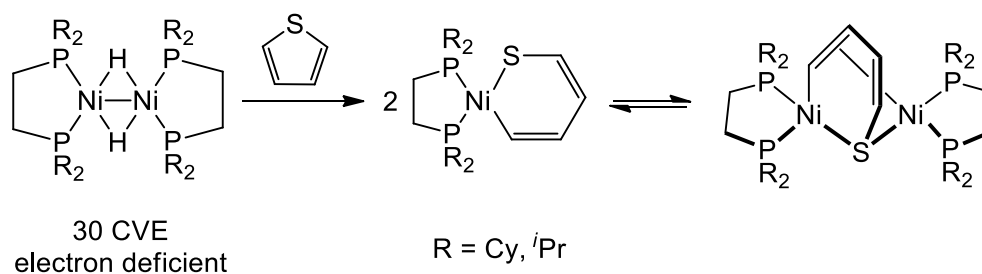
interactions with Ru centres and skeletal rearrangement afterwards.¹⁰⁶ The reaction with $t\text{BuSiH}_3$ produces a Ru_3 cluster with an unprecedented $\mu^3\text{-}\eta^2\text{:}\eta^2\text{:}\eta^2\text{-silane}$ structure, which demonstrating that all three Ru centres are involved in the reversible Si–H activation upon heating.¹⁰⁷ In addition, the Ru_3 cluster is also able to activate C–S¹⁰⁸, C–N¹⁰⁹, N–N¹¹⁰, etc. In depth mechanistic study demonstrated that the labile hydride ligands and multimetallic centres give it reactivity to a wide range of substrates. Reactivity studies concerning this cluster and its derivatives¹¹¹⁻¹¹⁴ have been ongoing since its preparation in 1994.



Scheme 1.11 Reversible H_2 gas absorption and release on the $[(\text{R}_3\text{P})\text{Rh}]_6\text{H}_{12}^{2+}$ cluster. Exact hydride locations in $[(\text{R}_3\text{P})\text{Rh}]_6\text{H}_{16}^{2+}$ are not known.

Apart from the organic molecule activation, transition metal clusters also show reactivity with small molecule gases such as H_2 , CO and CO_2 that are ideal feedstocks for large scale processes. A hexanuclear Rh cluster produced by Weller and co-workers¹¹⁵ provides an example of stoichiometric reactivity with hydrogen that shows the range of oxidation states available in the non-traditional clusters (**Scheme 1.11**). The octahedral cluster has 6 tertiary phosphine ligands and 12 hydride ligands. Each Rh is bound to a terminal phosphine and every 2 Rh are bridged by a hydride ligand. The CVE count is 76, which is very deficient compared to the 86 CVE predicted for typical octahedral clusters.

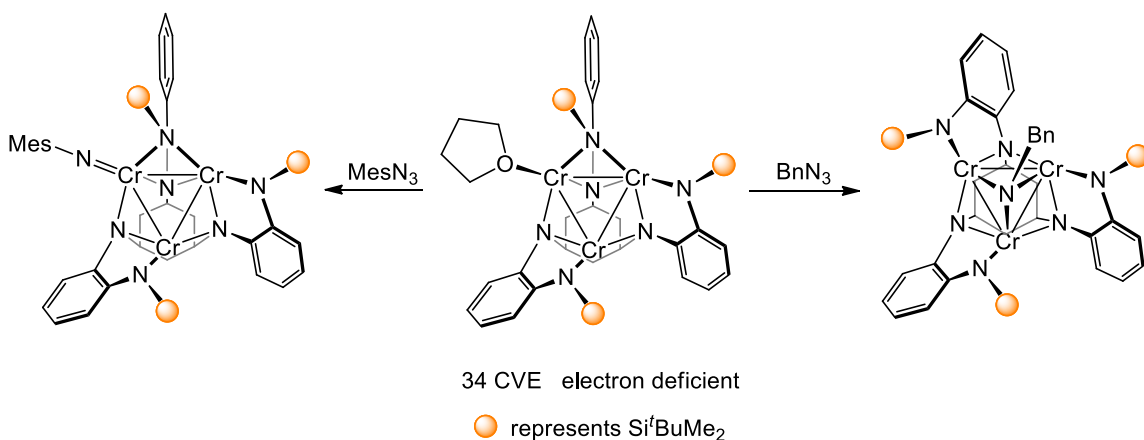
Despite the high hydride content, this cluster is stable under vacuum without losing hydride ligands. Instead, it gains 2 molecules of H₂ under 1 atm H₂ over 10 min in solution and adsorbs 2 H₂ under 4 h over 16 h in the solid state. The Ru₆H₁₆²⁺ cluster can be returned to Ru₆H₁₂²⁺ under vacuum or in the presence of H acceptors such as alkenes, producing corresponding alkanes. These are rare examples¹¹⁶⁻¹¹⁹ of reversible H₂ adsorption. This also shows the potential of this class of electron deficient cluster in difficult catalytic processes that require multi-electron transfer steps to substrates, rather than simply two available oxidation states separated by two electrons. Due to its reactivity in the solid state, the Rh₆ cluster gives a molecular model for H₂ gas storage as well as heterogeneous catalysis of alkene/arene hydrogenation. An NMR spectroscopy and isotope labeling study under D₂ atmosphere demonstrated exchange between hydride ligands and free H₂ gas. It is noteworthy that deuterium is also incorporated in the phosphine ligand, suggesting that phosphine or other ancillary ligands in cluster chemistry are not entirely innocent.



Scheme 1.12 Ni mediated C–S bond cleavage. Equilibrium between mononuclear nickel sulfide and dinuclear nickel sulfide proves the cooperative action of substrate on the both nickel centres.

Under the pressure of resource scarcity and environmental contamination as a result of the rapid development of modern industry, increasing attention is in polymetallic earth-abundant and less toxic first-row transition metals. Although not technically a cluster, in a paper by Jones and co-workers in 1999, it was shown that an electron deficient nickel dimer with 2 bridging hydride ligands reacts with sulphur containing aromatic compounds.¹²⁰ This Ni dimer can catalyse hydrodesulfurization (HDS, mainly catalyzed by Mo in

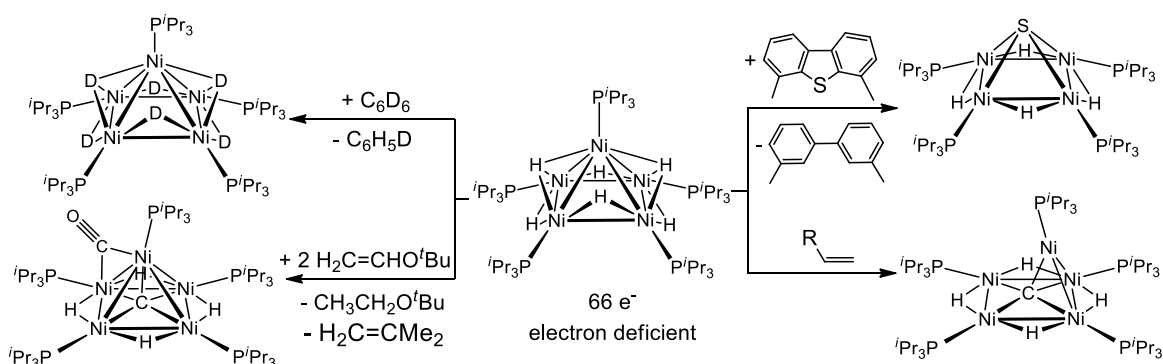
industry) of dibenzothiophene under 1 atm of H₂. Mechanistic studies shows that an equilibrium of nickel monomer and sulfide bridged Ni dimer appears when Ni dimer reacts with sulfur containing substrates, as shown in **Scheme 1.12**. The identification of intermediates demonstrates that the hydrodesulfurization is initialized by C–S bond cleavage with cooperative interactive with both nickel centres. This example shows that first-row transition metals are able to take place of second- and third-row metals to fulfil the urgent requirement of sustainability in the future.



Scheme 1.13 Ligand steric effects on single-site vs cooperative activation of azide by a Cr₃ cluster.

A modern example of an electron deficient 1st-row transition metal clusters is the trinuclear Cr complex supported by a hexadentate amine ligand shown in **Scheme 1.13**.¹²¹ This 34 e⁻ cluster is very electron deficient by the Lauher model that predicts 48 CVE. What interesting is, the cluster has a C₁ symmetry, although the free ligand has a symmetry of C₃. Single crystal X-ray diffraction shows that the three Cr centres have distinct metal coordination environments. One Cr binds to a THF molecule from solvent and three amides and interacts with an agostic C–H bond from the ^tBuMe₂Si group. Another metal coordinates to four amides, while the last one binds to three amides. The reaction with benzyl azide (BnN₃) in benzene or THF yields LCr₃ (μ³-NBn). However the reaction with bulkier mesityl azide (MesN₃) does not produce the μ³-NMes analogue. In benzene, the

NMes group replace the THF and binds to the Cr as an imido ligand; in THF, a C_3 LCr_3 (μ^3 -N) is generated. A mechanistic study suggests that the bulky t BuMe₂Si moiety hindered the pathway to the $[Cr_3]$ face, leading to the cooperative interaction with smaller BnN₃ and the single site interaction with MesN₃. Excess THF disfavours the species obtained dissociation of bound THF, and forces the MesN₃ access the $[Cr_3]$ face. This novel trimeric Cr cluster suggests that it is possible to switch between single-site and cooperative interactions on a cluster by tuning the properties of the ligands and/or solvents and thus synthesize different products through distinct mechanism.



Scheme 1.14 Cooperative C–C, C–O, C–S bond activation and H/D exchange on a Ni₅ cluster.

Our research group has previously explored 1st-row transition metal cluster chemistry, particularly with Ni. The synthesis of the pentanuclear nickel hydride cluster $[(iPr_3P)Ni]_5H_6$ was reported in 2012. This cluster has a rich chemistry of inert bond activation reactions, as summarized in **Scheme 1.14**.¹²² The cluster has a pseudosquare pyramidal *nido* geometry, with one phosphine ligand on each skeletal Ni and bridged by four μ^2 hydrides and two μ^3 hydrides. The electron count is 8 less than expected, making it another example of earth-abundant transition metal electron deficient cluster. It is able to facilitate the activation of unreactive $C(sp^2)$ – $C(sp^2)$ bonds. A carbon atom from alkene

substrate is extracted by the Ni₅ cluster and generates a new Ni₅ complex with a carbide ligand bridging the four basal Ni centre.¹²³ In the case of *tert*-butylvinyl ether, apart from the C=C bond cleavage, C(sp³)-O bond cleavage happened simultaneously, producing a Ni₅ cluster with a bridging carbide ligand and a bridging carbonyl ligand.¹²⁴ The Ni₅ cluster can also provoke the difficult “ultra-deep” hydrodesulfurization in 4,6-dimethyldibenzothiophene (4,6-Me₂DBT), which has long been a challenge in oil industry.¹²⁵ Furthermore, the cluster can catalyze H/D exchange on aromatic compounds facilely.^{122, 126} All of these reactivity studies demonstrate the versatile reactivities of this Ni₅ cluster to diverse substrates under mild condition. All these reactions suggest the possibility of late metal clusters capable of ground-breaking catalytic transformation of involving the rearrangement of typically unreactive skeletal bonds via cooperativity.

1.5 Dissertation Scope

Previous computational mechanistic studies in nickel catalyzed C(sp²)-O activation have conflicting conclusions regarding the number of ligand involved in the key difficult bond activation step of the catalytic cycle. The lack of easily accessible mono-ligand nickel complex is one of the obstacles to experimentally testing the proposed mechanisms. In Chapter 2, the preparation and fully characterization of the first Ni monophosphine complex and a series of derivatives will be shown. In Chapter 3, Ni mediated C(sp²)-O activation of alkenyl ethers will be discussed. Both LNi(0) and L₂Ni(0) were used in the mechanistic study. In Chapter 4, as a follow up on our previous work on C-O activation by a Ni₅ cluster, we tried new synthetic routes to polynuclear nickel complexes, including the Ni monophosphine complex introduced in Chapter 2. The role of the phosphine ligands in the formation and reactivity of these clusters is also investigated. In Chapter 5, we undertook a preliminary study of the reactions of LNi(0) and L₂Ni(0) with naphthyl substrates containing C-O bonds. Future work about C-O bond activation is listed.

1.6 References

1. M. D. Fryzuk, *Science*, 2013, **340**, 1530-1531.
2. J. D. Gilbertson, N. K. Szymczak and D. R. Tyler, *J. Am. Chem. Soc.*, 2005, **127**, 10184-10185.
3. B. M. Lindley, R. S. van Alten, M. Finger, F. Schendzielorz, C. Wurtele, A. J. M. Miller, I. Siewert and S. Schneider, *J. Am. Chem. Soc.*, 2018, **140**, 7922-7935.
4. M. E. Moret and J. C. Peters, *J. Am. Chem. Soc.*, 2011, **133**, 18118-18121.
5. M. Mori, *J. Organomet. Chem.*, 2004, **689**, 4210-4227.
6. F. Bellina and R. Rossi, *Chem. Rev.*, 2010, **110**, 1082-1146.
7. S. H. Cho, J. Y. Kim, J. Kwak and S. Chang, *Chem. Soc. Rev.*, 2011, **40**, 5068-5083.
8. R. Giri, B. F. Shi, K. M. Engle, N. Maugel and J. Q. Yu, *Chem. Soc. Rev.*, 2009, **38**, 3242-3272.
9. C. G. Jia, T. Kitamura and Y. Fujiwara, *Acc. Chem. Res.*, 2001, **34**, 633-639.
10. J. A. Labinger and J. E. Bercaw, *Nature*, 2002, **417**, 507-514.
11. H. Amii and K. Uneyama, *Chem. Rev.*, 2009, **109**, 2119-2183.
12. O. Blum, F. Frolow and D. Milstein, *J. Chem. Soc. Chem. Comm.*, 1991, 258-259.
13. T. Braun and F. Wehmeier, *Eur. J. Inorg. Chem.*, 2011, 613-625.
14. T. Ichitsuka, T. Fujita, T. Arita and J. Ichikawa, *Angew. Chem. Int. Ed.*, 2014, **53**, 7564-7568.
15. Q. Shen, Y. G. Huang, C. Liu, J. C. Xiao, Q. Y. Chen and Y. Guo, *J. Fluorine Chem.*, 2015, **179**, 14-22.
16. R. J. Young and V. V. Grushin, *Organometallics*, 1999, **18**, 294-296.
17. L. J. Goossen, K. Goossen and C. Stanciu, *Angew. Chem. Int. Ed.*, 2009, **48**, 3569-3571.
18. L. Guo and M. Rueping, *Acc. Chem. Res.*, 2018, **51**, 1185-1195.

19. B. Su, Z. C. Cao and Z. J. Shi, *Acc. Chem. Res.*, 2015, **48**, 886-896.
20. M. Tobisu and N. Chatani, *Acc. Chem. Res.*, 2015, **48**, 1717-1726.
21. M. Tobisu and N. Chatani, *Topics Curr. Chem.*, 2016, **374**.
22. X. Zhang, F. Jordan and M. Szostak, *Org. Chem. Front.*, 2018, **5**, 2515-2521.
23. K. J. Laidler, *Pure Appl. Chem.*, 1996, **68**, 149-192.
24. N. R. Council, *Catalysis Looks to the Future*, The National Academies Press, Washington, DC, 1992.
25. B. Rieger, L. S. Baugh, S. Kacker and S. Striegler, *Late Transition Metal Polymerization Catalysis*, WILEY-VCH, 2006.
26. L. B. Huang, M. Arndt, K. Goossen, H. Heydt and L. J. Goossen, *Chem. Rev.*, 2015, **115**, 2596-2697.
27. M. B. C. Bolm, *Transition Metals for Organic Synthesis*, WILEY-VCH, 2004.
28. C. H. Jun, C. W. Moon and D. Y. Lee, *Chemistry*, 2002, **8**, 2422-2428.
29. Y. J. Park, J. W. Park and C. H. Jun, *Acc. Chem. Res.*, 2008, **41**, 222-234.
30. C. H. Jun, *Chem. Soc. Rev.*, 2004, **33**, 610-618.
31. B. Rybtchinski and D. Milstein, *Angew. Chem. Int. Ed.*, 1999, **38**, 870-883.
32. K. Kruger, A. Tillack and M. Beller, *Chemsuschem*, 2009, **2**, 715-717.
33. M. Albrecht and M. M. Lindner, *Dalton Trans.*, 2011, **40**, 8733-8744.
34. Z. K. Yu, W. W. Jin and Q. B. Jiang, *Angew. Chem. Int. Ed.*, 2012, **51**, 6060-6072.
35. A. Nova, R. Mas-Balleste and A. Lledos, *Organometallics*, 2012, **31**, 1245-1256.
36. D. L. Anderson, *J. Geophys. Res.*, 1983, **88**, B41-B52.
37. D. C. Rees and J. B. Howard, *Curr. Opin. Chem. Biol.*, 2000, **4**, 559-566.
38. J. Kim and D. C. Rees, *Biochemistry-U.S.*, 1994, **33**, 389-397.
39. J. I. van der Vlugt, *Eur. J. Inorg. Chem.*, 2012, 363-375.

40. M. H. Perez-Temprano, J. A. Casares and P. Espinet, *Chem. Eur. J.*, 2012, **18**, 1864-1884.
41. S. F. McWilliams and P. L. Holland, *Acc. Chem. Res.*, 2015, **48**, 2059-2065.
42. B. H. S. Thimmappa, *Coordin. Chem. Rev.*, 1995, **143**, 1-34.
43. A. V. Petukhov, *Chem. Phys. Lett.*, 1997, **277**, 539-544.
44. G. Rothenberg, *Catalysis: Concepts and Green Applications*, Wiley-VCH, 2008.
45. S. Z. Tasker, E. A. Standley and T. F. Jamison, *Nature*, 2014, **509**, 299-309.
46. J. Cornella, E. Gomez-Bengoia and R. Martin, *J. Am. Chem. Soc.*, 2013, **135**, 1997-2009.
47. H. W. C. Rettenmeier, L. H. Gade, *Chemistry A European Journal*, 2014, **20**, 9657-9665.
48. J. C. T. O. Gutierrez, D. N. Primer, M. C. Kozlowski, *J. Am. Chem. Soc.*, 2015, **137**, 4896-4899.
49. J. R. J. Breitenfeld, M. D. Wodrich, X. Hu, *J. Am. Chem. Soc.*, 2013, **135**, 12004-12012.
50. C. A. R. J. Wenz, H. Wadepohl, L. H. Gade, *Chem. Commun.*, 2016, **52**, 202-205.
51. G. C. F. N. D. Schley, *J. Am. Chem. Soc.*, 2014, **136**, 16588-16593.
52. J. Cornella, C. Zarate and R. Martin, *Chem. Soc. Rev.*, 2014, **43**, 8081-8097.
53. X. Hong, Y. Liang and K. N. Houk, *J. Am. Chem. Soc.*, 2014, **136**, 2017-2025.
54. W.-N. Li and Z.-L. Wang, *RSC Adv.*, 2013, **3**, 25565.
55. G. A. Edouard, P. Kelley, D. E. Herbert and T. Agapie, *Organometallics*, 2015, **34**, 5254-5277.
56. M. Tobisu and N. Chatani, *Acc. Chem. Res.*, 2015, **48**, 1717-1726.
57. C. Wang, T. Ozaki, R. Takita and M. Uchiyama, *Chemistry*, 2012, **18**, 3482-3485.
58. L. Guo, C.-C. Hsiao, H. Yue, X. Liu and M. Rueping, *ACS Catal.*, 2016, **6**, 4438-4442.

59. E. Wenkert, E. L. Michelotti and C. S. Swindell, *J. Am. Chem. Soc.*, 1979, **101**.
60. J. W. Dankwardt, *Angew. Chem. Int. Ed.*, 2004, **43**, 2428-2432.
61. M. Tobisu, T. Shimasaki and N. Chatani, *Angew. Chem. Int. Ed.*, 2008, **47**, 4866-4869.
62. K. W. Quasdorf, X. Tian and N. K. Garg, *J. Am. Chem. Soc.*, 2008, **130**, 14422-14423.
63. T. Shimasaki, Y. Konno, M. Tobisu and N. Chatani, *Org. Lett.*, 2009, **11**, 4890-4892.
64. H. Ogawa, H. Minami, T. Ozaki, S. Komagawa, C. Wang and M. Uchiyama, *Chemistry*, 2015, **21**, 13904-13908.
65. T. Wititsuwannakul, Y. Tantirungrotechai and P. Surawatanawong, *ACS Catal.*, 2016, **6**, 1477-1486.
66. L. Xu, L. W. Chung and Y.-D. Wu, *ACS Catal.*, 2016, **6**, 483-493.
67. Zhe Li, Song-Lin Zhang, Yao Fu, Qing-Xiang Guo and L. Liu, *J. Am. Chem. Soc.*, 2009, **131**, 8815-8823.
68. K. Muto, J. Yamaguchi, A. Lei and K. Itami, *J. Am. Chem. Soc.*, 2013, **135**, 16384-16387.
69. R. J. Somerville, L. V. A. Hale, E. Gomez-Bengoa, J. Bures and R. Martin, *J. Am. Chem. Soc.*, 2018, **140**, 8771-8780.
70. J. Cornella and R. Martin, *Org. Lett.*, 2013, **15**, 6298-6301.
71. P. W. Jolly and K. Jonas, *Angew. Chem. Int. Ed.*, 1968, **7**, 731-&.
72. J. A. Hatnean, R. Beck, J. D. Borrelli and S. A. Johnson, *Organometallics*, 2010, **29**, 6077-6091.
73. Y. Hoshimoto, Y. Hayashi, H. Suzuki, M. Ohashi and S. Ogoshi, *Organometallics*, 2014, **33**, 1276-1282.
74. R. G. T. Nickel, C. Krueger, K. R. Poeschke, *Angew. Chem.*, 1994, **106**, 908-910.
75. N. Yoshikai, H. Matsuda and E. Nakamura, *J. Am. Chem. Soc.*, 2008, **130**, 15258-15259.
76. Z. J. Bryan and A. J. McNeil, *Chem. Sci.*, 2013, **4**, 1620-1624.

77. S. K. Sontag, J. A. Bilbrey, N. E. Huddleston, G. R. Sheppard, W. D. Allen and J. Locklin, *J. Org. Chem.*, 2014, **79**, 1836-1841.
78. S. Zhu, M. M. Shoshani and S. A. Johnson, *Chem. Commun.*, 2017, **53**, 13176-13179.
79. C. Massera and G. Frenking, *Organometallics*, 2003, **22**, 2758-2765.
80. L. G. Xie and Z. X. Wang, *Chemistry*, 2011, **17**, 4972-4975.
81. M. Tobisu, T. Takahira, T. Morioka and N. Chatani, *J. Am. Chem. Soc.*, 2016, **138**, 6711-6714.
82. M. Tobisu, T. Takahira and N. Chatani, *Org. Lett.*, 2015, **17**, 4352-4355.
83. M. Tobisu, T. Takahira, A. Ohtsuki and N. Chatani, *Org. Lett.*, 2015, **17**, 680-683.
84. M. Tobisu, A. Yasutome, H. Kinuta, K. Nakamura and N. Chatani, *Org. Lett.*, 2014, **16**, 5572-5575.
85. Q. C. Zhang, X. Wang, Q. Qian and H. G. Gong, *Synthesis-Stuttgart*, 2016, **48**, 2829-2836.
86. Z. He, F. Song, H. Sun and Y. Huang, *J. Am. Chem. Soc.*, 2018, **140**, 2693-2699.
87. R. B. Bedford, N. J. Gower, M. F. Haddow, J. N. Harvey, J. Nunn, R. A. Okopie and R. F. Sankey, *Angew. Chem. Int. Ed.*, 2012, **51**, 5435-5438.
88. T. Leon, A. Correa and R. Martin, *J. Am. Chem. Soc.*, 2013, **135**, 1221-1224.
89. M. Padmanaban, A. T. Biju and F. Glorius, *Org. Lett.*, 2011, **13**, 98-101.
90. F. O. Arp and G. C. Fu, *J. Am. Chem. Soc.*, 2005, **127**, 10482-10483.
91. W. A. Warr, *Chemical Structures 2: The International Language of Chemistry*, Springer Berlin Heidelberg, 1993.
92. D. A. Pratt, J. S. Wright and K. U. Ingold, *J. Am. Chem. Soc.*, 1999, **121**, 4877-4882.
93. B. T. Guan, S. K. Xiang, B. Q. Wang, Z. P. Sun, Y. Wang, K. Q. Zhao and Z. J. Shi, *J. Am. Chem. Soc.*, 2008, **130**, 3268-3269.
94. K. Huang, G. Li, W. P. Huang, D. G. Yu and Z. J. Shi, *Chem. Commun.*, 2011, **47**, 7224-7226.

95. D. G. Yu, X. Wang, R. Y. Zhu, S. Luo, X. B. Zhang, B. Q. Wang, L. Wang and Z. J. Shi, *J. Am. Chem. Soc.*, 2012, **134**, 14638-14641.
96. Q. Zhou, H. D. Srinivas, S. Dasgupta and M. P. Watson, *J. Am. Chem. Soc.*, 2013, **135**, 3307-3310.
97. E. J. Tollefson, L. E. Hanna and E. R. Jarvo, *Acc. Chem. Res.*, 2015, **48**, 2344-2353.
98. M. C. Chabrie, *Compt. Rend.*, 1907, **144**.
99. E. L. Muetterties, *J. Organomet. Chem.*, 1980, **200**, 177-190.
100. W. N. L. R. Hoffmann, *J. Chem. Phys.*, 1962, **37**.
101. K. Wade, *Chem. Commun.*, 1971, 792-793.
102. A. J. Welch, *Chem. Commun.*, 2013, **49**, 3615-3616.
103. J. W. Lauher, *J. Am. Chem. Soc.*, 1978, **100**, 5305-5315.
104. R. Peters, *Cooperative Catalysis: Designing Efficient Catalysts for Synthesis*, Wiley-VCH, 2015.
105. H. Suzuki, Y. Takaya, T. Takemori and M. Tanaka, *J. Am. Chem. Soc.*, 1994, **116**, 10779-10780.
106. T. Takao and H. Suzuki, *B. Chem. Soc. Jpn.*, 2014, **87**, 443-458.
107. M. Nagaoka, H. Tsuruda, M. Amako, H. Suzuki and T. Takao, *Angew. Chem. Int. Ed.*, 2015, **54**, 14871-14874.
108. K. Matsubara, R. Okamura, M. Tanaka and H. Suzuki, *J. Am. Chem. Soc.*, 1998, **120**, 1108-1109.
109. T. Takao, S. Horikoshi, T. Kawashima, S. Asano, Y. Takahashi, A. Sawano and H. Suzuki, *Organometallics*, 2018, **37**, 1598-1614.
110. Y. Nakajima and H. Suzuki, *Organometallics*, 2003, **22**, 959-969.
111. T. Takao, H. Suwa, R. Okamura and H. Suzuki, *Organometallics*, 2012, **31**, 1825-1831.
112. T. Takao, T. Kawashima, H. Kanda, R. Okamura and H. Suzuki, *Organometallics*, 2012, **31**, 4817-4831.
113. T. Kaneko, H. Suwa, T. Takao and H. Suzuki, *Organometallics*, 2013, **32**, 737-740.

114. T. Kuzutani, Y. Torihata, H. Suzuki and T. Takao, *Organometallics*, 2016, **35**, 2543-2556.
115. S. K. Brayshaw, M. J. Ingleson, J. C. Green, J. S. McIndoe, P. R. Raithby, G. Kociok-Kohn and A. S. Weller, *J. Am. Chem. Soc.*, 2006, **128**, 6247-6263.
116. L. J. Farrugia, M. Green, D. R. Hankey, A. G. Orpen and F. G. A. Stone, *Chem. Commun.*, 1983, 310-312.
117. R. D. Adams, B. Captain and M. D. Smith, *Angew. Chem. Int. Ed.*, 2006, **45**, 1109-1112.
118. A. M. Arif, T. A. Bright, R. A. Jones and C. M. Nunn, *J. Am. Chem. Soc.*, 1988, **110**, 6894-6895.
119. W. Paw, D. K. Bower, D. J. Bierdeman, J. B. Keister and E. M. Schulman, *J. Coord. Chem.*, 1996, **39**, 199-210.
120. D. A. Vicic and W. D. Jones, *J. Am. Chem. Soc.*, 1999, **121**, 7606-7617.
121. A. K. Bartholomew, C. E. Juda, J. N. Nessralla, B. Lin, S. G. Wang, Y. S. Chen and T. A. Betley, *Angew. Chem. Int. Ed.*, 2019, **58**, 5687-5691.
122. R. Beck, M. Shoshani and S. A. Johnson, *Angew. Chem. Int. Ed.*, 2012, **51**, 11753-11756.
123. M. M. Shoshani and S. A. Johnson, *Nat. Chem.*, 2017, **9**, 1282-1285.
124. M. M. Shoshani, V. Semeniuchenko and S. A. Johnson, *Chem. Eur. J.*, 2018, **24**, 14282-14289.
125. M. M. Shoshani and S. A. Johnson, *Inorg. Chem.*, 2015, **54**, 11977-11985.
126. M. M. Shoshani, J. Y. Liu and S. A. Johnson, *Organometallics*, 2018, **37**, 116-126.

Chapter 2 Versatile (Cy₃P)Ni(η^6 -arene) Nickel

Monophosphine Precursor

Chapter 2 reproduced by permission of The Royal Society of Chemistry from the published work: DOI: 10.1039/C7CC08416A

2.1 Introduction

Interest in Ni complexes has intensified over the last decade, not only for their potential application as economical replacement of their heavier Pd congeners in catalysis,¹ but also due to their unique reactivities.² Nickel monophosphine arene adducts have been proposed as highly reactive intermediates capable of difficult C–O bond activation steps in Ni catalyzed cross-coupling reactions. Phosphine supported complexes of the type Ni(PR₃)_n (where n = 2, 3, 4) are ubiquitous Ni(0) precursors for both stoichiometric and catalytic transformations.^{3–8} Recently, PCy₃ supported Ni complexes have been used extensively in catalytic cross-coupling reactions featuring C–O bond functionalization.^{9–16} A number of computational studies have examined the role of Ni(PCy₃)_n species in these reactions, and both the monophosphine Ni(PCy₃)^{17–22} and diphosphine Ni(PCy₃)₂²³ moieties have been hypothesized to mediate the difficult C–O bond activation steps. Reactive sources of Ni(0) bearing a single N-heterocyclic carbene ligand, such as (η^6 -arene)Ni(NHC), are easily prepared (**Figure 2.1a**).²⁴ In contrast, only a single related phosphine complex, (η^6 -arene)Ni(^tBu₂PCH₂P^tBu₂), has been structurally characterized

(**Figure 2.1b**); due to the presence of a diphosphine supporting ligand and its decomposition in solution above $-30\text{ }^{\circ}\text{C}$, this species is not a synthetically useful $(\text{R}_3\text{P})\text{Ni}$ precursor.²⁵

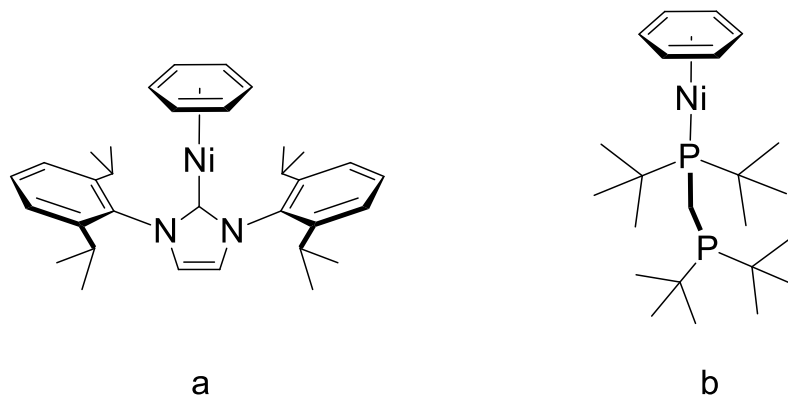
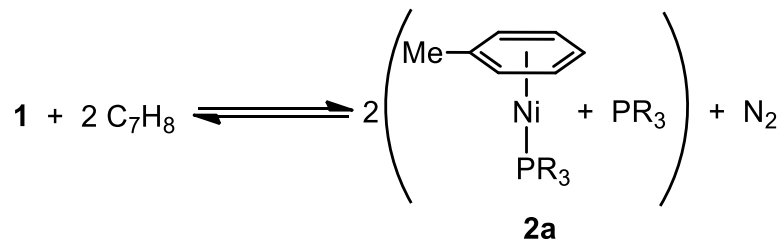


Figure 2.1 An example of $(\text{NHC})\text{Ni}(\eta^6\text{-arene})$, where arene is C_6H_6 , NHC is IPr (1,3-bis(2,6-diisopropylphenyl)imidazol-2-ylidene); b) The structure of $(t\text{Bu}_2\text{PCH}_2\text{P}^t\text{Bu}_2)\text{Ni}(\eta^6\text{-C}_6\text{H}_6)$.

The *triisopropylphosphine* supported dinitrogen complex $[(t\text{Pr}_3\text{P})_2\text{Ni}]_2(\mu\text{-N}_2)$ was proposed to react in aromatic solvents such as benzene, toluene or mesitylene to give equilibrium amounts of $(t\text{Pr}_3\text{P})\text{Ni}(\eta^6\text{-arene})$ in solution (**Scheme 2.1**);²⁶ however, attempts to isolate and verify the structure of these species by single crystal X-ray diffraction failed both due to the difficulty in removing the high boiling point P^tPr_3 produced and the oily nature of the product. A synthetically versatile precursor for monophosphine species, such as $(\text{PCy}_3)\text{Ni}$, are entirely lacking; such a species would enable much-needed experimental validation of the different computationally supported mechanistic hypotheses for C–O bond functionalization.



Scheme 2.1 Equilibrium reaction of complex **1** with toluene.

The similar Tolman cone angles^{27, 28}, percent buried volume²⁹ and electronic parameters for ⁱPr₃P and Cy₃P suggested that the reactions of [(Cy₃P)₂Ni]₂(μ-N₂) (**1**) with arenes might be expected to provide (Cy₃P)Ni(η⁶-arene) complexes; however, despite the use of complex **1** for almost 50 years,^{17, 30-40} only the species [(Cy₃P)₂Ni]N₂, (Cy₃P)₂Ni and (Cy₃P)₃Ni have been reported in benzene solutions of **1**.⁴¹ Herein, we reinvestigate this chemistry, and provide a practical synthetic route to complexes of the type (Cy₃P)Ni(η⁶-arene).

2.2 Results and Discussion

Solutions of [(Cy₃P)₂Ni]₂(μ-N₂) (**1**) in pentane at room temperature gave ³¹P{¹H} NMR spectra with a single peak at δ 31.1. A similar spectrum is observed in THF. However, when **1** was dissolved in toluene, the sharp resonance associated with **1** broadened and diminished and two new resonances, with an integral ratio of 1:1, were observed at δ 46.5 and δ 10.3. The former is assigned as (Cy₃P)Ni(η⁶-PhMe) (**2a**) and the latter is from unbound Cy₃P (**Figure 2.2**).

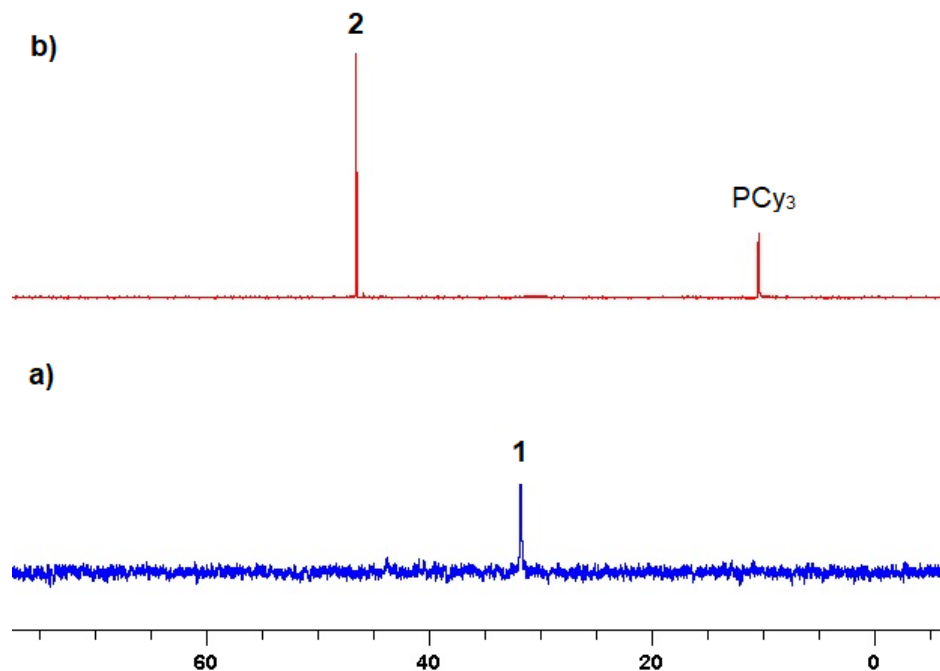


Figure 2.2 $^{31}\text{P}\{^1\text{H}\}$ NMR of a) Complex **1** in pentane and b) Complex **1** in toluene.

The variable-temperature (VT) $^{31}\text{P}\{^1\text{H}\}$ NMR supports that this entropically favoured reaction is enthalpically disfavoured, and regenerates **1** and toluene as the temperature is lowered. As shown in **Figure 2.3**, at all temperatures studied the resonance for **2a** is sharp, which indicates that the equilibrium process is slow relative to the NMR time scale. The large variance in literature reported $^{31}\text{P}\{^1\text{H}\}$ NMR chemical shifts for **1** is consistent with a number of the reported shifts being obtained in aromatic solvents.^{42, 43}

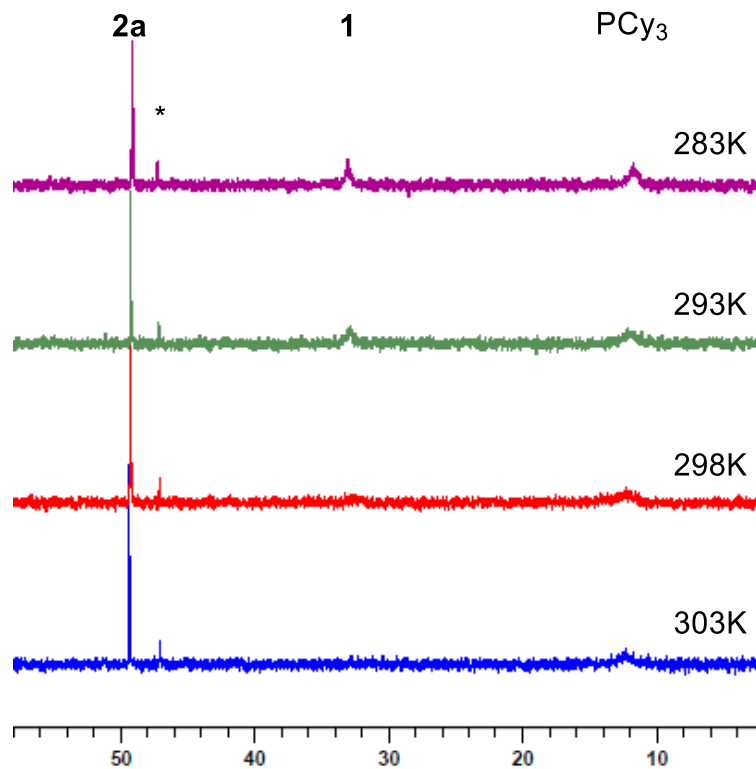


Figure 2.3 VT-³¹P{¹H} NMR of complex **1** in toluene. The integral of **1** increases as the temperature decreases. * is O=PCy₃.

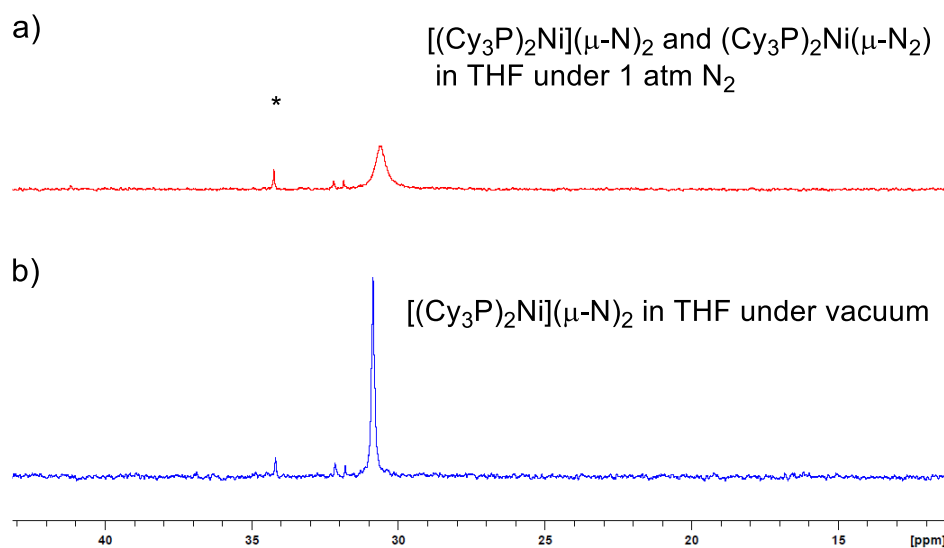
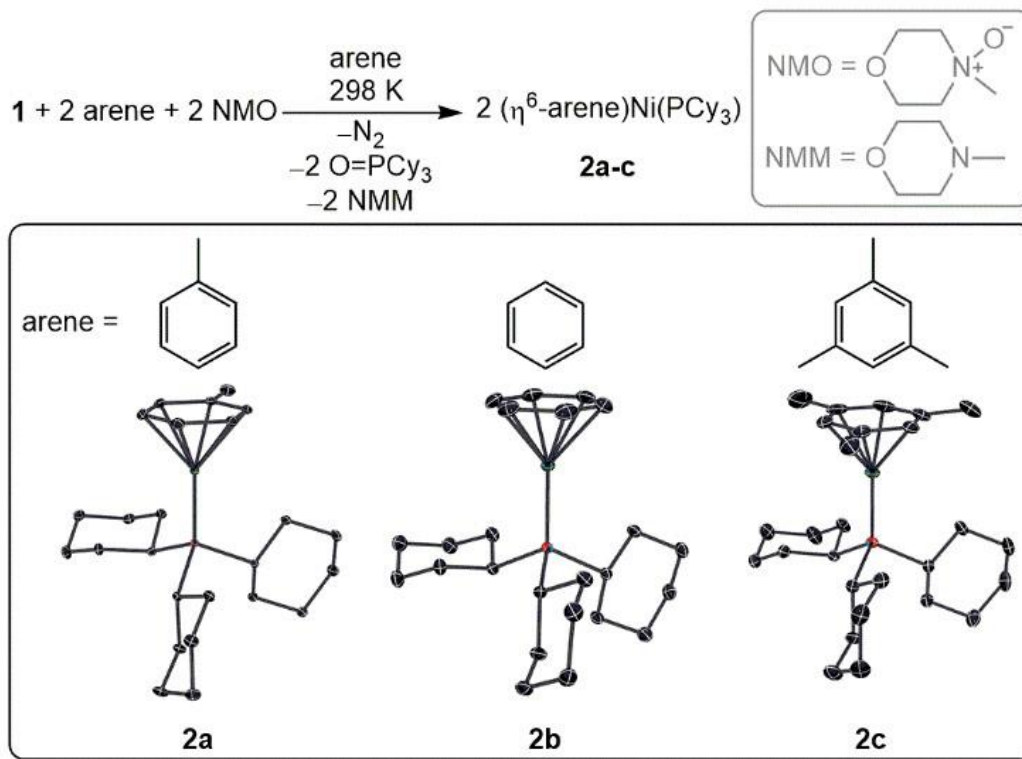


Figure 2.4 ³¹P{¹H} NMR of a) Complex **1** in THF under N₂ atmosphere and b) Complex **1** in THF under vacuum.

In the $^{31}\text{P}\{^1\text{H}\}$ of **1** under N_2 atmosphere, a broad singlet peak was observed. When the THF solution was exposed under vacuum, as shown in **Figure 2.4**, a much sharper singlet peak was observed, which suggests that a mononuclear species $[(\text{Cy}_3\text{P})_2\text{Ni}](\mu\text{-N}_2)$ was generated. The application of vacuum to arene solutions with equilibrium amounts of **1** generates only $(\text{Cy}_3\text{P})\text{Ni}(\eta^6\text{-arene})$ and PCy_3 , which suggests that the species **1** and its mononuclear counterpart $[(\text{Cy}_3\text{P})_2\text{Ni}](\mu\text{-N}_2)$ are the only species bearing two phosphines per Ni. There is no evidence for $[(\text{Cy}_3\text{P})_2\text{Ni}]$, which was previously proposed to be present in solution and commonly invoked in computations;^{18, 19, 21-23} There was also no evidence for the previously reported complex $(\text{Cy}_3\text{P})_3\text{Ni}$, even in the presence of added PCy_3 (**Scheme 2.1**).

The isolation of **2a** in the presence of unbound PCy_3 failed due to their similar solubilities, and in the presence of N_2 only **1** is obtained. Attempts to use Lewis acids to trap free PCy_3 , such as AlMe_3 or $\text{B}(\text{C}_6\text{F}_5)_3$, failed due to the decomposition of **2a**. Reaction of a toluene solution of **1** with *N*-methylmorpholine *N*-oxide (NMO), a mild oxidant often applied in biochemistry and organic synthesis⁴⁴⁻⁴⁸ gave **2a** and the byproduct *N*-methylmorpholine (NMM). The oxidation was selective, with no evidence of oxidation at Ni,⁴⁹ although the use of excess NMO did result in the decomposition of **2a**. The volatile NMM byproduct was removed under vacuum, whereas the $\text{O}=\text{PCy}_3$ generated is less soluble in pentane than **2a**, and was separated by recrystallization from a dilute pentane solution at $-40\text{ }^\circ\text{C}$ as colourless crystals. After the separation of $\text{O}=\text{PCy}_3$ and NMM, pure **2a** was isolated in 34% yield as pale yellow crystals from a concentrated pentane solution cooled to $-40\text{ }^\circ\text{C}$. The modest isolated yield is due to the solubility of **2a**, and NMR spectroscopy of the crude reaction mixture shows near quantitative conversion. Complex **2a** is stable in the solid state at room temperature under an inert gas atmosphere for weeks. Solutions of **2a** in *n*-pentane decompose over hours via the precipitation of metallic Ni and the liberation of arene and PCy_3 , the latter of which results in a reestablishment of the equilibrium of the remaining **2a** with **1**. Similar reaction conditions can be used to generate other arene adducts, such as with benzene (**2b**) and mesitylene (**2c**), as shown in Scheme 2.2.



Scheme 2.2 Isolation of toluene (**2a**), benzene (**2b**) and mesitylene (**2c**) complexes from **1** by oxidation of unbound PCy₃ with NMO.

The solid-state structure of complexes **2a-c** were determined by X-ray diffraction. The structure of **2a** is shown below in **Figure 2.5**. All structures confirm the proposed structures of these 18-electron, two-coordinate Ni complexes.

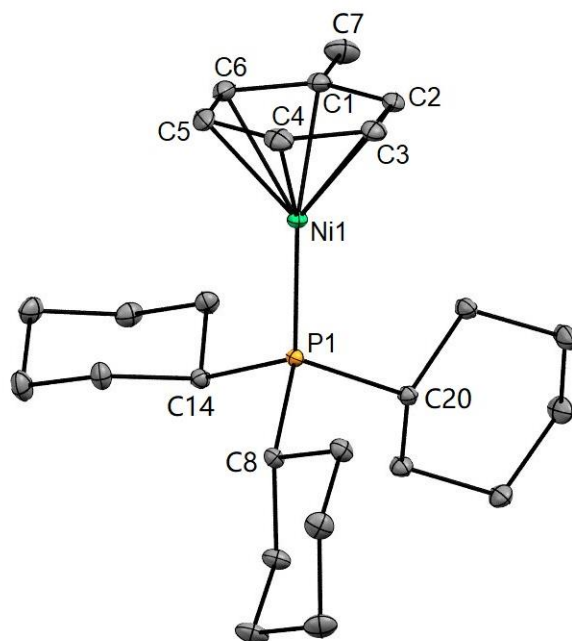
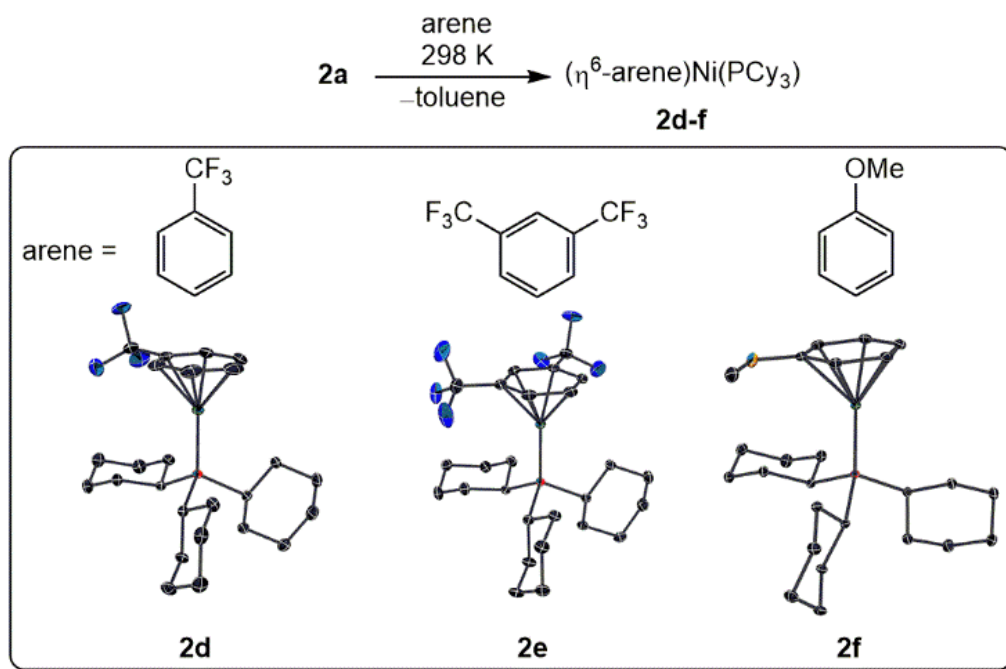


Figure 2.5 ORTEP depiction of **2a**.




Scheme 2.3 Use of **2a** as a (Cy₃P)Ni transfer reagent in the synthesis of complexes of *α,α,α*-trifluorotoluene (**2d**), 1,3- bis(trifluoromethyl)benzene (**2e**) and anisole (**2f**).

Complex **2a** is a convenient source of the (Cy₃P)Ni moiety, which is readily transferred to other arenes at room temperature. When **2a** is dissolved in *α,α,α*-trifluorotoluene at room temperature, new resonances are immediately observed in the ³¹P{¹H} and ¹⁹F NMR spectra. Removal of the solvent under vacuum provides (Cy₃P)Ni(η⁶-C₆H₅CF₃) (**2d**). Similar reaction conditions using 1,3- bis(trifluoromethyl)benzene gives (Cy₃P)Ni[η⁶-1,3-(CF₃)₂C₆H₄] (**2e**), and anisole provides (Cy₃P)Ni(η⁶-C₆H₅OMe) (**2f**), as shown in **Scheme 2.3**. The structures of **2d-f** in the solid-state were all determined by X-ray crystallography.

The equilibrium transfer of (Cy₃P)Ni from **2a** is influenced by the electronics of the recipient arene. For example, solutions of **2a** with added fluorobenzene showed low intensity signals in the ¹⁹F and ³¹P{¹H} NMR that could be attributed to equilibrium formation of (Cy₃P)Ni(η⁶-C₆H₅F); however, this complex proved too unstable in solution to isolate. A similar result was obtained with *N,N*-dimethylaniline. Reactions with the difluorobenzenes **2a** showed no new ¹⁹F and ³¹P{¹H} NMR resonances that could be attributed to the isomers of (Cy₃P)Ni(η⁶-C₆H₄F₂). The decreased propensity to bind to fluorinated aromatics is opposite to the trend observed in the chemistry of Ni(PR₃)₂, where more fluorinated arenes form more stable adducts,⁵⁰⁻⁵² though other metal complexes are known where fluorinated arenes form less thermodynamically favourable adducts.⁵³ The effect of arene substituents on the binding of the (PCy₃)Ni moiety was quantified from the equilibria reached when an equimolar mixture of competing arenes and toluene were added to substoichiometric **2a**. Equilibria concentrations of the new (Cy₃P)Ni(η⁶-arene) species and **2a** were determined immediately by ³¹P{¹H} NMR spectroscopy, and remained unchanged when the solutions were monitored for several hours. The Gibbs free energy changes for these reactions were determined from the equilibrium constants, and are shown in **Scheme 2.4**. The results show that electron-withdrawing CF₃ substituents form the most thermodynamically stable adducts. Substituents with lone pairs, such as *N,N*-dimethylaniline, anisole and fluorobenzene all give less stable adducts. In these cases, the arene with the more electronegative substituents form the least stable adducts. Some structural trends in these (Cy₃P)Ni(η⁶-arene) complexes match the thermodynamic data.

ΔG (kJ·mol ⁻¹)	Arene
2.7	fluorobenzene
2.7	anisole
1.0	<i>N,N</i> -Dimethylaniline
0.1	mesitylene
0	toluene
-0.4	benzene
-1.6	α, α, α -trifluorotoluene
-5.6	1,3-bis(trifluoromethyl)benzene

2a

 toluene/arene
 1 : 1 mixture

 (Cy₃P)Ni(η^6 -arene)

Scheme 2.4 Determination of Gibbs free energy change (ΔG) for equilibrium (Cy₃P)Ni transfer from **2a** to arenes.

In the structure of **2f** the Ni-C bond to the *ipso* carbon is the longest in the complex. Similarly, in **2d**, the shortest Ni-C bond is to the *ipso* carbon. Comparatively less is known about electronic effects in (NHC)Ni(η^6 -arene) compounds.²⁴ Selective bond lengths of compounds **2a-f** are listed in **Table 2.1**.

Table 2.1 Selective Bond Lengths of (Cy₃P)Ni(η⁶-arene) Complexes

Arene	Average Ni-C(arene) bond length (Å)	Ni- <i>ipso</i> -C bond length (Å)	Ni-arene centre distance (Å)
anisole	2.129(3)	2.157(3)	1.596
mesitylene	2.131(6)	2.136(6) ^a	1.597
toluene	2.127(1)	2.136(1)	1.594
benzene	2.119	N/A	1.587
α,α,α-trifluorotoluene	2.114(2)	2.083(2) ^a	1.582
1,3-bis(trifluoromethyl)benzene	2.114(2)	2.101(2) ^a / 2.103(2) ^b	1.579

^a Average Ni-*ipso*-C bond length

^b Bond distance between Ni and C at site 2

2.3 Summary and Conclusions

This work studied the properties of **1** in depth and corrects a longstanding error in the solution nature of **1**, a commonly used (Cy₃P)₂Ni(0) precursor. We firmly proved the equivalence between [(R₃P)₂Ni]₂(μ-N₂) and (R₃P)Ni(η⁶-arene) (R = PCy₃ and P^{*i*}Pr₃) in aromatic compounds under N₂ atmosphere. The addition of *N*-methylmorpholine *N*-oxide to arene solutions of [(Cy₃P)₂Ni]₂(μ-N₂) allows for the synthesis, fully characterization and determination of important electronic effects in thermodynamic stability of a series of stable (Cy₃P)Ni(η⁶-arene) complexes. More importantly, the isolation of these species allows for the use of **2a–f** as reactive sources of the (Cy₃P)Ni moiety, demonstrates their viability as intermediates and provides an experimental means to test the hypothesized importance of the (Cy₃P)Ni moiety in bond activation and catalysis. Work is underway to

experimentally verify the role of (Cy₃P)Ni in C–O bond oxidative addition predicted by DFT calculations, and the use of **2a-f** as catalyst precursors.

2.4 Experimental Section

2.4.1 General Procedures

All experiments were performed under an N₂ atmosphere using either standard Schlenk techniques or a glovebox. Dry, oxygen-free solvents were employed throughout. Anhydrous pentane, toluene, and α,α,α -trifluorotoluene were purchased from Alfa Aesar and used as received. Anisole, mesitylene, hexamethyldisiloxane (HMDSO) and 1,3-bis(trifluoromethyl)benzene were purchased from Sigma Aldrich, deoxygenated by freeze-pump-thaw three times and dried by passing through a column of activated alumina. ¹H, ³¹P{¹H}, ¹³C{¹H}, and ¹⁹F{¹H} NMR spectra were recorded on a Bruker AMX spectrometer operating at 500 MHz. All chemical shifts are recorded in parts per million, and all coupling constants are reported in hertz. ¹H NMR spectra were referenced to (Me₃Si)₂O (δ 0.065)⁵⁴⁻⁵⁶ with respect to tetramethylsilane at δ 0.00. ³¹P{¹H} NMR spectra were referenced to external 85% H₃PO₄ at δ 0.00. ¹³C{¹H} NMR spectra were referenced to solvent resonances ((Me₃Si)₂O, δ 1.94). ¹⁹F{¹H} NMR spectra were referenced to an external sample of 80% CCl₃F in CDCl₃ at δ 0.00. Elemental analyses were performed by the Center for Catalysis and Materials Research, Windsor, Ontario. Trimethylaluminum solution (2.0 M in toluene) was purchased from Sigma Aldrich and used as received. Nickel(II) acetylacetonate was purchased from Alfa Aesar. *N*-Methylmorpholine *N*-oxide (NMO) and tricyclohexylphosphine (PCy₃) was purchased from Oakwood Products, Inc. [(Cy₃P)₂Ni]₂(μ -N₂) (**1**) was prepared according to the method of Jolly.⁵⁷ All of the solid compounds mentioned above were deoxygenated under vacuum before use.

2.4.2 Synthesis and Characterization of Complexes

Synthesis and Characterization of (Cy₃P)Ni(η^6 -PhMe) (2a) To a stirring solution of [(Cy₃P)₂Ni]₂(μ -N₂) (**1**) (2.00 g, 1.58 mmol) in 50 mL toluene, *N*-methylmorpholine *N*-oxide (NMO) (0.370 g, 3.16 mmol) was added over the course of 20 min. The solution turned from dark red to orange over the course of the addition. All volatiles were removed under vacuum and the remaining residue was dissolved in 50 mL of *n*-pentane. The mixture was filtered through Celite[®] and the solution was cooled to -40 °C for 12 h. Tricyclohexylphosphine oxide (O=PCy₃) precipitated from solution as an off-white solid and was removed by cold filtration through Celite. The filtrate was dried under vacuum, and then redissolved in 5 mL pentane and filtered through Celite. Cooling to -40 °C for 12 h provided **2a** as orange crystals suitable for single crystal X-ray diffraction. The product was collected by filtration and dried under vacuum (yield 0.468 g, 34.4 %). ¹H NMR (HMDSO, 500 MHz, 298 K): δ 1.13-1.28 (m, 18H, PCHCH₂CH₂CH₂), 1.66-1.74 (m, 15H, PCHCH₂CH₂CH₂), 2.22 (s, 3H, C₆H₅CH₃), 5.75 (accidentally coincident s, 5H, C₆H₅CH₃). ³¹P{¹H} NMR (HMDSO, 202.5 MHz, 298 K): δ 47.6 (s). ¹³C{¹H} (HMDSO, 125.8 MHz, 298 K): δ 22.01 (s, C₆H₅CH₃), 27.15 (s, PCHCH₂CH₂CH₂), 28.10 (d, ³J_{C-P} = 11 Hz, PCHCH₂CH₂), 31.27 (d, ²J_{C-P} = 5.7 Hz, PCHCH₂), 35.02 (d, ¹J_{C-P} = 17.6 Hz, PCH), 89.47 (s, *m*-toluene C), 89.97 (s, *p*-toluene C), 92.29 (s, *o*-toluene C), 102.00 (s, *ipso*-CCH₃). Anal. Calcd for C₂₅H₄₁NiP (MW 431.26): C, 69.63; H, 9.58. Found: C, 69.68; H, 9.50.

Synthesis and Characterization of (Cy₃P)Ni(η^6 -Ph) (2b) Complex **2a** (400 mg, 0.93 mmol) was dissolved in 15 mL of benzene. After 10 min of stirring, all volatiles were removed under vacuum. The remaining residue was dissolved in 10 mL of *n*-pentane and filtered through a plug of Celite, then cooled to -40 °C for 16 h. Yellow crystals of **2b** were isolated, washed with -40 °C *n*-pentane, and dried under vacuum (yield 117 mg, 30.2%). ¹H NMR (HMDSO, 500 MHz, 298 K): δ 1.10-1.28 (m, 18H, PCHCH₂CH₂CH₂), 1.57-1.82 (m, 15H, PCHCH₂), 5.85 (s, 6H, benzene-CH). ³¹P{¹H} NMR (HMDSO, 202.5 MHz, 298 K): δ 46.5 (s). ¹³C{¹H} (HMDSO, 125.8 MHz, 298K): δ 27.19 (s, PCHCH₂CH₂CH₂), 28.19 (d, ³J_{C-P} = 11 Hz, PCHCH₂CH₂), 31.37 (d, ²J_{C-P} = 5.6 Hz, PCHCH₂), 35.03 (d, ¹J_{C-P} = 18.2

Hz, PCH), 90.39 (s, benzene-CH). Anal. Calcd for C₂₅H₄₁ONiP (MW 417.23): C, 69.09; H, 9.42. Found: C, 69.37; H, 9.56.

Synthesis and Characterization of (Cy₃P)Ni(η⁶-1,3,5-Me₃C₆H₃) (2c) To a stirring solution of **1** (520 mg, 0.410 mmol) in 10 mL mesitylene and 5 mL pentane, *N*-methylmorpholine *N*-oxide (NMO) (96 mg, 0.821 mmol) was added over the course of 20 min. The solution was stirred for an additional 30 min, at which point all volatiles were removed. The residue was dissolved in 30 mL pentane and filtered the solution through Celite. The filtrate was cooled to -40 °C for 6 h, then filtered through Celite to remove O=PCy₃. The volume of solution was reduced to 2 mL under vacuum and filtered through a plug of Celite. The solution was then cooled to -40 °C for 16 h which yielded orange cubic crystals suitable for single crystal X-Ray diffraction. Crystals of **2c** were collected, washed with cold pentane and dried under vacuum (87 mg, yield 23.1 %). ¹H NMR (HMDSO, 500 MHz, 298 K): δ 1.08-1.26 (m, 18H, PCHCH₂CH₂CH₂), 1.65-1.73 (m, 15H, PCHCH₂CH₂CH₂), 2.17 (s, 9H, CCH₃), 5.63 (s, 3H, mesitylene CH). ³¹P{¹H} NMR (HMDSO, 202.5 MHz, 298 K): δ 49.5 (s). ¹³C{¹H} (HMDSO, 125.8 MHz, 298 K): δ 21.87 (s, CCH₃), 27.20 (s, PCHCH₂CH₂CH₂), 28.12 (d, ³J_{C-P} = 11 Hz, PCHCH₂CH₂), 31.27 (d, ²J_{C-P} = 6.0 Hz, PCHCH₂), 35.31 (d, ¹J_{C-P} = 17 Hz, PCH), 94.17 (s, mesitylene CH), 100.17 (s, mesitylene CCH). Anal. Calcd for C₂₅H₄₁ONiP (MW 447.26): C, 67.13; H, 9.24. Found: C, 66.92; H, 9.27.

Synthesis and Characterization of (Cy₃P)Ni(η⁶-CF₃C₆H₅) (2d) Complex **2a** (400 mg, 0.93 mmol) was dissolved in 15 mL of α, α, α-trifluorotoluene. After 10 min of stirring, the solution was evaporated under vacuum. The residue was dissolved in 6 mL of *n*-pentane, filtered through a plug of Celite, and cooled to -40 °C for 12 h. Dark yellow-orange crystals of **2d** precipitated. The crystals were collected and washed with cold pentane and dried under vacuum (121 mg, yield 26.9%). ¹H NMR (HMDSO, 500 MHz, 298 K): δ 1.13-1.20 (m, 18H, PCHCH₂CH₂CH₂), 1.70-1.73 (m, 15H, PCHCH₂), 6.02 (m, 3H, *m*- and *p*-trifluorotoluene H), 6.14 (m, 2H, *o*-trifluorotoluene H). ³¹P{¹H} NMR (HMDSO, 202.5 MHz, 298 K): δ 45.5 (s). ¹³C{¹H} (HMDSO, 125.8 MHz, 298 K): δ 26.97 (s, PCHCH₂CH₂CH₂), 27.98 (d, ³J_{C-P} = 11 Hz, PCHCH₂CH₂), 31.10 (d, ²J_{C-P} = 5.5 Hz,

PCHCH₂), 34.47 (d, ¹J_{C-P} = 18 Hz, PCH), 86.11 (s), 89.36 (s), 89.70 (s). ¹⁹F{¹H} (HMDSO, 470.6 MHz, 298 K): δ -61.05 (s). Anal. Calcd for C₂₅H₃₈F₃NiP (MW 485.23): C, 61.88; H, 7.89. Found: C, 61.57; H, 8.21.

Synthesis and Characterization of (Cy₃P)Ni[η⁶-1,3-(CF₃)₂C₆H₄] (2e) Complex **2a** (400 mg, 0.93 mmol) was dissolved in 15 mL of 1,3-bis-(trifluoromethyl)benzene. After 10 min of stirring, all volatiles were removed under vacuum. The remaining residue was dissolved in 5 mL of *n*-pentane, filtered through a plug of Celite, and cooled to -40 °C for 16 h. Complex **2e** was isolated as orange-red crystals (142 mg, 27.7 %). ¹H NMR (HMDSO, 500 MHz, 298 K): δ 1.11-1.32 (m, 18H, PCH₂CH₂CH₂CH₂), 1.68-1.74 (m, 15H, PCHCH₂), 6.16 (m, 1H, CF₃CCHCH), 6.26 (m, 2H, CF₃CCHCHCH), 6.41 (1H, CF₃CCHCCF₃). ³¹P{¹H} NMR (HMDSO, 202.5 MHz, 298 K): δ 43.1 (s). ¹³C{¹H} (HMDSO, 125.8 MHz, 298K): δ 24.9 (s, 3C), 26.0 (d, 6C, ³J_{C-P} = 10.8 Hz), 29.0 (d, 6C, ²J_{C-P} = 4.2 Hz), 32.2 (d, 3C, ¹J_{C-P} = 19.6 Hz), 80.3 (s), 83.1 (s), 83.4 (s), 87.2 (s). ¹⁹F{¹H} (HMDSO, 470.6 MHz, 298 K): δ -61.80 (s). Anal. Calcd for C₂₅H₃₈F₃NiP (MW 553.23): C, 56.45; H, 6.74. Found: C, 56.53; H, 6.94.

Synthesis and Characterization of (Cy₃P)Ni(η⁶-PhOMe) (2f) Complex **2a** (500 mg, 1.11 mmol) was dissolved in 15 mL of anisole. After 15 min of stirring, all volatiles were removed under vacuum. The remaining residue was dissolved in 5 mL of *n*-pentane, filtered through a plug of Celite, and cooled to -40 °C for 16 h. Complex **2f** was isolated as dark yellow-orange crystals and dried under vacuum (yield 0.129 g, 24.9%). ¹H NMR (HMDSO, 500 MHz, 298 K): δ 1.17-1.27 (m, 18H, PCHCH₂CH₂CH₂), 1.67-1.74 (m, 15H, PCHCH₂), 3.62 (s, 3H, OCH₃), 5.69 (m, 1H, *p*-anisole CH), 5.73 (m, 2H, *o*-anisole CH), 5.79 (m, 2H, *m*-anisole CH). ³¹P{¹H} NMR (HMDSO, 202.5 MHz, 298 K): δ 48.3 (s). ¹³C{¹H} (HMDSO, 125.8 MHz, 298K): δ 27.14 (s, PCHCH₂CH₂CH₂), 28.12 (d, ³J_{C-P} = 11 Hz, PCHCH₂CH₂), 31.27 (d, ²J_{C-P} = 5.6 Hz, PCHCH₂), 35.13 (d, ¹J_{C-P} = 17.8 Hz, PCH), 54.61 (s, OCH₃), 80.91 (s, *m*-toluene C), 86.95 (s, *o*-toluene C), 88.47 (s, *p*-toluene C), 102.93 (s, COCH₃). Anal. Calcd for C₂₅H₄₁ONiP (MW 447.26): C, 67.14; H, 9.24. Found: C, 66.92; H, 9.27.

2.4.3 Equilibrium Studies of **1** and **1-PⁱPr₃**

NMR scale reaction of [(ⁱPr₃P)₂Ni]₂(μ-N₂) (1-PⁱPr₃**) and toluene in the absence of NMO** **1-PⁱPr₃** was prepared according to the literature method⁵⁸. 10 mg of **1-PⁱPr₃** (0.0127 mmol) was dissolved in 0.6 mL of pentane and only one singlet peak at δ 43.8 ppm was observed in the ³¹P{¹H} NMR spectrum. When 10 mg of N₂[Ni(PⁱPr₃)₂]₂ was dissolved in toluene (0.6 mL, 5.65 mmol) at room temperature, the resonance corresponding to PⁱPr₃ (δ 19.8 ppm) and (ⁱPr₃P)Ni(η⁶-PhMe) appear in the ³¹P{¹H} NMR spectrum.

NMR scale reaction of **1 and toluene in the absence of NMO** A solution of **1** (10 mg, 0.00789 mmol) in 0.6 mL pentane was analyzed by ³¹P{¹H} NMR and features one singlet resonance at δ 31.1. When 10 mg of **1** was dissolved in 0.6 mL of toluene in a J. Young tube, two singlet resonances were observed at δ 46.5 and δ 10.3 which correspond to **2a** and PCy₃, respectively. Degassing the solution by three freeze-pump-thaw cycles did not affect these two resonances.

NMR scale reaction of **2a and PCy₃ under 1 atm of N₂** 6 mg (0.014 mmol) of **2a** and 4 mg (0.014 mmol) of PCy₃ was dissolved in pentane at room temperature under 1 atm N₂. The reaction reached equilibrium in 1 h. A resonance corresponding to **1** was observed at δ 31.0.

Variable-temperature NMR of **1 in toluene** 10 mg of **1** was fully dissolved in 0.6 mL toluene and ³¹P{¹H} MMR data was collected at 283, 293, 293 and 303 K.

Equilibrium between [(Cy₃P)₂Ni]₂(μ-N₂) and (Cy₃P)₂Ni(μ-N₂) A solution of **1** (10 mg, 0.023 mmol) was dissolved in 0.6 mL of THF and transferred to a J. Young NMR tube. A ³¹P{¹H} NMR spectrum of the solution was collected at room temperature and featured a broad resonance (W_{1/2} = 121 Hz) at δ 30.6 ppm. The J. Young NMR tube was cooled in liquid nitrogen and the N₂ atmosphere was removed under vacuum. The ³¹P{¹H} NMR spectrum was then recollectd in the absence of N₂. A much sharper singlet (W_{1/2} = 15 Hz) was observed at δ 30.9.

Arene competition reactions with 2a 10 mg of **2a** (0.0232 mmol) was dissolved in a mixture of anisole (25.1 mg, 0.232 mmol), dimethylaniline (28.1 mg, 0.232 mmol), fluorobenzene (22.3 mg, 0.232 mmol) and *n*-pentane (0.60 mL) in an NMR tube. The reaction was monitored through $^{31}\text{P}\{^1\text{H}\}$ NMR at room temperature over a period of 6 h. The reaction reached equilibrium in 30 min. The spectrum was simulated using line-fitting in TopSpin 3.5pl7. The ratio of **2a**, **2f**, $(\text{Cy}_3\text{P})\text{Ni}(\eta^6\text{-C}_6\text{H}_5\text{F})$ (**2g**) and $(\text{Cy}_3\text{P})\text{Ni}(\eta^6\text{-Me}_2\text{NC}_6\text{H}_5)$ (**2h**) at equilibrium was 1:3.40:3.28:6.77. In another experiment, 8 mg of **2a** was dissolved in a mixture of benzene (0.170 mL, 1.89 mmol), mesitylene (0.260 mL, 1.89 mmol) and toluene (0.200 mL, 1.89 mmol). The reaction was monitored through $^{31}\text{P}\{^1\text{H}\}$ NMR at room temperature over a period of 6 h and the reaction reached equilibrium in 30 min. The integral ratio of **2a**, **2b** and **2c** was 1:1.19:0.98, respectively. In a third experiment, a similar method as described above was used to compete **2a** (8mg), with 0.200 mL toluene, 0.230 mL α, α, α -trifluorotoluene (1.89 mmol) and 0.290 mL 1,3-bis(trifluoromethyl) benzene (1.89 mmol). The ratio of the integrals of these three analogues was determined to be 1:2:12. The Gibbs free energy of the reaction was calculated using the equation $\Delta G = -RT\ln K$ ($R = 8.314 \text{ kJ/mol}$).

2.5 X-ray Crystallography

Table 2.2 Crystallographic Data for Complexes **2a-2f**

Compound	2a	2b	2c	2d	2e	2f
Chemical Formula	$\text{C}_{25}\text{H}_{41}\text{NiP}$	$\text{C}_{24}\text{H}_{39}\text{NiP}$	$\text{C}_{27}\text{H}_{45}\text{NiP}$	$\text{C}_{25}\text{H}_{38}\text{F}_3\text{NiP}$	$\text{C}_{26}\text{H}_{37}\text{F}_6\text{NiP}$	$\text{C}_{25}\text{H}_{41}\text{NiOP}$
Formula Weight	431.26	417.23	459.31	485.23	553.23	447.26
Temp	173(2) K	173(2) K	173(2) K	173(2) K	173(2) K	173(2) K
Crystal system	Triclinic	Monoclinic	Monoclinic	Monoclinic	Monoclinic	Triclinic
Space group	P -1	P2(1)/n	P2(1)/c	P2(1)/c	C2/c	P -1

a/ Å	8.6764(6)	9.8511(11)	12.7379(14)	11.8792(7)	16.921(4)	8.6352(5)
b/ Å	9.5709(7)	22.745(2)	9.3650(11)	9.2062(6)	9.399(2)	9.7092(6)
c/ Å	15.6496(11)	9.8693(10)	21.990(3)	22.9722(15)	32.999(8)	15.6942(10)
α / °	96.519(2)	90	90	90	90	97.5800(10)
β / °	99.003(2)	92.166(2)	104.542(2)	104.1810(10)	99.990(4)	99.4610(10)
γ / °	115.531(2)	90	90	90	90	115.0380(10)
V/ Å ³	1134.08(14)	2209.7(4)	2539.2(5)	2435.7(3)	5169(2)	1145.68(12)
Z	2	4	4	4	8	2
D _{calc} /g cm ⁻³	1.263	1.254	1.201	1.323	1.422	1.297
μ (Mo-K α) / mm ⁻¹	0.933	0.956	0.838	0.894	0.868	0.93
F(000)	468	904	4256	1032	2320	484
Reflection collected	56664	72724	8145	60724	49098	32139
Independent reflections	9957	9693	6405	8797	7542	25298
R(int)	4.42	4.35	twinned	3.90	7.54	twinned
R1 (I > 2 σ (I))	3.37	3.07	5.52	3.60	4.34	6.38
R1(all)	5.47	4.57	7.78	5.62	8.79	9.18
wR2(all)	7.19	6.65	14.53	9.04	8.66	10.95
GOF	1.0210	1.0560	1.1440	1.0430	1.0340	1.0920

R1: also known as the R-value, represents the agreement between calculated and observed models.

wR2: similar to R1, but refers to squared F-values.

GOF: goodness of fit parameter.

2.6 References

1. A. Suzuki, *Angew. Chem. Int. Ed.*, 2011, **50**, 6722-6737.
2. Y. Tamaru, *Modern Organonickel Chemistry (Wiley-VCH)*, 2005.
3. M. C. Neary and G. Parkin, *Dalton Trans.*, 2016, **45**, 14645-14650.
4. S. D. Ittel, *Inorg. Synth.*, 1990, **28**, 98-104.
5. C. Lei, Y. J. Yip and J. S. Zhou, *J. Am. Chem. Soc.*, 2017, **139**, 6086-6089.
6. D. Pollak, R. Goddard and K. R. Porschke, *J. Am. Chem. Soc.*, 2016, **138**, 9444-9451.
7. J. A. Hatnean, R. Beck, J. D. Borrelli and S. A. Johnson, *Organometallics*, 2010, **29**, 6077-6091.
8. L. B. Han, C. Zhang, H. Yazawa and S. Shimada, *J. Am. Chem. Soc.*, 2004, **126**, 5080-5081.
9. B. Yang and Z. X. Wang, *J. Org. Chem.*, 2017, **82**, 4542-4549.
10. Y. Gu and R. Martin, *Angew. Chem. Int. Ed.*, 2017, **56**, 3187-3190.
11. N. Iranpoor and F. Panahi, *Org. Lett.*, 2015, **17**, 214-217.
12. J. Xiao, J. Yang, T. Chen and L. B. Han, *Chem. Commun.*, 2016, **52**, 2157-2160.
13. M. Tobisu, T. Takahira, T. Morioka and N. Chatani, *J. Am. Chem. Soc.*, 2016, **138**, 6711-6714.
14. L. Guo, X. Liu, C. Baumann and M. Rueping, *Angew. Chem. Int. Ed.*, 2016, **55**, 15415-15419.

15. H. Yue, L. Guo, H. H. Liao, Y. Cai, C. Zhu and M. Rueping, *Angew. Chem. Int. Ed.*, 2017, **56**, 4282-4285.
16. M. R. Harris, L. E. Hanna, M. A. Greene, C. E. Moore and E. R. Jarvo, *J. Am. Chem. Soc.*, 2013, **135**, 3303-3306.
17. J. Cornella, E. Gomez-Bengoa and R. Martin, *J. Am. Chem. Soc.*, 2013, **135**, 1997-2009.
18. H. Xie, Y. Li, L. Wang, J. Kuang, Q. Lei and W. Fang, *Dalton Trans.*, 2017, **46**, 13010-13019.
19. S.-Q. Zhang, B. L. H. Taylor, C.-L. Ji, Y. Gao, M. R. Harris, L. E. Hanna, E. R. Jarvo, K. N. Houk and X. Hong, *J. Am. Chem. Soc.*, 2017, **139**, 12994-13005.
20. Z. Li, S.-L. Zhang, Y. Fu, Q.-X. Guo and L. Liu, *J. Am. Chem. Soc.*, 2009, **131**, 8815-8823.
21. H. Ogawa, H. Minami, T. Ozaki, S. Komagawa, C. Wang and M. Uchiyama, *Chemistry*, 2015, **21**, 13904-13908.
22. X. Hong, Y. Liang and K. N. Houk, *J. Am. Chem. Soc.*, 2014, **136**, 2017-2025.
23. M. C. Schwarzer, R. Konno, T. Hojo, A. Ohtsuki, K. Nakamura, A. Yasutome, H. Takahashi, T. Shimasaki, M. Tobisu, N. Chatani and S. Mori, *J. Am. Chem. Soc.*, 2017, **139**, 10347-10358.
24. Y. Hoshimoto, Y. Hayashi, H. Suzuki, M. Ohashi and S. Ogoshi, *Organometallics*, 2014, **33**, 1276-1282.
25. T. Nickel, R. Goddard, C. Krueger and K. R. Poeschke, *Angew. Chem. Int. Ed.*, 1994, **106**, 908-910 (See also *Angew Chem , Int Ed Engl* , 1994, 1933(1998), 1879-1982).

26. R. Beck, M. Shoshani, J. Krasinkiewicz, J. A. Hatnean and S. A. Johnson, *Dalton Trans.*, 2013, **42**, 1461-1475.
27. T. E. Muller and D. M. P. Mingos, *Transit. Metal Chem.*, 1995, **20**, 533-539.
28. C. A. Tolman, *Chem. Rev.*, 1977, **77**, 313-348.
29. H. Clavier and S. P. Nolan, *Chem. Commun.*, 2010, **46**, 841-861.
30. P. W. Jolly and K. Jonas, *Angew. Chem. Int. Ed.*, 1968, **7**, 731-732.
31. K. S. Kanyiva, N. Kashihara, Y. Nakao, T. Hiyama, M. Ohashib and S. Ogoshi, *Dalton Trans.*, 2010, **39**, 10483-10494.
32. C. S. Yeung and V. M. Dong, *J. Am. Chem. Soc.*, 2008, **130**, 7826-7827.
33. M. Aresta, A. Dibenedetto, E. Quaranta, M. Lanfranchi and A. Tiripicchio, *Organometallics*, 2000, **19**, 4199-4207.
34. M. Y. Darensbourg, M. Ludwig and C. G. Riordan, *Inorg. Chem.*, 1989, **28**, 1630-1634.
35. Kyalo Stephen Kanyiva, Natsuko Kashihara, Yoshiaki Nakao, Tamejiro Hiyama, Masato Ohashib and S. Ogoshi, *Dalton Trans.*, 2010, **39**, 10483-10494.
36. M. Aresta, E. Quaranta, A. Dibenedetto, P. Giannoccaro, I. Tommasi, M. Lanfranchi and A. Tiripicchio, *Organometallics*, 1997, **16**, 834-841.
37. K. Osakada, H. Hayashi, M. Maeda, T. Yamamoto and A. Yamamoto, *Chem. Lett.*, 1986, 597-600.
38. G. Favero, A. Morvillo and A. Turco, *J. Organomet. Chem.*, 1983, **241**, 251-257.
39. M. G. Mason and J. A. Ibers, *J. Am. Chem. Soc.*, 1982, **104**, 5153-5157.

40. M. Aresta, C. F. Nobile, V. G. Albano, E. Forni and M. Manassero, *Chem. Comm.*, 1975, 636-637.
41. P. W. Jolly, K. Jonas, C. Kruger and Y.-H. Tsay, *J. of Organomet. Chem.*, 1971, **33**, 109-122.
42. C. S. Yeung and V. M. Dong, *J. Am. Chem. Soc.*, 2008, **130**, 7826-7827.
43. J. Cornella, E. Gomez-Bengoia and R. Martin, *J. Am. Chem. Soc.*, 2013, **135**, 1997-2009.
44. B. Khumraksa, W. Phakhodee and M. Pattarawarapan, *Tetrahedron Lett.*, 2013, **54**, 1983-1986.
45. S. Singh, P. Chauhan, M. Ravi, I. Taneja, Wahajuddin and P. P. Yadav, *RSC Adv.*, 2015, **5**, 61876-61880.
46. S. Yruegas, D. C. Patterson and C. D. Martin, *Chem. Commun.*, 2016, **52**, 6658-6661.
47. A. T. Nelson, M. J. Kolar, Q. Chu, I. Syed, B. B. Kahn, A. Saghatelian and D. Siegel, *J. Am. Chem. Soc.*, 2017, **139**, 4943-4947.
48. T. Maehara, K. Motoyama, T. Toma, S. Yokoshima and T. Fukuyama, *Angew. Chem. Int. Ed.*, 2017, **56**, 1549-1552.
49. M. M. Shoshani and S. A. Johnson, *Inorg. Chem.*, 2017 Accepted, ic-2017-02546u.R02541.
50. S. A. Johnson, J. A. Hatnean and M. E. Doster, *Prog. Inorg. Chem.*, 2012, **57**, 255-352.
51. S. A. Johnson, N. M. Mroz, R. Valdizon and S. Murray, *Organometallics*, 2011, **30**, 441-457.

52. S. A. Johnson, E. T. Taylor and S. J. Cruise, *Organometallics*, 2009, **28**, 3842-3855.
53. S. D. Pike, M. R. Crimmin and A. B. Chaplin, *Chem. Commun.*, 2017, **53**, 3615-3633.
54. K. H. Tatsuki Kitayama, Springer Laboratory, 2013.
55. M. A. Farag, A. Porzel, E. A. Mahrous, M. M. El-Massry and L. A. Wessjohann, *Anal. Bioanal. Chem.*, 2015, **407**, 1937-1949.
56. S. Losio, G. Leone, F. Bertini, G. Ricci, M. C. Sacchi and A. C. Boccia, *Polym. Chem.*, 2014, **5**, 2065-2075.
57. P. W. Jolly and K. Jonas, *Inorg. Synth.*, 1974, **15**.
58. R. Beck, M. Shoshani, J. Krasinkiewicz, J. A. Hatnean and S. A. Johnson, *Dalton Trans.*, 2013, **42**, 1461-1475.

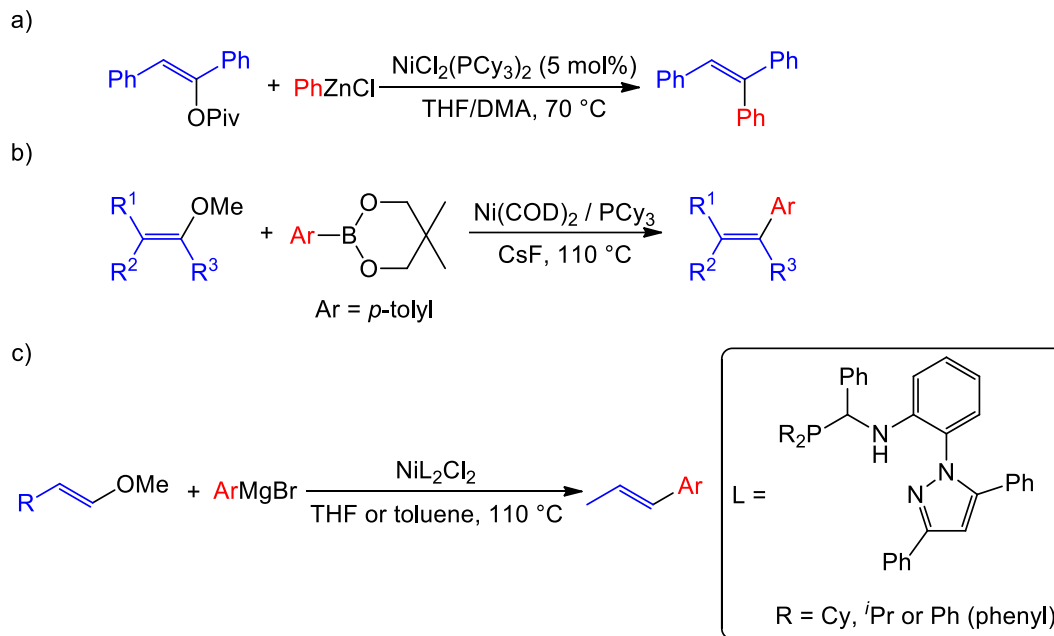
Chapter 3 Nickel C(sp²)-O Bond Cleavage by Oxidative Addition and β -Oxygen Elimination to give Esters from Coupling of Vinyl Ethers or Cross Coupling of Vinyl Ethers and Aldehydes

3.1 Introduction

Over the past decades, the application of ethers as electrophilic substrates in cross-coupling reactions has increased, because of their lower toxicity and price than traditional halide electrophiles. Ethers have the potential to become the preferred building blocks in organic and pharmaceutical syntheses, though the greater difficulty in activating C(sp²)-O bonds vs the carbon-halogen equivalents provides a need for new catalysts. Many zerovalent nickel complexes can cleave C(sp²)-O bonds and several catalytic cross-coupling reactions that utilize nickel catalysts have been developed¹⁻⁸. The application of nickel catalysts provides lower cost, improved sustainability and helps avoid heavy metal pollution from the heavier transition metal catalysts more commonly utilized in traditional cross-coupling. A number of studies have examined the mechanism C(sp²)-O activation and catalysis by nickel complexes, where both LNi and L₂Ni fragments are implicated in the transition state of C-O bond cleavage by oxidative addition mechanisms.⁹⁻¹⁶ Our goals

are to uncover mechanistic details about the ability of Ni to activate of C–O bonds, to enable new catalytic transformation with a versatile scope of attractive substrates.

The complexes $(\text{Cy}_3\text{P})\text{Ni}(\eta^6\text{-arene})$ developed by our group and $[(\text{Cy}_3\text{P})_2\text{Ni}]_2(\mu\text{-N}_2)$ (**1**)¹⁷ provide useful sources of LNi and L_2Ni moieties to investigate the mechanism of C–O bond activation, where $\text{L} = \text{PCy}_3$. Unfortunately in studies with the less reactive substrates of interest, like PhOMe, these complexes led to slow decomposition to Ni metal and PCy_3 over weeks at 298 K, or hours in refluxing toluene, and with $(\text{Cy}_3\text{P})\text{Ni}(\eta^6\text{-PhOMe})$ as the only observed species.¹⁸ Seeking to target new substrates we investigated alkenyl ethers. As summarized in **Scheme 3.1**, few examples of nickel catalyzed cross-coupling of alkenyl ethers have been reported,¹⁹⁻²³ and mechanistic studies with these substrates are entirely absent. We also investigated the reaction of $\text{L}_n\text{Ni}(0)$ with 2-methoxynaphthalene and 2-naphthyl acetate. The preliminary results of these two substrates will be discussed later in Chapter 5. This chapter describes the discovery of intriguing reactivity of Ni(0) complexes with alkenyl ethers and a mechanistic study that demonstrates multiple mechanisms for C–O bond cleavage.

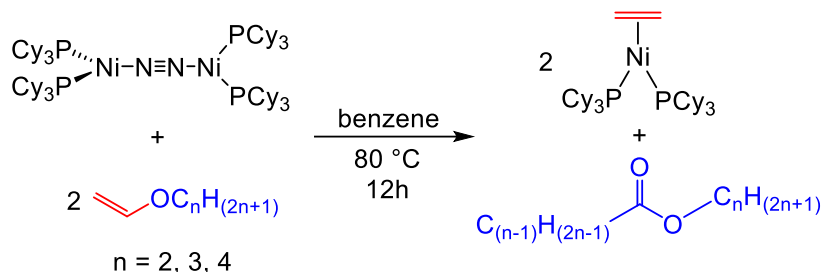


Scheme 3.1 Examples of Ni catalyzed cross-coupling reactions of alkenyl ethers and nucleophiles through C(sp²)-O bond activation. a) Negishi-style cross-coupling of alkenyl pivalate and organic zinc reagent catalyzed by NiCl₂(PCy₃)₂. b) Suzuki-Miyaura-style cross-coupling of alkenyl ethers and boronic ester catalyzed by Ni(COD)₂/PCy₃. c) Kumada-type cross-coupling of alkenyl ethers and aromatic Grignard reagent catalyzed by nickel phosphine complex.

3.2 Results and Discussion

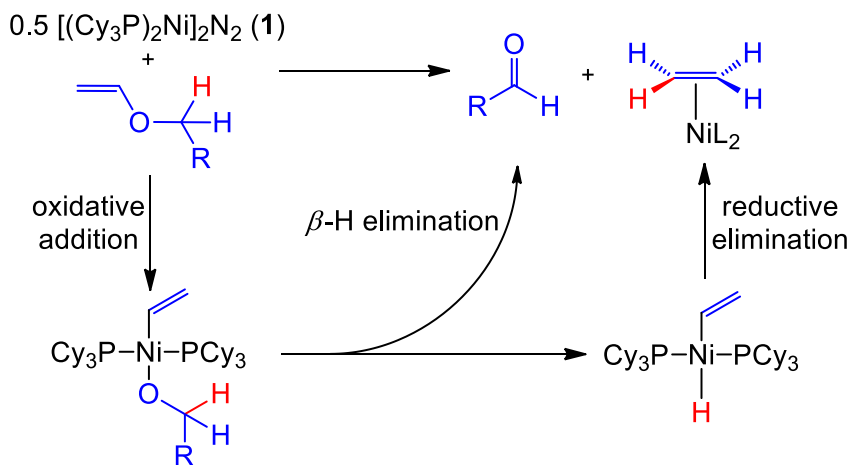
Stoichiometric conversion of alkenyl ethers to esters. When a benzene solution of [(Cy₃P)₂Ni]₂(μ-N₂) (**1**) and two equivalents of the vinyl ether EtOCH=CH₂ and were heated in an 80 °C bath for 12 h, the only significant product observed by ³¹P{¹H} NMR was the known ethylene complex (Cy₃P)₂Ni(η²-C₂H₄),¹⁴ as shown in **Scheme 3.2**. The unanticipated stoichiometric organic product was determined to be the ester MeCO₂Et. To clarify the source of the carbon chains in this product, which could arise from the ethyl or vinyl substituents, the same reactions was repeated with different alkyl substituents. The reaction using ⁿPrOCH=CH₂ gave EtCO₂Pr, and the reaction with ⁿBuOCH=CH₂ gave

ⁿPrCO₂Bu, as shown in **Scheme 3.2**, which shows that all the carbon atoms in the organic product are derived from the alkyl substituent of the vinyl ether.



Scheme 3.2 Reactions of H₂C=CHOEt, H₂C=CHOⁿPr and H₂C=CHOⁿBu with [(Cy₃P)₂Ni]₂(μ-N₂) (**1**) in benzene to give esters upon heating.

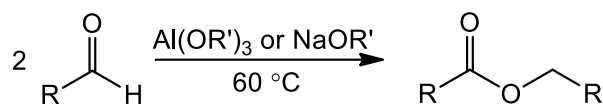
Ruling out nickel catalysed Tishchenko coupling of aldehydes. There is precedent in Ni chemistry for C(sp²)-O bond activation to be followed by β-H elimination, to give aldehydes. This reactivity as applied to this system could convert EtOCH=CH₂ into acetaldehyde and produce (Cy₃P)₂Ni(η²-C₂H₄), as shown in **Scheme 3.3**. No aldehyde or any other organic intermediate was observed during the reaction of EtOCH=CH₂ with [(Cy₃P)₂Ni]₂(μ-N₂) (**1**) shown in **Scheme 3.2**.



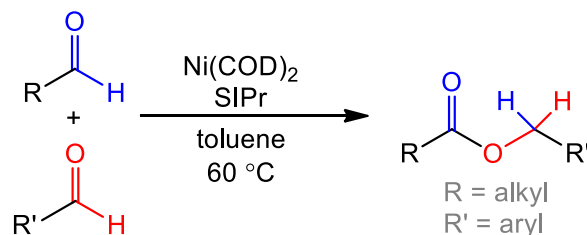
Scheme 3.3 Precedented mechanism for the production of aldehydes from C-O bond oxidative addition and β-H elimination as applied to system under study.

The absence of aldehyde as an observable intermediate does not rule out its slow production followed by rapid consumption in further reaction steps to produce esters. In fact, the nickel catalysed coupling of aldehydes to give esters has been demonstrated previously.²⁴ The reactivity observed here is conceivably a variant on a transition metal catalysed version of the Tishchenko reaction. The organic Tishchenko reaction²⁵ is depicted in **Scheme 3.4**, part A, and couples two aldehydes to give an ester. This reaction does not provide a selective route to cross-coupling of two aldehydes; however, it has been found that nickel catalyzed variants to this reaction using bulky N-heterocyclic carbene ligands allow the cross coupling of aryl and alkyl substituted aldehydes to selectively provide a single ester, as shown in **Scheme 3.4**, part B.^{24, 26} To test if the production of esters in the reaction of $\text{EtOCH}=\text{CH}_2$ is simply the result of acetaldehyde production followed by a Ni-catalysed Tishchenko reaction, we directly reacted complex **1** with acetaldehyde, as shown in **Scheme 3.4**, part C. Even after heating, no production of MeCO_2Et was observed, ruling out the possibility that the formation of esters shown in **Scheme 3.2** is from the nickel catalysed coupling of aldehydes.

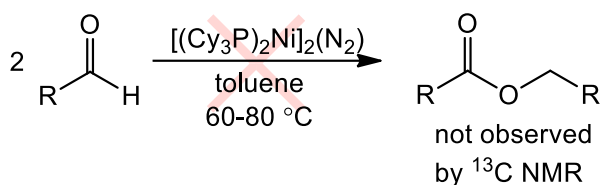
A) Tishchenko Reaction:



B) Nickel catalysed cross Tishchenko:

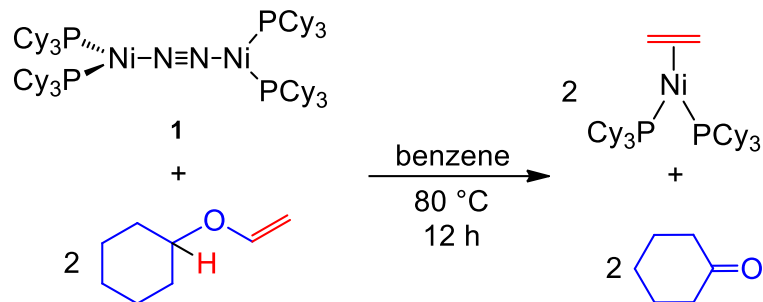


C) Failed nickel catalysed Tishchenko:



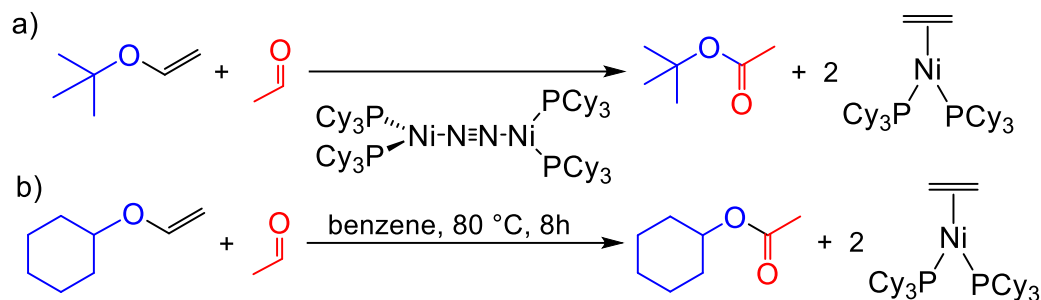
Scheme 3.4 a) Aluminum or sodium alkoxide catalyzed aldehyde condensation (typical Tishchenko reaction without selectivity to cross-coupling of two aldehydes). b) Nickel catalyzed Tishchenko reaction with the assistance of NHC or PCy₃ ligand. The substrates include at least one aryl ester. SIPr = 1,3-(2,6-bis(isopropyl)phenyl)imidazolidine. c) Reaction of aldehydes with stoichiometric amount of $[(\text{Cy}_3\text{P})_2\text{Ni}]_2(\mu\text{-N}_2)$ (**1**) does not produce an ester.

Aldehyde intermediates. The failure of this system to couple aldehydes does not rule out aldehydes as an intermediate in the reaction mechanism, and the reaction of **1** with CyOCH=CH_2 , where Cy = cyclohexyl, generates cyclohexanone and $(\text{Cy}_3\text{P})_2\text{Ni}(\eta^2\text{-CH}_2\text{=CH}_2)$ cleanly upon heating. This confirms that the $\text{C}(\text{sp}^2)\text{-O}$ bond activation followed by $\beta\text{-H}$ elimination mechanism shown previously in **Scheme 3.3** is possible under the reaction conditions.



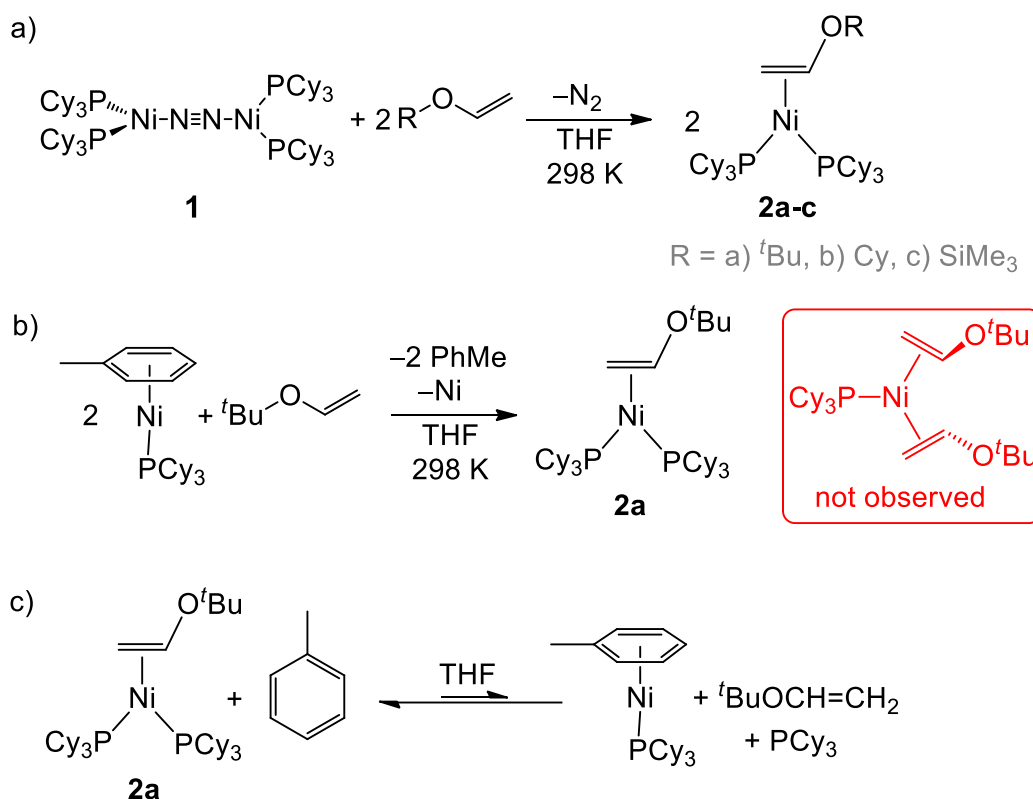
Scheme 3.5 The reaction of $[(\text{Cy}_3\text{P})_2\text{Ni}]_2(\mu\text{-N}_2)$ (**1**) and $\text{CyOCH}=\text{CH}_2$ at $80\text{ }^\circ\text{C}$ produces cyclohexanone and $(\text{Cy}_3\text{P})_2\text{Ni}(\eta^2\text{-C}_2\text{H}_4)$.

To test the possibility that aldehydes generated from vinyl ethers could react with vinyl ethers to give esters a direct reaction of the pair of reagents was attempted. The vinyl ether $t\text{BuOCH}=\text{CH}_2$, which cannot undergo $\beta\text{-H}$ elimination after $\text{C}(\text{sp}^2)\text{-O}$ bond activation to give either an aldehyde or ketone, was reacted with acetaldehyde and complex **1**. As shown in **Scheme 3.6 a**, this reaction yielded the cross-coupled ester product. This reaction does not require an ether resistant to $\beta\text{-H}$ elimination after $\text{C}(\text{sp}^2)\text{-O}$ bond activation. As shown in **Scheme 3.6 b**, the reaction of $\text{CyOCH}=\text{CH}_2$ with acetaldehyde and **1** also give the cross coupled ester product. This occurs without the production of cyclohexanone, as observed in the reaction shown in **Scheme 3.5** above, suggestion a pathway for homocoupling of vinyl ethers to esters where the $\text{C}(\text{sp}^2)\text{-O}$ bond activation is rate limiting, and the reaction of aldehydes with vinyl ethers to provide esters is faster. This explains the absence of any observable aldehyde intermediates in the homocoupling of vinyl ethers to esters.



Scheme 3.6 a) The cross-coupling of $t\text{BuOCH}=\text{CH}_2$ and acetaldehyde mediated by $[(\text{Cy}_3\text{P})_2\text{Ni}]_2(\mu\text{-N}_2)$ (**1**). MeCOO^tBu and $(\text{Cy}_3\text{P})_2\text{Ni}(\eta^2\text{-C}_2\text{H}_4)$ are produced. b) The cross-coupling of $\text{CyOCH}=\text{CH}_2$ and acetaldehyde mediated by $[(\text{Cy}_3\text{P})_2\text{Ni}]_2(\mu\text{-N}_2)$ (**1**). MeCOOCy and $(\text{Cy}_3\text{P})_2\text{Ni}(\eta^2\text{-C}_2\text{H}_4)$ are produced.

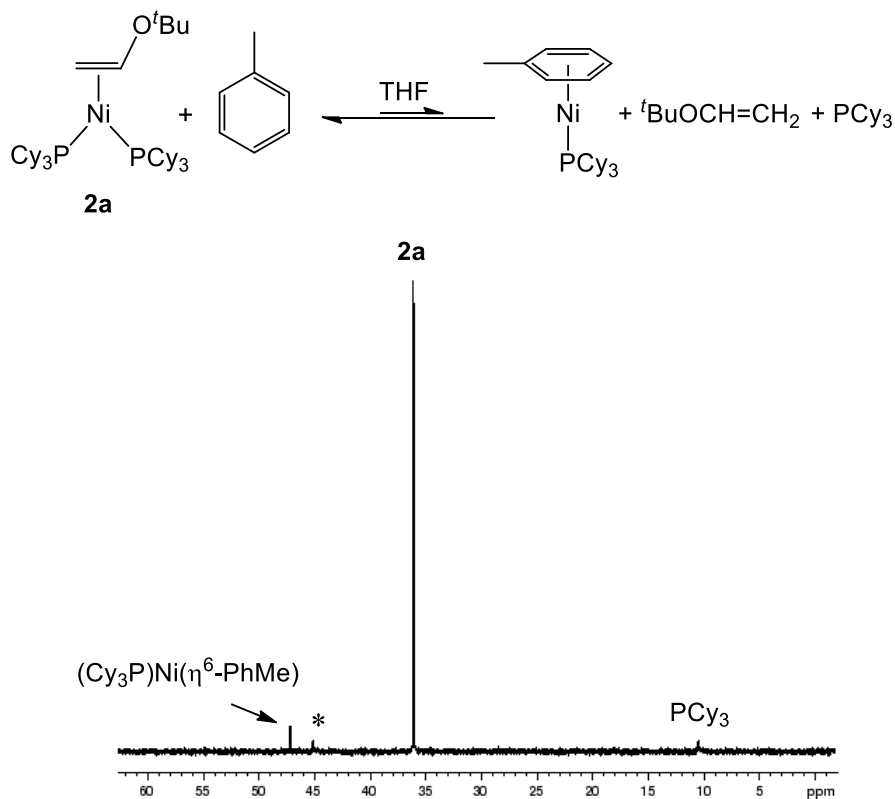
Isolated Ni(0) vinyl ether intermediates. In an attempt to get further insight into the mechanism of ester formation we sought to search for intermediates in the reaction. The reaction of a red solution of **1** immediately provided a dark yellow solution of $(\text{Cy}_3\text{P})_2\text{Ni}(\eta^2\text{-H}_2\text{C}=\text{CHO}^t\text{Bu})$ (**2a**) with the visible loss of N_2 gas. Similar reactions using $\text{CyOCH}=\text{CH}_2$ and $\text{Me}_3\text{SiOCH}=\text{CH}_2$ generated the analogues $(\text{Cy}_3\text{P})_2\text{Ni}(\eta^2\text{-H}_2\text{C}=\text{CHOCy})$ (**2b**) and $(\text{Cy}_3\text{P})_2\text{Ni}(\eta^2\text{-H}_2\text{C}=\text{CHOSiMe}_3)$ (**2c**). The yields appeared quantitative of $[(\text{Cy}_3\text{P})_2\text{Ni}]_2(\mu\text{-N}_2)$ (**1**) in THF with $t\text{BuOCH}=\text{CH}_2$ by $^{31}\text{P}\{^1\text{H}\}$ NMR.



Scheme 3.7 a) The reaction of ROCH=CH₂ and [(Cy₃P)₂Ni]₂(μ-N₂) (**1**) produces (Cy₃P)₂Ni(η²-H₂C=CHOR) (**2a-c**). b) The reaction of (Cy₃P)Ni(η⁶-PhMe) with ^tBuOCH=CH₂ also produces **2a**. c) The equilibrium of **2a** and (Cy₃P)Ni(η⁶-PhMe) in THF.

The chemistry of these vinyl ether adducts is different from vinylstannanes, germanes and silanes, which readily form monophosphine complexes (Cy₃P)Ni(η²-H₂C=CHER₃), where ER₃ is a SnR₃, GeR₃ or SiR₃ substituent, and are readily prepared from Ni(COD)₂.²⁷ Complexes **2a** and analogues cannot be accessed from the reaction of Ni(COD)₂ (COD = 1,5-cyclooctadiene) with PCy₃ and vinyl ether. The use of excess η²-H₂C=CHOR in these reactions did not yield any observable monophosphine complexes of the type (Cy₃P)Ni(η²-H₂C=CHOR)₂. As shown in **Scheme 3.7 b**, even the reaction of the monophosphine source (Cy₃P)Ni(η⁶-PhMe) with η²-H₂C=CHO^tBu in a ratio of 1:1 in THF only yielded **2a**, with decomposition of an equivalent of (Cy₃P)Ni(η⁶-PhMe) to Ni metal providing the additional PCy₃ required. Evidence of the relative thermodynamic instability of these vinyl ether complexes is provided by the equilibrium observed shown in **Scheme**

3.7 c. When **2a** is dissolved in THF and an equivalent of toluene is added the equilibrium formation of a small amount of $(\text{Cy}_3\text{P})\text{Ni}(\eta^6\text{-PhMe})$ was observed. The $^{31}\text{P}\{^1\text{H}\}$ NMR of this reaction mixture is shown in **Scheme 3.8**.



Scheme 3.8 The $^{31}\text{P}\{^1\text{H}\}$ NMR spectrum showing the equilibrium formation of $(\text{Cy}_3\text{P})\text{Ni}(\eta^6\text{-PhMe})$ and PCy_3 upon addition of toluene to a THF solution of **2a**, as shown in **Scheme 3.7 c**. * is $\text{O}=\text{PCy}_3$.

Complexes **2a-c** were isolated as bright yellow powders by recrystallization from pentane at $-40\text{ }^\circ\text{C}$, with yields of 84.4%, 76.7% and 64.9%, respectively. Crystals of **2a** suitable for single crystal X-ray diffraction were recrystallized from its saturated hexamethyldisiloxane (HMDSO) solution by slow evaporation at room temperature. The solid-state structure of **2a** is depicted in **Figure 3.1**. The nickel centre features a trigonal planar geometry with coordination of two PCy_3 ligand and a η^2 -bound vinyl group. The

C2–O1 and C1–C2 bond distances of 1.413(2) and 1.402(3) Å are longer than the bond distances of 1.368(10) and 1.322(9) in free H₂C=CHO'Bu,²⁸ which is caused by π back-donation from the nickel to the vinyl group. The structure is similar to other (Cy₃P)₂Ni(η^2 -alkene) complexes.²⁹⁻³²

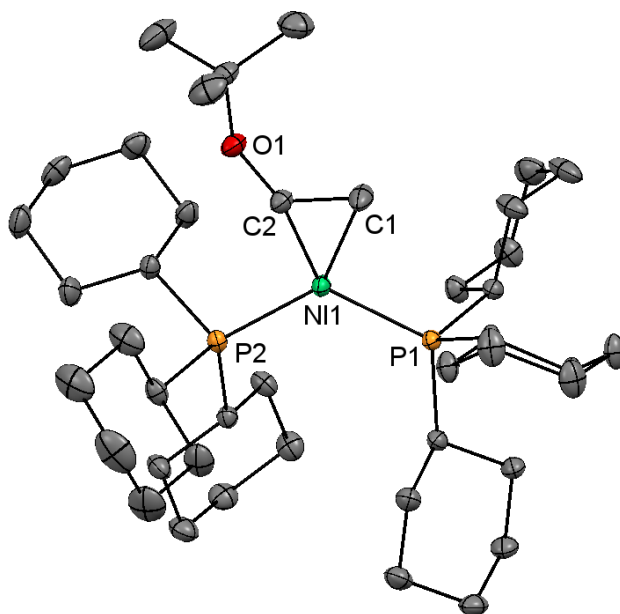


Figure 3.1 Solid state structure of **2a**. Hydrogen atoms were omitted for clarity. Selected bond length (unit: Å): Ni–C(1) = 1.968(2); Ni–C(2) = 1.978(2); Ni–P(1) = 2.1971(5); Ni–P(2) = 2.1854(6); C(1)–C(2) = 1.402(3); C(2)–O(1) = 1.413(2). Selected bond angles (unit: °): C(1)–Ni–C(2) = 41.63(7); Ni–C(1)–C(2) = 69.6(1); Ni–C(2)–C(1) = 68.8(1); P(1)–Ni–P(2) = 117.98(2).

The solid molecular structure of **2a** has C_1 symmetry, but the $^{31}\text{P}\{^1\text{H}\}$ NMR spectrum at room temperature only shows a single resonance at δ 36.3. When the solution is cooled the resonances decoalesce and give a slow exchange spectrum at -20 °C that features second order AB doublets with a $^2J_{\text{PP}}$ of 39 Hz, as shown in **Figure 3.2**. The fluxional process likely results from a low barrier to rotation around the Ni-alkene bond, as no evidence of exchange with free vinyl ether is observed.

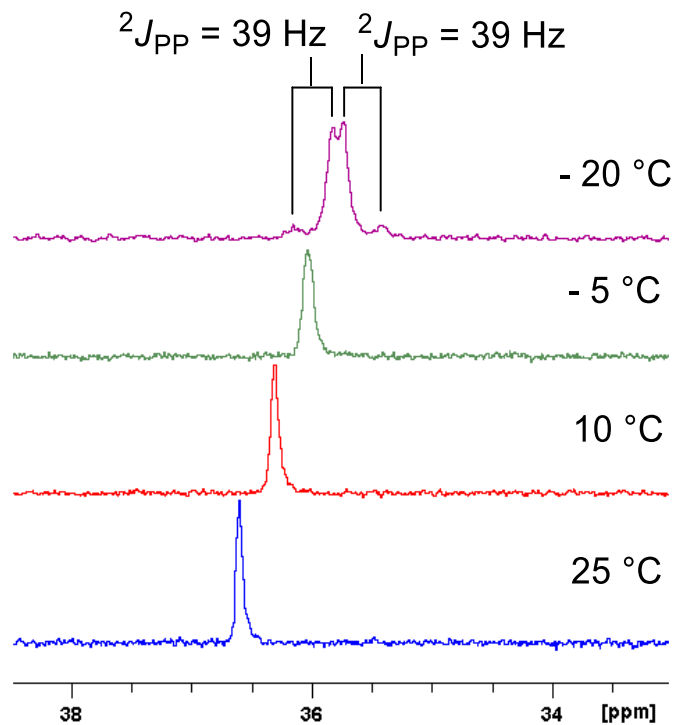
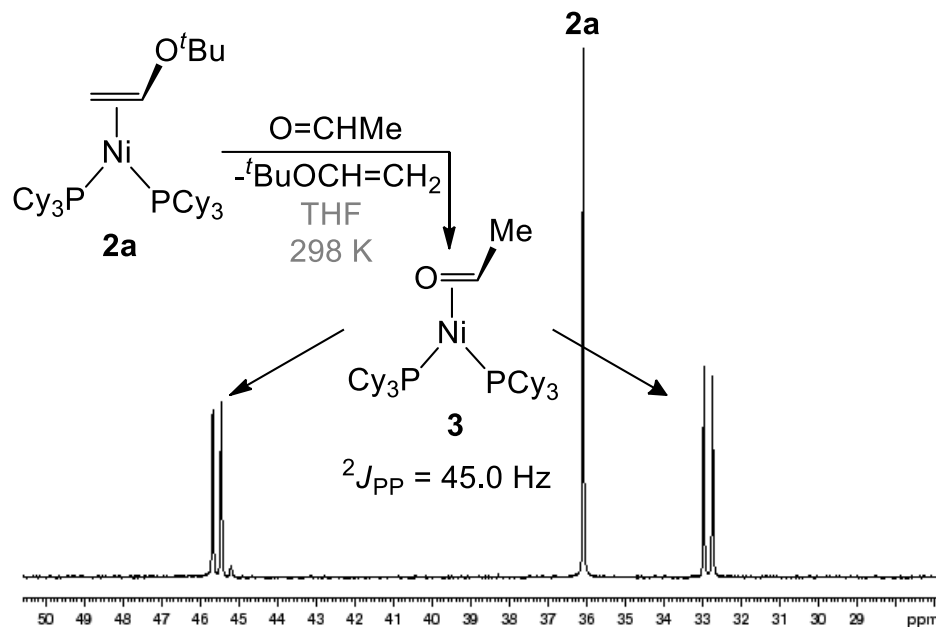


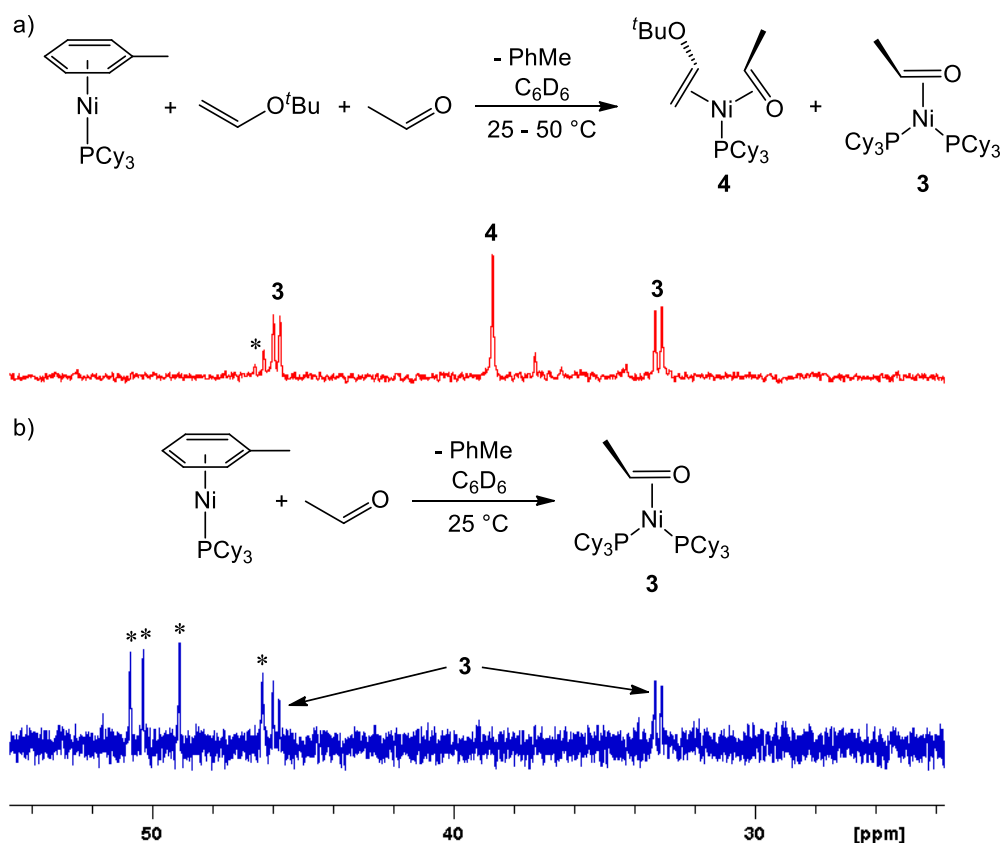
Figure 3.2 The variable-temperature $^{31}\text{P}\{^1\text{H}\}$ of **2a** in HMDSO.

Reaction of Ni(0) vinyl ethers with acetaldehyde. As previously shown in **Scheme 3.6**, a solution of aldehyde, vinyl ether and $[(\text{Cy}_3\text{P})_2\text{Ni}]_2(\mu\text{-N}_2)$ (**1**) heated to $80\text{ }^\circ\text{C}$ gives an ether as a coupling product and $(\text{Cy}_3\text{P})_2\text{Ni}(\eta^2\text{-H}_2\text{C}=\text{CH}_2)$. Monitoring this mixture even at room temperature shows the conversion to a different new nickel complex in the $^{31}\text{P}\{^1\text{H}\}$ NMR with two ^{31}P environments and a $^2J_{\text{PP}}$ of 45 Hz, as shown in **Scheme 3.9**. Comparison to literature values reveals that this complex is $(\text{Cy}_3\text{P})_2\text{Ni}(\eta^2\text{-O}=\text{CHMe})$ (**3**)¹⁴. Over time the reaction goes to completion; even in the presence of added $t\text{BuOHC}=\text{CH}_2$ no equilibrium amount of **2a** was observed.



Scheme 3.9 The $^{31}\text{P}\{^1\text{H}\}$ NMR spectrum of the reaction of **2a** with acetaldehyde at room temperature to give $(\text{Cy}_3\text{P})_2\text{Ni}(\eta^2\text{-O=CHMe})$ (**3**).

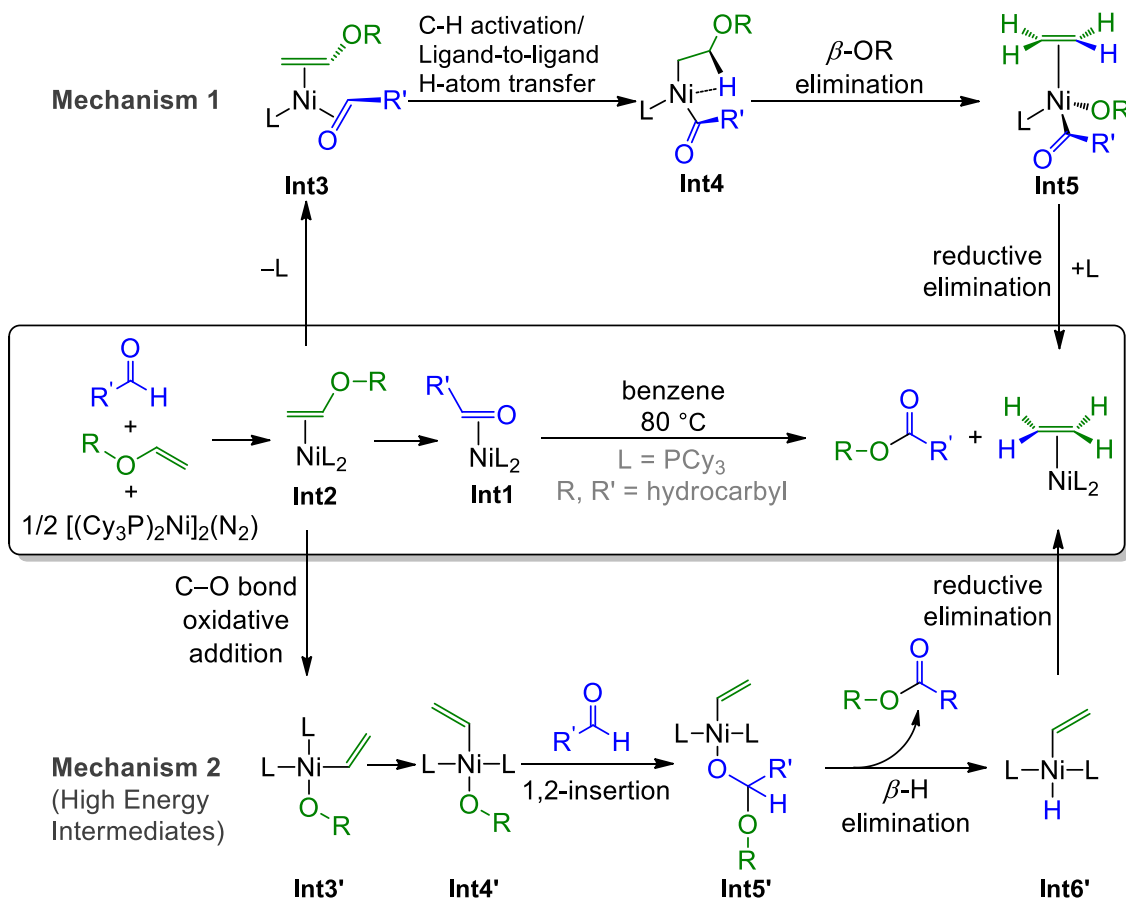
Reaction of $\text{LNi}(0)$ with vinyl ether and acetaldehyde. As shown in **Scheme 3.10 a**, the reaction of $(\text{Cy}_3\text{P})\text{Ni}(\eta^6\text{-PhMe})$ and stoichiometric amount of $t\text{BuOCH=CH}_2$ and O=CHMe produces complex **3** and a new species **4** with a chemical shift of δ 38.2 in $^{31}\text{P}\{^1\text{H}\}$ NMR spectrum. Gentle heating of the reaction solution leads to the decomposition of nickel complexes but not the full conversion of complex **3** to **4**. As shown in **Scheme 3.10**, the singlet peak was not observed in the reaction of $(\text{Cy}_3\text{P})\text{Ni}(\eta^6\text{-PhMe})$ with O=CHMe , ruling out the possibility of $(\text{Cy}_3\text{P})\text{Ni}(\eta^2\text{-O=CMe})_2$. Complex **4** is probably the monophosphine complex $(\text{Cy}_3\text{P})\text{Ni}(\eta^2\text{-O=CHMe})(\eta^2\text{-}t\text{BuOCH=CH}_2)$ (**4**). Further characterizations are needed to verify the structure.



Scheme 3.10 a) The reaction of (Cy₃P)Ni(η⁶-PhMe) with stoichiometric amount of ^tBuOCH=CH₂ and O=CHMe. Both complex **4** and **5** were generated. b) The reaction of (Cy₃P)Ni(η⁶-PhMe) with 2 equivalent of O=CHMe. Only Complex **3** was produced, which rules out the possibility of (Cy₃P)Ni(η²-O=CHMe)₂. * are unidentified products.

Mechanistic Proposals. Two mechanistic manifolds were considered for the coupling of aldehydes and vinyl ethers by Ni(0), as shown in **Scheme 3.11**. The reaction of [(Cy₃P)₂Ni]₂(μ-N₂) (**1**), ^tBuOCH=CH₂ and O=CHMe favours the production of **Int1** over **Int2**, as shown in the central stoichiometric pathway. The upper **Mechanism 1** proceeds by the loss of PCy₃ to give (Cy₃P)Ni(H₂C=CHO^tBu)(O=CHMe) (**Int3**). The bound acetaldehyde can then performs a nickel-mediated ligand-to-ligand hydrogen atom transfer, which is equivalent to a combined C–H bond oxidative addition followed by 1,2-insertion, to give β-agostic **Int4**. The C–O bond activation step then proceeds by β-OR

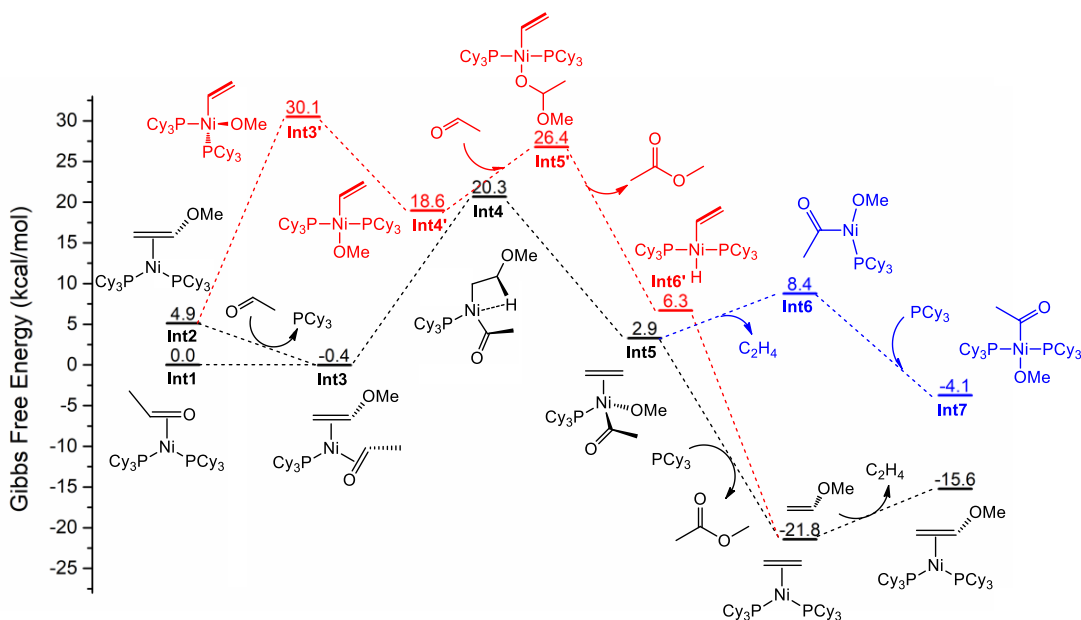
elimination to give Int5. This pathway is analogous to that proposed for catalytic C–H stannylation, germylation and silylation by Ni.³³



Scheme 3.11 Two mechanisms of Ni mediated production of ester from vinyl ether and acetaldehyde, differing by mechanism of the C–O bond cleavage step. **Mechanism 1** features a β -OR elimination step, whereas **Mechanism 2** operates by a more classical C–O bond oxidative addition.

Mechanism 2 proceeds from **Int2** via C–O bond oxidative addition, and then requires insertion of the aldehyde to give **Int5'**, followed by a β -H elimination step to give **Int6'** and the ester product. Reductive elimination from **Int6'** gives $(\text{Cy}_3\text{P})_2\text{Ni}(\eta^2\text{-}$

H₂C=CH₂). The rapid insertion of acetaldehyde into the Ni–OR bond of **Int4'** seems questionable, as it is unlikely to be thermodynamically favourable and would have to proceed more rapidly than favourable β -H elimination from **Int4'**. In order to compare the feasibility of the two proposed mechanisms, DFT calculations were performed. For the sake of calculation resource and time, reactions energies were determined using MeOCH=CH₂ as the vinylmethyl ether. As shown in **Scheme 3.12**, the Gibbs free energy of each intermediate was calculated in kcal/mol.



Scheme 3.12 DFT calculations of intermediates in the 2 plausible mechanisms. Mechanism 2 is in red. Mechanism 1 is shown in black and the blue one is an off-cycle reaction pathway considered in Mechanism 1.

Although these are not the activation energies for reactions that could be used to discriminate preferred pathways, the relative energy of the species involved gives some indication that **Mechanism 1** is the most likely for the coupling of aldehydes and vinyl ethers. In the second mechanism, **Int3'** features a relatively high energy of more than 30 kcal/mol, whereas the highest energy intermediate in **Mechanism 1** is only 20.3 kcal/mol higher energy than **4**. The calculation suggests that **Mechanism 1** is more favoured than

acetaldehyde insertion to vinyl ether. We also calculated another pathway possible for **Int5**. Ethylene dissociates from Ni centre and PCy₃ ligand fill the vacant site. But the energy of **Int6** is much higher than (Cy₃P)₂Ni(η²-CH=CH₂), excluding the possibility of this side reaction. Finally, in order to prove if the reaction has the potential to be optimized to a catalysis, we compared the energies of (Cy₃P)₂Ni(η²-CH=CH₂) and (Cy₃P)₂Ni(η²-MeOCH=CH₂). The energy of (Cy₃P)₂Ni(η²-MeOCH=CH₂) is 6 kcal/mol higher than (Cy₃P)₂Ni(η²-CH=CH₂), which demonstrated that the exchanging may be completed by mild heating. However, experimental study does not match with the calculation result. Starting materials and catalytic amount of [(Cy₃P)₂Ni]₂(μ-N₂) were dissolved in toluene and refluxed for 72 h under N₂ flow. The reactions were monitored by NMR spectroscopy but no sign of ester was observed. In addition, it is noteworthy that the optimized structure of **Int5** has a tetrahedral geometry, which is unusual for a Ni(II) complex. We also calculated the Gibbs free energy of the triplet state of **Int5** and found it to be less stable than its singlet state. Calculations about the transition states is needed to complete the mechanism and help us understand the reaction further.

3.3 Conclusions and Future Work

In this work, Ni mediate alkenyl C(sp²)-O activation was discussed. Unlike the ambiguity about the number of involved ligand in Ni catalyzed aromatic C(sp²)-O activation, alkenyl C(sp²)-O activation starts from a NiL₂ adduction. Ester is produced as the final organic product. We also developed a method of producing asymmetric esters from vinyl ether and acetaldehyde. Tishchenko reaction is usually applied to produce symmetric esters using only one kind of acetaldehyde. It is hard to avoid multiple productions when using 2 kinds of acetaldehydes. The method offered here could produce designated ester by using corresponding ether and ester without separation of byproducts. The DFT study demonstrated that the key step in the mechanism is C-H activation of acetaldehyde and hydroalkylation happened on Ni centre. In-depth DFT study is required to complete the mechanism so that we can better understand the reaction and design

catalytic system in the future. The preparation and characterization of intermediates will offer solid evidence to verify the proposed mechanism.

3.4 Experimental section

3.4.1 General Procedure

All experiments were performed under an N₂ atmosphere using either standard Schlenk techniques or a glovebox unless otherwise mentioned. Dry, oxygen-free solvents were employed throughout. Anhydrous pentane, toluene, benzene and tetrahydrofuran (THF) were purchased from Sigma Aldrich and used as received. All ¹H, ³¹P{¹H}, and ¹³C{¹H} NMR spectra were recorded on a Bruker AMX spectrometer operating at 500 MHz. All chemical shifts are recorded in parts per million, and all coupling constants are reported in hertz. ¹H NMR spectra were referenced to C₆D₆ (δ 7.16), CDCl₃ (δ 7.26) or hexamethyldisiloxane (HMDSO) (δ 0.065) with respect to tetramethylsilane at δ 0.00. ³¹P{¹H} NMR spectra were referenced to an external 85% H₃PO₄ sample at δ 0.00. ¹³C{¹H} NMR spectra were referenced to C₆D₆ (δ 128.05), CDCl₃ (δ 77.16) or HMDSO (δ 1.94)³⁴⁻³⁶. Elemental analyses were performed by the Center for Catalysis and Materials Research, Windsor, Ontario. Tricyclohexylphosphine (PCy₃) was purchased from Oakwood Products, Inc and was deoxygenated under vacuum before use. C₆D₆ and CD₃Cl were purchased from Cambridge Isotope Laboratory. Hexamethyldisiloxane (HMDSO) was purchased from Alfa Aesar. *tert*-butylvinylether, cyclohexylvinylether, vinyloxy-trimethylsilane, ethylvinylether, *n*-propylvinylether, and *n*-butylvinylether were purchased from Sigma Aldrich. These liquid organic compounds were deoxygenated by freeze-pump-thaw three times and dried by passing through a column of activated alumina. Ethyl acetate, acetaldehyde, propyl butyrate, butyl valerate, cyclohexyl acetate, cyclohexanone and acetaldehyde were purchased from Sigma Aldrich and used as received. Celite was purchased from Sigma Aldrich, deoxygenated and dried by heating at 200 °C under vacuum before use. [(Cy₃P)₂Ni]₂(μ-N₂) was prepared using a modification method of Aresta.³⁷ NaK was used as the reducing agent instead of sodium sand.

In the DFT calculations, the M06³⁸ method and the def2svp³⁹ basis set were used.

3.4.2 Synthesis and Characterization of Complexes

Synthesis and Characterization of (Cy₃P)₂Ni(η²-C₂H₃O^tBu) (2a) 0.45 g (0.36 mmol) of [(Cy₃P)₂Ni]₂(μ-N₂) (**1**) was dissolved in 35 mL THF and 0.09 g of *tert*-butylvinyl ether was added to the solution. The colour of the solution turned from dark red to dark yellow. Stirred the solution for 0.5 h and dried the solution under vacuum. Extracted the solid residue by pentane and filter through Celite. Cooled down to -40 °C for 16 h and bright yellow microcrystalline solid precipitated. Collected 0.39 g yellow solid (yield 84.4%). Crystals suitable for single crystal X-ray diffraction was recrystallized from saturated HMDSO solution by slow evaporation at room temperature. ¹H NMR (HMDSO, 500 MHz, 298 K): δ 1.20 (s, 9H, C(CH₃)₃), 1.25-1.55 (m, 30H, CHCH₂), 1.96 (dd, ³J_{HH} = 8.5 Hz, ²J_{HH} = 4.1 Hz, 1H, vinyl-*H*) 1.70-2.07 (m, 36H, CHCH₂CH₂CH₂), 4.39 (ddt, ³J_{HH} = 8.5 Hz, ³J_{HH} = 5.9 Hz, ³J_{HP} = 3.0 Hz, 1H, vinyl-*H*). ³¹P{¹H} NMR (HMDSO, 202.5 MHz, 298 K): δ 36.3 (s). ¹³C{¹H} (HMDSO, 125.8 MHz, 298 K): δ 27.3 (s, CHCH₂CH₂CH₂), 28.4 (vt, ²J_{P-C} + ⁴J_{P-C} = 4.5 Hz, CHCH₂), 28.5 (vt, ²J_{P-C} + ⁴J_{P-C} = 4.5 Hz, CHCH₂), 28.8 (s, CCH₃), 30.9 (s, CHCH₂CH₂), 31.1 (s, CHCH₂CH₂), 37.3 (s, CH), 38.5 (vt, ¹J_{P-C} + ³J_{P-C} = 6.3 Hz, vinyl-CH₂), 73.5 (s, C(CH₃)₃), 81.0 (vt, ¹J_{P-C} + ³J_{P-C} = 9.5 Hz, vinyl-CH). Anal. Calcd for C₄₂H₇₈NiOP₂ (MW 719.71): C, 70.09; H, 10.92. Found: C, 69.68; H, 10.50.

Synthesis and Characterization of (Cy₃P)₂Ni(η²-C₂H₃OCy) (2b) 0.4 g (0.32 mmol) of [(Cy₃P)₂Ni]₂(μ-N₂) (**1**) was dissolved in 30 mL THF and 0.12 g (0.95 mmol) of cyclohexylvinylether was added to the solution. After stirring for 30 min at room temperature, solvent was evaporated under vacuum and the residue was extracted by pentane. Yellow microcrystalline solid precipitated after cooling down to -40 °C for 16 h. Collected the solid by filtration and the yield is 0.36 g (yield 76.7%). ¹H NMR (HMDSO, 500 MHz, 298 K): δ 1.23-1.58 (m, 35H, CHCH₂), 1.61 (dd, ³J_{HH} = 9.2 Hz, ²J_{HH} = 4.5 Hz, 1H, vinyl-*H*), 1.68-2.02 (m, 42H, CHCH₂CH₂CH₂), 3.38 (ddt, ³J_{HH} = 3.6 Hz, ²J_{HH} = 4.5 Hz, ³J_{HP} = 8.0 Hz, 1H, vinyl-*H*), 4.46 (ddt, ³J_{HH} = 3.6 Hz, ³J_{HH} = 9.2 Hz, ³J_{HP} = 4.6 Hz, 1H, vinyl-*H*). ³¹P{¹H} NMR (HMDSO, 202.5 MHz, 298 K): δ 36.8 (s). ¹³C{¹H} (HMDSO, 125.8 MHz, 298 K): δ 24.2 (s, OCHCH₂CH₂CH₂), 26.8 (s, OCHCH₂CH₂), 27.3 (s, PCHCH₂CH₂CH₂), 28.46 (vt, ²J_{P-C} + ⁴J_{P-C} = 4.7 Hz, PCHCH₂), 28.53 (vt, ²J_{P-C} + ⁴J_{P-C} = 4.7

Hz, PCHCH₂), 30.98 (s, PCHCH₂CH₂/CHCH₂), 31.09 (s, CHCH₂CH₂/CHCH₂), 32.4 (s, OCHCH₂), 35.1 (vt, ¹J_{P-C} + ³J_{P-C} = 6.3 Hz, vinyl-CH₂), 37.3 (br, PCH), 79.1 (m, OCH), 87.4 (vt, ¹J_{P-C} + ³J_{P-C} = 10.0 Hz, vinyl-CH). Anal. Calcd for C₄₄H₈₀NiOP₂ (MW 745.74): C, 70.87; H, 10.81. Found: C, 70.39; H, 11.02.

Synthesis and Characterization of (Cy₃P)₂Ni(η²-C₂H₃OSiMe₃) (2c) 0.4 g (0.32 mmol) of [(Cy₃P)₂Ni]₂(μ-N₂) (**1**) was dissolved in 30 mL THF and 0.11 g (0.95 mmol) of trimethylsilylvinylether was added to the solution. After stirring for 30 min at room temperature, solvent was evaporated under vacuum and the residue was extracted by pentane. Yellow microcrystalline solid precipitated after cooling down to -40 °C for 16 h. Collected the solid by filtration and the yield is 0.32 g (yield 67.9%). ¹H NMR (HMDSO, 500 MHz, 298 K): δ 0.10 (s, 9H, Si(CH₃)₃), 1.25-1.55 (m, 30H, CHCH₂), 1.59 (dd, ²J_{HH} = 8.3 Hz, ³J_{HH} = 5.0 Hz, 1H, vinyl-H), 1.73-1.99 (m, 36H, CHCH₂CH₂CH₂), 4.65 (ddt, ³J_{HH} = 8.2 Hz, ³J_{HH} = 5.0 Hz, ³J_{HP} = 5.6 Hz, 1H, vinyl-H). ³¹P{¹H} NMR (HMDSO, 202.5 MHz, 298 K): δ 36.7 (s). ¹³C{¹H} (HMDSO, 125.8 MHz, 298 K): δ 27.4 (s, CHCH₂CH₂CH₂), 28.4 (vt, ²J_{P-C} + ⁴J_{P-C} = 4.5 Hz, CHCH₂), 28.5 (vt, ¹J_{P-C} + ³J_{P-C} = 4.5 Hz, CHCH₂CH₂/CHCH₂), 28.8 (s, CCH₃), 30.9 (s, CHCH₂CH₂/CHCH₂), 31.1 (s, CHCH₂CH₂/CHCH₂), 37.3 (s, CH), 38.5 (vt, ¹J_{P-C} + ³J_{P-C} = 6.3 Hz, vinyl-CH₂), 73.5 (s, C(CH₃)₃), 81.0 (vt, ¹J_{P-C} + ³J_{P-C} = 9.5 Hz, vinyl-CH). Anal. Calcd for C₂₄H₇₈NiOP₂ (MW 503.51): C, 57.25; H, 15.61. Found: C, 56.73; H, 15.78.

3.4.3 Equilibrium Study

2a and 3 10 mg (Cy₃P)₂Ni(η²-C₂H₃O^tBu) (**2a**) (0.014 mmol) was fully dissolved in 0.5 mL THF. 42 mg ^tBuOCH=CH₂ (0.42 mmol) and 18 mg O=CHMe (0.42 mmol) was added to the solution. Only **3** was observed in ³¹P{¹H} NMR spectrum, which proved that there is no equilibrium between **2a** and **3**.

2a and (Cy₃P)Ni(η⁶-PhMe) 42 mg ^tBuOCH=CH₂ (0.42 mmol), 39 mg PhMe (0.42 mmol) and 10 mg (Cy₃P)₂Ni(η²-C₂H₃O^tBu) (0.014 mmol) was fully dissolved in mL ^tBuOCH=CH₂ stock solution. The reaction reached to the equilibrium after 6 h at room

temperature. The ratio of 2a and (Cy₃P)Ni(η⁶-PhMe) is 91: 9 according to the integral of the ³¹P{¹H} NMR spectrum.

3.4.4 The Synthesis and Characterization of Organic Products from Vinyl Ethers and [(Cy₃P)₂Ni](μ-N₂) (1)

General Procedure A 28 mg (0.02 mmol) of **1** and 0.05 mmol vinyl ether were dissolved in 0.6 ml C₆D₆ in a J. Young tube. The solution was refluxed gently in an oil bath for 12 h. The reaction solution was cooled down to room temperature, filtered it and characterized the organic products by ¹³C NMR spectroscopy.

General Procedure B 28 mg (0.02 mmol) of **1**, 3 μL (0.05 mmol) acetaldehyde and 0.05 mmol vinyl ether were dissolved in 0.6 ml C₆D₆ in a J. Young tube. The solution was refluxed gently in an oil bath for 12 h. The reaction solution was cooled down to room temperature, filtered and characterized the organic products by ¹³C NMR spectroscopy.

Cyclohexanone Procedure A. ¹³C{¹H} (C₆D₆, 125.8 MHz, 298 K): δ 25.1 (s, CCH₂CH₂CH₂), 27.1 (s, CCH₂CH₂), 41.9 (s, CCH₂), 209.1 (s, CO).

Ethyl acetate Procedure A. ¹³C{¹H} (C₆D₆, 125.8 MHz, 298 K): δ 14.1 (s, OCH₂CH₃), 20.9 (s, CCH₃), 60.1 (s, OCH₂), 170.4 (s, carbonyl-CO).

Propyl ester Procedure A. ¹³C{¹H} (C₆D₆, 125.8 MHz, 298 K): δ 13.76 (s, OCH₂CH₂CH₃), 13.83 (s, CCH₂CH₃), 19.5 (s, OCH₂CH₂), 27.0 (s, CCH₂), 63.9 (s, OCH₂), 172.8 (s, carbonyl-CO).

Butyl ester Procedure A. ¹³C{¹H} (CDCl₃, 125.8 MHz, 298 K): δ 14.1 (s, CH₃), 18.5 (s, OCH₂CH₂CH₂), 19.2 (s, CCH₂CH₂), 22.8 (s, OCH₂CH₂), 31.7 (s, CCH₂), 36.4 (s, OCH₂CH₂), 64.2 (s, OCH₂), 174.0 (s, carbonyl-CO).

Cyclohexyl acetate Procedure B. ¹³C{¹H} (CDCl₃, 125.8 MHz, 298 K): δ 21.6 (s, CHCH₂CH₂CH₂), 24.0 (s, CHCH₂CH₂), 25.5 (s, CHCH₂), 31.8 (s, CH), 72.8 (s, OCH₃), 170.8 (s, carbonyl-CO)

Tert-Butyl acetate Procedure B. $^{13}\text{C}\{^1\text{H}\}$ (C_6D_6 , 125.8 MHz, 298 K): δ 20.1 (s, OCH₃), 49.3 (s, CCH₃), 170.0 (s, carbonyl-CO).

3.5 X-ray Crystallography

Table 3.1 Crystallographic Data for Complex **2a**

Compound	2a
Chemical Formula	C ₄₂ H ₇₈ NiOP ₂
Formula Weight	719.71
Temp	170 K
Crystal system	Monoclinic
Space group	P 2 ₁ /c
a/ Å	16.0021(19)
b/ Å	13.4384(15)
c/ Å	19.432(2)
α/ °	90
β/ °	96.677(3)
γ/ °	90
V/ Å ³	4150.4(8)
Z	4
D _{calc} /g cm ⁻³	1.152
μ(Mo-Kα) / mm ⁻¹	0.574
F(000)	1584.0
Reflection collected	116646
Independent reflections	9528
R(int)	5.14
R1 (I > 2σ(I))	3.17
R1(all)	
wR2(all)	7.91
GOF	1.028

R1: also known as the R-value, represents the agreement between calculated and observed models.

wR2: similar to R1, but refers to squared F-values.

GOF: goodness of fit parameter.

3.6 References

1. Y. Gu and R. Martin, *Angew. Chem. Int. Ed.*, 2017, **56**, 3187-3190.
2. L. Guo, X. Liu, C. Baumann and M. Rueping, *Angew. Chem. Int. Ed.*, 2016, **55**, 15415-15419.
3. M. R. Harris, L. E. Hanna, M. A. Greene, C. E. Moore and E. R. Jarvo, *J. Am. Chem. Soc.*, 2013, **135**, 3303-3306.
4. N. Iranpoor and F. Panahi, *Org. Lett.*, 2015, **17**, 214-217.
5. M. Tobisu, T. Takahira, T. Morioka and N. Chatani, *J. Am. Chem. Soc.*, 2016, **138**, 6711-6714.
6. J. Xiao, J. Yang, T. Chen and L. B. Han, *Chem. Commun.*, 2016, **52**, 2157-2160.
7. B. Yang and Z. X. Wang, *J. Org. Chem.*, 2017, **82**, 4542-4549.
8. H. Yue, L. Guo, H. H. Liao, Y. Cai, C. Zhu and M. Rueping, *Angew. Chem. Int. Ed.*, 2017, **56**, 4282-4285.
9. S.-Q. Zhang, B. L. H. Taylor, C.-L. Ji, Y. Gao, M. R. Harris, L. E. Hanna, E. R. Jarvo, K. N. Houk and X. Hong, *J. Am. Chem. Soc.*, 2017, **139**, 12994-13005.
10. H. Xie, Y. Li, L. Wang, J. Kuang, Q. Lei and W. Fang, *Dalton Trans.*, 2017, **46**, 13010-13019.
11. M. C. Schwarzer, R. Konno, T. Hojo, A. Ohtsuki, K. Nakamura, A. Yasutome, H. Takahashi, T. Shimasaki, M. Tobisu, N. Chatani and S. Mori, *J. Am. Chem. Soc.*, 2017, **139**, 10347-10358.
12. H. Ogawa, H. Minami, T. Ozaki, S. Komagawa, C. Wang and M. Uchiyama, *Chemistry*, 2015, **21**, 13904-13908.

13. X. Hong, Y. Liang and K. N. Houk, *J. Am. Chem. Soc.*, 2014, **136**, 2017-2025.
14. J. Cornella, E. Gomez-Bengoia and R. Martin, *J. Am. Chem. Soc.*, 2013, **135**, 1997-2009.
15. Z. Li, S.-L. Zhang, Y. Fu, Q.-X. Guo and L. Liu, *J. Am. Chem. Soc.*, 2009, **131**, 8815-8823.
16. X. Li and X. Hong, *J. Organomet. Chem.*, 2018, **864**, 68-80.
17. P. W. Jolly and K. Jonas, *Angew. Chem. Int. Ed.*, 1968, **7**, 731-732.
18. S. Zhu, M. M. Shoshani and S. A. Johnson, *Chem. Commun.*, 2017, **53**, 13176-13179.
19. L. Guo, X. Liu, C. Baumann and M. Rueping, *Angew. Chem. Int. Ed.*, 2016, **55**, 15415-15419.
20. B. J. Li, Y. Z. Li, X. Y. Lu, J. Liu, B. T. Guan and Z. J. Shi, *Angew. Chem. Int. Ed.*, 2008, **47**, 10124-10127.
21. B. J. Li, D. G. Yu, C. L. Sun and Z. J. Shi, *Chem. Eur. J.*, 2011, **17**, 1728-1759.
22. T. Shimasaki, Y. Konno, M. Tobisu and N. Chatani, *Org. Lett.*, 2009, **11**, 4890-4892.
23. L. G. Xie and Z. X. Wang, *Chem. Eur. J.*, 2011, **17**, 4972-4975.
24. S. Ogoshi, Y. Hoshimoto and M. Ohashi, *Chem. Commun.*, 2010, **46**, 3354-3356.
25. V. E. Tishchenko, *Journal of the Russian Physico-Chemical Society*, 1906, **38**, 355-418.
26. Y. Hoshimoto, M. Ohashi and S. Ogoshi, *J. Am. Chem. Soc.*, 2011, **133**, 4668-4671.
27. M. R. Elsby and S. A. Johnson, *J. Am. Chem. Soc.*, 2017, **139**, 9401-9407.

28. C. Leibold and H. Oberhammer, *J. Am. Chem. Soc.*, 1998, **120**, 1533-1537.
29. D. Brauer and C. Krüger, *Inorg. Chem.*, 1977, **16**, 884-891.
30. A. P. Jarvis, D. M. Haddleton, J. A. Segal and A. McCamley, *Dalton Trans.*, 1995, 2033-2040.
31. G. D. Jones and D. A. Vasic, *Organometallics*, 2005, **24**, 3821-3823.
32. M. Ohashi, T. Taniguchi and S. Ogoshi, *J. Am. Chem. Soc.*, 2011, **133**, 14900-14903.
33. M. R. Elsby, J. Y. Liu, S. Zhu, L. F. Hu, G. P. Huang and S. A. Johnson, *Organometallics*, 2019, **38**, 436-450.
34. M. A. Farag, A. Porzel, E. A. Mahrous, M. Mo'men and L. A. Wessjohann, *Anal. Bioanal. Chem.*, 2015, **407**, 1937-1949.
35. T. Kitayama and K. Hatada, *NMR spectroscopy of polymers*, Springer Science & Business Media, 2013.
36. S. Losio, G. Leone, F. Bertini, G. Ricci, M. C. Sacchi and A. C. Boccia, *Polym. Chem.*, 2014, **5**, 2065-2075.
37. M. Aresta, C. Nobile and A. Sacco, *Inorganica Chim. Acta*, 1975, **12**, 167-178.
38. Y. Zhao, D. G. Truhlar, *Theor. Chem. Acc.*, 2008, **120**, 215-241.
39. F. Weigend and R. Ahlrichs, *Phys. Chem. Chem. Phys.*, 2005, **7**, 3297-3305.

Chapter 4 The Formation of Nickel Hydride Clusters:

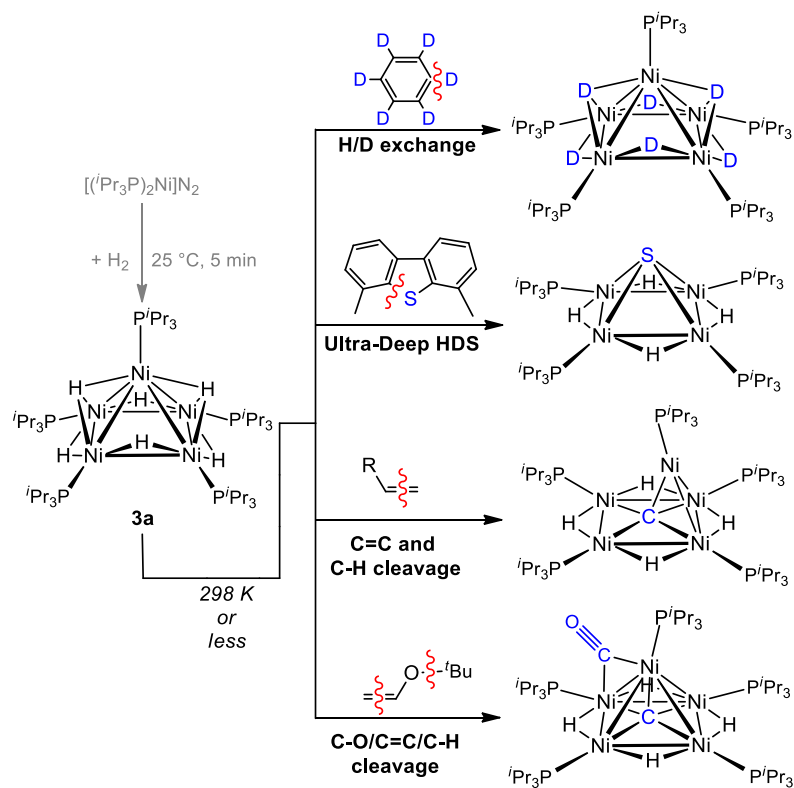
Influence of Phosphines and Intermediates

4.1 Introduction

Transition metal hydride clusters have a history of more than 80 years¹. They were first synthesized from late metal carbonyl complexes through protonation by acids or oxidative addition to hydrogen sources.²⁻⁷ More recently, the trend of research is moving to non-carbonyl transition metal clusters supported by tertiary phosphines, cyclopentadienyl or hydride ligand because such type of clusters are usually electron deficient, which featuring them unique properties and reactivities. They can be applied in various fields such as in cooperative catalysis,⁸⁻¹³ electrochemistry,¹⁴⁻¹⁶ surface chemistry,¹⁷⁻²⁰ etc. Cluster mediated cooperative catalysis in particular is expanding rapidly because of its ability to efficiently activate and functionalize inert bonds that are hard to be cleaved by other type of catalysts.

First-row transition metals have received increased attention in catalysis and bond activation chemistry, due to the higher earth abundance of these metals. Their abundance provides a lower price comparing to second- and third-row transition metals and improved sustainability; however, these metals of less reactive for typical inert-bond activation reactions like C–H activation, and are thus limited in scope for these modern applications. Cooperative reactivity is a commonly posited approach for overcoming first-row transition

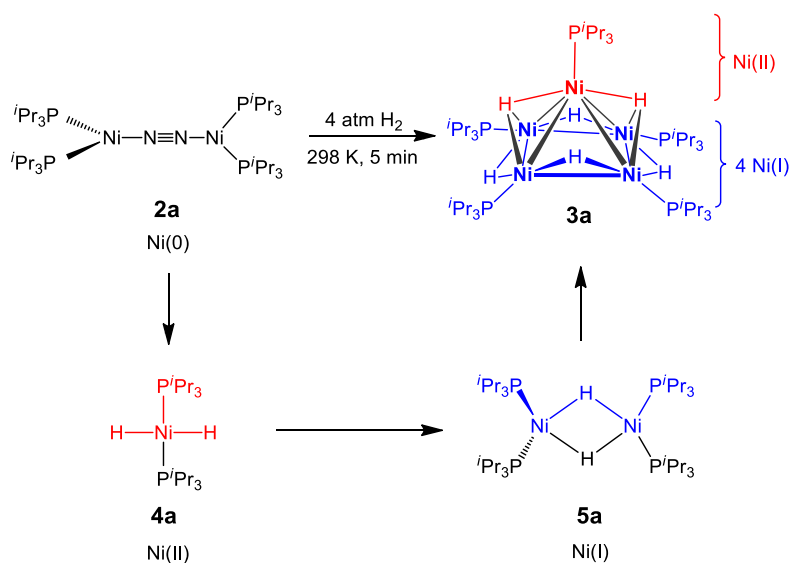
metals diminished abilities in bond-activation. Cooperativity is used to describe scenarios where multiple metals work together to assist in reactions. Cluster chemistry provides an obvious entry to complexes capable of cooperative activation of traditionally unreactive substrates. Many clusters supported by ligands like carbonyls feature great stability, but with increased stability often comes lackluster reactivity. Such complexes typically have a large HOMO-LUMO gap offered by strong field ligands and favourable valence electron counts.



Scheme 4.1 Synthesis and selected reactivity of the pentanuclear nickel hydride cluster $[(iPr_3P)_2Ni]_2(\mu-N_2)$ (**2a**).

There are only a handful of examples of clusters supported by only hydrides and phosphine donors, which includes examples with late first-row transition metals such as Co and Ni. These clusters have unusually low valence electron counts that could signal potential for reactivity. In 2012, our group reported the synthesis of the

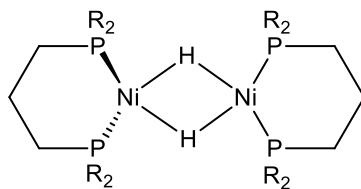
triisopropylphosphine supported pentanuclear nickel hydride cluster, $[(i\text{Pr}_3\text{P})\text{Ni}]_5\text{H}_6$ (**3a**).²¹ As shown in **Scheme 4.1**, the reaction of H_2 gas with the Ni(0) dinitrogen complex $[(i\text{Pr}_3\text{P})_2\text{Ni}]_2(\mu\text{-N}_2)$ (**2**)²² leads to the clean assembly of cluster **3a**. Complex **3a** is capable of a wide range of inert bond activation reactions under ambient conditions, which include H/D exchange,²³ C=C,²⁴ C–O, C–H²⁵ and C–S²⁶ bond cleavage. Remarkably, complex **3a** features considerable functional group tolerance, selectively performing carbon atom abstraction from alkenes even in the presence of typically more reactive species like amines or even water.



Scheme 4.2 Plausible mechanism of the formation of complex **3a** from **2a** under 4 atm H_2 atmosphere.

The mechanistic study about clusters is still at its early stage and has not made much progress yet, which hindered the advanced development of transition metal cluster chemistry and its further applications in industry. Also, the study of how the ancillary ligands influence the synthesis of clusters is absent to the best of our knowledge. In this chapter, we tested the scope of tertiary phosphines that could help stabilize a $(\text{LNi})_5\text{H}_6$ (L = tertiary phosphine ligand) style cluster. We also did mechanistic study by monitoring the

reaction of H₂ gas and complex **2a** or its derivatives and assigned and characterized one of the intermediates.



Barnett et al. Chem. Ber **1977**, 3900

Figure 4.1 The structure of L₂Ni(μ-H)₂ synthesized by Barnett and co-workers in 1977.

As shown in **Scheme 4.2**, we raised a plausible mechanism of the formation of cluster **3a** based on the nickel moieties in the cluster. The pentanuclear complex is basically composed of a capping moiety and four basal fragments with each nickel atom is supported by a P^{*i*}Pr₃P ligand. The capping nickel is bound by two hydride ligands, so it could arise a *trans*-(^{*i*}Pr₃P)NiH₂ complex (**4a**) with one of the phosphine ligand replaced by the basal part. Each two adjacent nickel atoms are bridged by one μ-H ligand, which resemble the structure of a known dinuclear nickel complex, (L₂)₂Ni(μ-H)₂, where L₂ is a bidentate phosphine ligand (the chemical structure is shown in **Figure 1.1**.²⁷ Based on the properties of the cluster, we proposed that two intermediates, *trans*-(^{*i*}Pr₃P)₂NiH₂ (**4a**) and [(^{*i*}Pr₃P)₂Ni]₂(μ-H)₂ (**5a**) formed first when complex **2a** was exposed to H₂ environment. Two [(^{*i*}Pr₃P)₂Ni]₂(μ-H)₂ (**5a**) consisted the base of the cluster. One of the phosphine ligand of *trans*-(^{*i*}Pr₃P)₂NiH₂ (**4a**) dissociated and the (^{*i*}Pr₃P)NiH₂ moiety capped the base and generated the final product. However, there is no promising experimental evidence so far to support this mechanism.

4.2 Results and Discussion

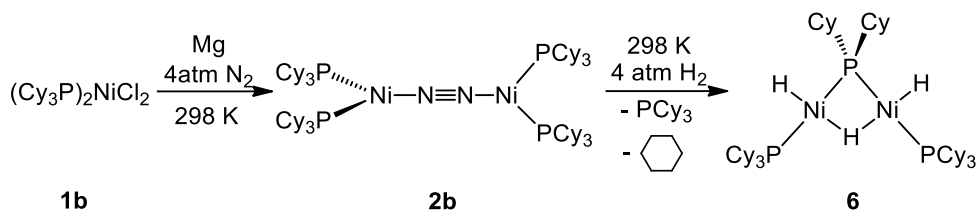
4.2.1 Phosphine Scope

Table 4.1 Key Physical Parameters of Phosphines

Phosphine	Cone Angle ($^{\circ}$) ²⁸	% V_{bur} ²⁹	Electronic Parameter (cm^{-1})
PEt ₃	132	32.7	2062
PPh ₃	145	34.5	2069
PCy ₂ Me	146	33.4	2056
P ⁱ Pr ₂ Et	151	36.0	2056
PⁱPr₃	160	37.6	2059
PCy ₃ /PCyp ₃	160	37.1	2056
P ^t Bu ₂ Me	161	37.0	2059
P ^t Bu ₂ Et	165	39.2	2060

In the case of our phosphine supported nickel cluster, it might be expected that steric constraints are important for the formation of these clusters. With large phosphines there is not enough space to form a pentanuclear cluster, which may lead to the formation of a complex with lesser nuclearity; with small phosphines it may be harder for phosphine ligands to depart from the Ni(I) intermediate to build up the base of the cluster. To extend the range of the phosphines, find out the upper and lower limits in terms of steric effect and study the similarities and differences of them in the preparation of polynuclear complexes, we started the study from the phosphines with similar Tolman cone angles^{28, 30} and percentage buried volumes (% V_{bur})²⁹ to PⁱPr₃, followed by phosphines with obviously larger or smaller steric hindrance. The phosphines and their important physical parameters are listed in **Table 4.1** and the result of each phosphine will be discussed in detail in the following paragraphs.

4.2.1.1 Hydrogenation of Tricyclohexylphosphine Supported Ni(0)



Scheme 4.3 The synthesis of **6** from **2b** under 4 atm H₂ atmosphere.

The phosphines ⁱPr₃P and Cy₃P have similar electronic parameters of 2056 and 2059 cm⁻¹ and steric parameters. Both phosphines have Tolman cone angles near 160° and % V_{bur} of 32.3 and 31.8% respectively, as shown in **Table 4.1**. These standard measures of phosphine donors suggest that they should support similar Ni hydride chemistry, but this did not prove to be true. The PCy₃ supported Ni(0) chemistry was easily accessed via the known complex, [(Cy₃P)₂Ni]₂(μ-N₂) (**2b**), the first synthesized and characterized Ni(0) dinitrogen complex.³¹ Complex **2b** was synthesized by a modification to the literature procedure,⁵ using sodium-potassium alloy (NaK) for the reduction of (Cy₃P)₂NiCl₂ (**1b**). Unlike (iPr₃P)₂NiCl₂ (**1a**) the more convenient reductant of freshly ground Mg failed to reduce **1b**.

Instead of the anticipated pentanuclear hydride cluster, the reaction of **2b** and H₂ gas produced a dinuclear Ni(II) hydride complex, [(Cy₃P)HNi]₂(μ-PCy₂)(μ-H) (**6**). The complex is thermally stable at room temperature over a period of months. The electron counting of each Ni nucleus is 16 e⁻. X-ray quality dark yellow crystals were recrystallized from pentane at -40 °C with a moderate yield of 35.4%. The solid-state molecular structure and selected bond lengths and angles are shown in **Figure 4.2**. Ni, P atoms and hydride ligands are all in the same plane and both nickels are square planar, bridged by a μ-PCy₂ moiety and a μ-H ligand. The molecule has approximate C_{2v} symmetry.

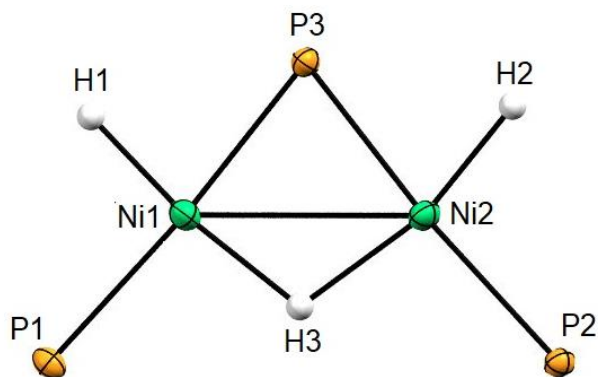


Figure 4.2 ORTEP depiction of **6**. The cyclohexyl groups are omitted for clarity. Selected bond distances (unit: Å): Ni(1)-H(1) = 1.52(2); Ni(1)-H(3) = 1.67; Ni(2)-H(2) = 1.47; Ni(2)-H(3) = 1.59(2); Ni(1)-P(1) = 2.1689(5); Ni(1)-P(3) = 2.0960(4); Ni(2)-P(2) = 2.1709(6); Ni(2)-P(3) = 2.1039(6). Selected bond angles (unit: °): P(3)-Ni(1)-H(3) = 88.2(7)°; P(3)-Ni(2)-H(3) = 90.0(8)°; Ni(1)-P(3)-Ni(2) = 76.22(2)°; Ni(1)-H(3)-Ni(2) = 106(1)°; H(1)-Ni(1)-P(3) = 76.8(8)°; H(2)-Ni(2)-P(3) = 82.1(8)°; H(3)-Ni(1)-P(1) = 96.6(7)°; H(3)-Ni(2)-P(2) = 94.1(8)°.

The $^{31}\text{P}\{^1\text{H}\}$ NMR chemical shifts of the terminal phosphines (P1 and P2) and bridging phosphide (P3) were observed at δ 50.8 and 155.8, respectively. The peaks of terminal hydride (H1 and H2) and bridging hydride (H3) ligands in ^1H NMR were observed at δ -9.18 and -12.85, respectively. The terminal hydrides give a second-order AA'XX'Z multiplet due to the magnetic inequivalence of the terminal phosphines. The simulated ^1H NMR of hydrides of complex **6** is compared to the experimental spectrum shown in **Figure 4.3**, and provides an excellent fit using the coupling constants $^2J_{\text{H1H3}} = ^2J_{\text{H2H3}} = 10.9$ Hz; $^2J_{\text{H3P3}} = 32.2$ Hz; $^2J_{\text{H3P1}} = ^2J_{\text{H3P2}} = 16.8$ Hz; $^2J_{\text{H1P1}} = ^2J_{\text{H2P2}} = 28.5$ Hz; $^2J_{\text{H1P2}} = ^2J_{\text{H2P1}} = 8.0$ Hz; $^2J_{\text{H1P3}} = ^2J_{\text{H2P3}} = 41.0$ Hz.

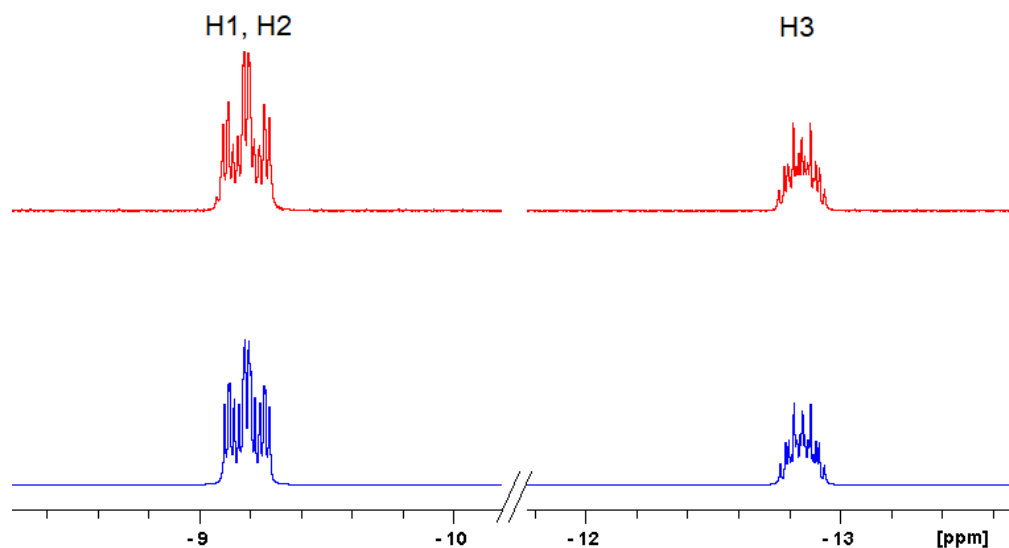
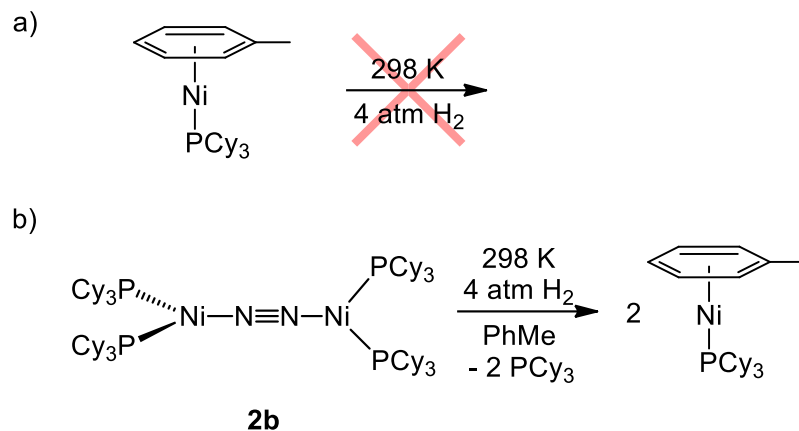


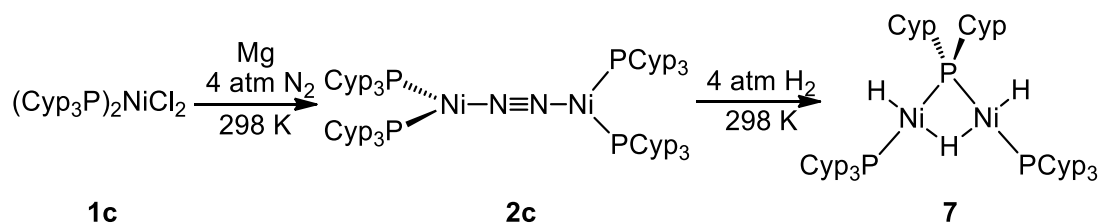
Figure 4.3 The experimental (red) and modeled (blue) hydride ligands peaks in ^1H NMR spectrum of **6**. The modelling software is Bruker TopSpin 4.0.6.

As shown in **Scheme 4.4a**, the monophosphine nickel complex $(\text{Cy}_3\text{P})\text{Ni}(\eta^6\text{-PhMe})$ was also tested as a Ni(0) source for hydride chemistry.³² This easily prepared precursor has the advantage of bearing a single phosphine donor, which is ideal for the preparation of clusters like complex **2a** that also features a single phosphine per Ni. Remarkably, no reaction was observed when a THF solution of $(\text{Cy}_3\text{P})\text{Ni}(\eta^6\text{-PhMe})$ was exposed to H_2 . Furthermore, as shown in **Scheme 4.4b**, when the dinitrogen complex **2b** was dissolved in toluene, which generates $(\text{Cy}_3\text{P})\text{Ni}(0)(\eta^6\text{-PhMe})$ and PCy_3 *in situ* (see Chapter 2), no reaction with H_2 was observed, in contrast to the formation of **6** observed in THF. The low reactivity of the $(\text{Cy}_3\text{P})\text{Ni}(\eta^6\text{-PhMe})$ suggests that concerted oxidative addition to this species must feature a large barrier.



Scheme 4.4 a) The reaction of $(\text{C}_3\text{H}_5)_3\text{P}(\eta^6\text{-PhMe})\text{Ni}$ with 4 atm H_2 gas does not produce polynuclear nickel hydride complexes. b) The reaction of **2b** with 4 atm H_2 gas in toluene only produces $(\text{C}_3\text{H}_5)_3\text{P}(\eta^6\text{-PhMe})\text{Ni}$.

4.2.1.2 Hydrogenation of Tricyclopentylphosphine Supported Ni(0)

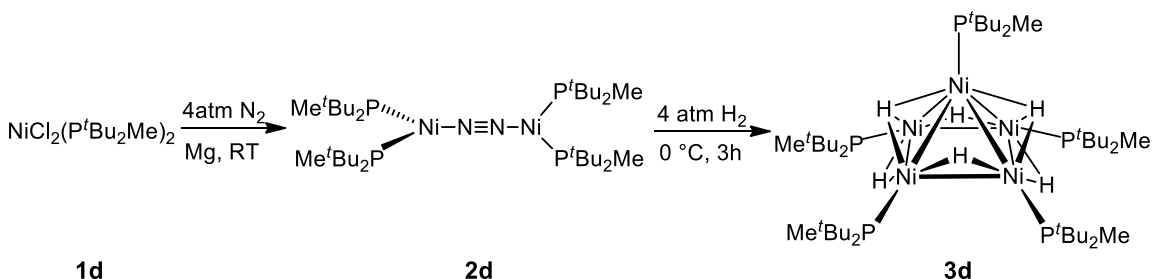


Scheme 4.5 The synthesis of **7** from **2c** under 4 atm H_2 atmosphere.

As shown in **Scheme 4.5**, the second phosphine studied was tricyclopentylphosphine (PCyp_3), which has similar physical and chemical properties to PCy_3 . $\text{NiCl}_2(\text{PCyp}_3)_2$ (**1c**) was reduced by activated Mg over a period of 16 hours and produced $[(\text{Cyp}_3\text{P})_2\text{Ni}]_2(\mu\text{-N}_2)_2$ (**2c**). The reaction of **2c** with H_2 gas under 4 atm pressure in pentane produced the PCyp_3 analogue of **6**, $[(\text{Cyp}_3\text{P})\text{HNi}]_2(\mu\text{-PCyp}_2)(\mu\text{-H})$ (**7**). Dark yellow cubic crystals suitable for single crystal diffraction were recrystallized from pentane after cooling down to $-40\text{ }^\circ\text{C}$ for 7 days. The yield of **7** was much lower than **6** because of unidentified side reactions. The solid structure highly resembles complex **6**. The chemical shifts of terminal and bridging hydride ligands were observed at $\delta -8.71$ and -12.13 ,

respectively. The terminal hydride peak is also second-order because of the magnetically inequivalent P atoms. The chemical shifts of terminal and bridging phosphorus in $^{31}\text{P}\{^1\text{H}\}$ were observed at δ 51.2 and 162.0, respectively.

4.2.1.3 The Preparation of Pentanuclear Cluster from Di-tert-butylmethylphosphine Supported Dinitrogen Complex



Scheme 4.6 The synthesis of the pentanuclear nickel cluster **3d** under from **2d** under 4 atm H_2 atmosphere.

As shown in **Table 4.1**, di-tert-butylmethylphosphine ($\text{P}^t\text{Bu}_2\text{Me}$) has a Tolman cone angle similar to P^iPr_3 , PCy_3 and PCyp_3 . We adopted the same methodology of the preparation of **2a-c** and successfully synthesized the dinitrogen complex $[(^t\text{Bu}_2\text{MeP})_2\text{Ni}]_2(\mu\text{-N}_2)$ (**2d**) from $[(^t\text{Bu}_2\text{MeP})_3\text{P}]_2\text{NiCl}_2$ (**1d**), using activated Mg as the reducing agent. The full reduction of **1d** to $\text{L}_2\text{Ni}(0)$ complex was completed in only 1 hour at 298 K under 4 atm N_2 environment, which is only 1/3 of the time needed to fully reduce complex **1a**. When the pentane solution of **2d** was exposed to 4 atm H_2 environment, the $\text{P}^t\text{Bu}_2\text{Me}$ analogue of **3a**, $[(^t\text{Bu}_2\text{MeP})\text{Ni}]_5\text{H}_6$ (**3d**) was generated (shown in **Scheme 4.6**). The synthesis of **3d** in benzene or toluene proved to be a failure because of the generation of $(^t\text{Bu}_2\text{MeP})\text{Ni}(\eta^6\text{-arene})$ which has been proved to be not reactive to H_2 gas. Complex **3d** is even more thermally sensitive than **3a**. In solid state, complex **3d** completely decomposed to nickel metal and phosphine over one week at room temperature under N_2 gas atmosphere. The preparation of **3d** has to be performed at a temperature as low as -15

°C. Dark brown cubic crystals suitable for single crystal X-ray diffraction were recrystallized from the pentane solution of the reaction at -40 °C with a yield of 20.4%.

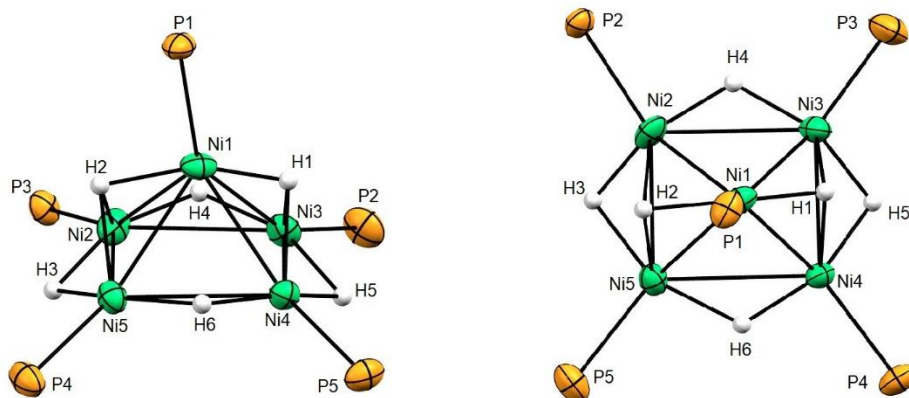


Figure 4.4 Solid state molecular structure of cluster **3d** was determined by single crystal X-ray diffraction. Both side view (left) and top view (right) are shown here. *Tert*-butyl and methyl groups are omitted for clarity. Selected bond distances (unit: Å): Ni(1)-Ni(2) = 2.4279(6); Ni(1)-Ni(3) = 2.4621(6); Ni(1)-Ni(4) = 2.4167(8); Ni(1)-Ni(5) = 2.4477(7); Ni(2)-Ni(3) = 2.6353(6); Ni(2)-Ni(5) = 2.4021(8); Ni(3)-Ni(4) = 2.3936(8); Ni(4)-Ni(5) = 2.6656(6); Ni(1)-P(1) = 2.218(2); Ni(2)-P(2) = 2.199(2); Ni(3)-P(3) = 2.189(1); Ni(4)-P(4) = 2.175(1). Selective bond angles (unit: °): Ni(2)-Ni(3)-Ni(4) = 90.43(2)°; Ni(3)-Ni(4)-Ni(5) = 89.72(2)°; Ni(4)-Ni(5)-Ni(2) = 89.52(2)°; Ni(5)-Ni(2)-Ni(3) = 90.25(2)°; Ni(2)-Ni(1)-Ni(4) = 95.05(2)°; Ni(3)-Ni(1)-Ni(5) = 93.41(2)°; Ni(2)-Ni(1)-Ni(3) = 65.21(2)°; Ni(3)-Ni(1)-Ni(4) = 58.75(2)°; Ni(4)-Ni(1)-Ni(5) = 66.45(2)°; Ni(5)-Ni(1)-Ni(2) = 59.03(2)°.

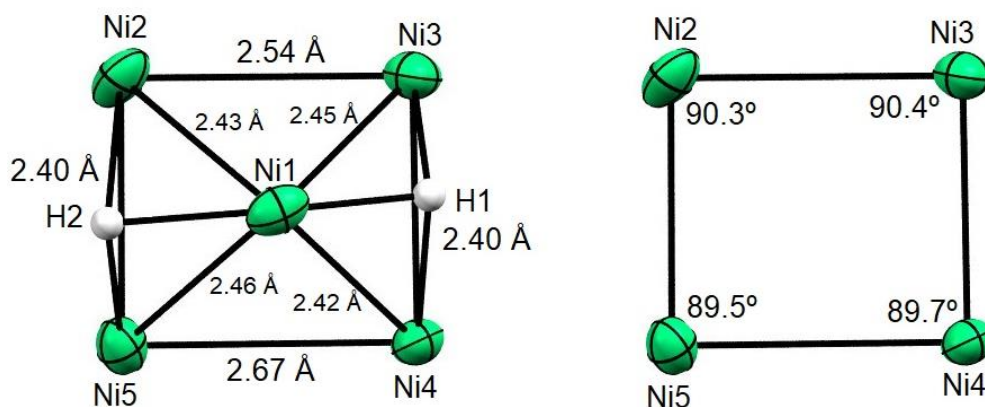
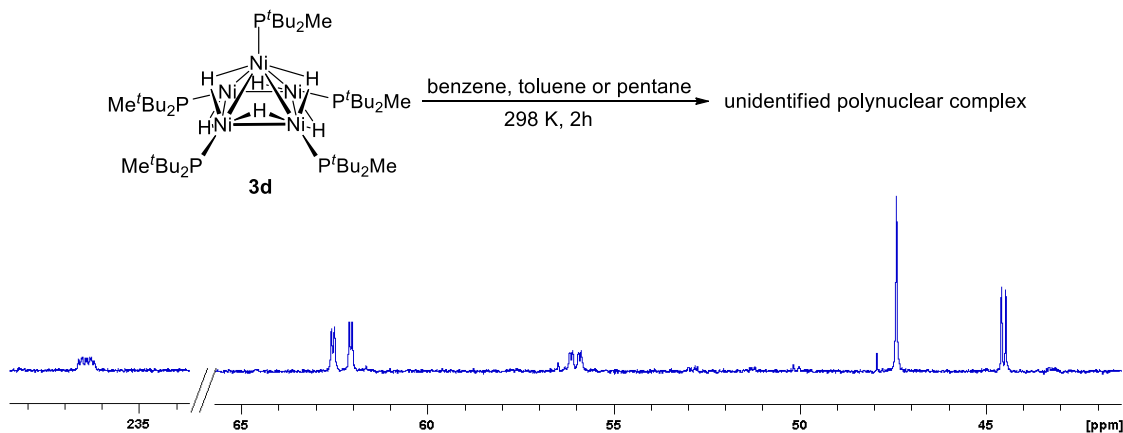


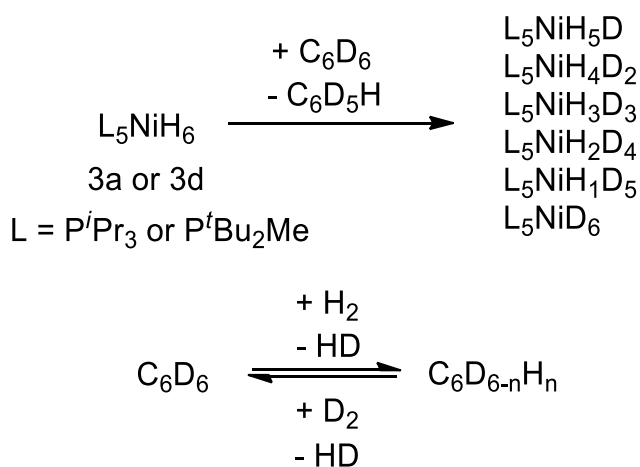
Figure 4.5 Nickel framework of **3d** with selected approximate bond lengths and bond angles.

Same as the complex **3a**, the geometry of the cluster **3d** is also a slightly distorted rectangular pyramid. Both side view and top view of **3d** are given in **Figure 4.4**. The four basal nickel atoms form a slightly distorted rectangle, with two paralleled edges (Ni(2)-Ni(3) = 2.54 Å; Ni(4)-Ni(5) = 2.67 Å) marked longer than the other two paralleled sides (Ni(2)-Ni(5) = 2.40 Å; Ni(3)-Ni(4) = 2.40 Å); the four angles of the base are very close to right angle (90.3°, 90.4°, 89.5°, 89.7°); and the distances between the top Ni(1) to the four basal nickels are approximately equal to each other (2.42 Å, 2.43 Å, 2.45 Å, 2.46 Å), which means the orthogonal projection of Ni(1) to the basal plane is approximately at the centre of the basal planar. Each basal Ni-Ni edge is bridged by a μ -H ligand. H(3) and H(5) are below the basal plane while H(4) and H(6) are above the basal plane. The plane of Ni(1)-Ni(2)-Ni(5) and Ni(1)-Ni(3)-Ni(4) are capped by a μ^3 -H hydride ligand, H(2) and H(1). The coordination environment of the top Ni(1) is close to *trans*-L₂Ni(II)H₂ (L is phosphine ligand), with one of the phosphine ligand replaced by the (LNi)₄H₄ basal moiety. Ni(3) and Ni(4) are bridged by H(1) and H(5), resembling the known Ni(I) complex (L₂Ni)₂(μ -H)₂, with one of the phosphine ligand replaced by the capping Ni(1) moiety. Ni(2) and Ni(5) are in the same chemical environment.



Scheme 4.7 The $^{31}\text{P}\{^1\text{H}\}$ NMR of the decomposition product of complex **3d** in benzene, toluene or pentane.

The extremely high instability of **3d** also leads to its decomposition in benzene, toluene and pentane, providing a same product. We failed to isolate the decomposition product because of its high solubility. From its $^{31}\text{P}\{^1\text{H}\}$ NMR as shown in **Scheme 4.7**, we found there were six chemical inequivalent phosphorous and one of the peak was observed at δ 238, which indicates that **3d** probably decomposed through a P–C bond cleavage process in the presence of benzene/toluene/pentane and produced a pentanuclear cluster with C_1 symmetry.



Scheme 4.8 H/D exchange between C_6D_6 and complex **3a** or **3d**.

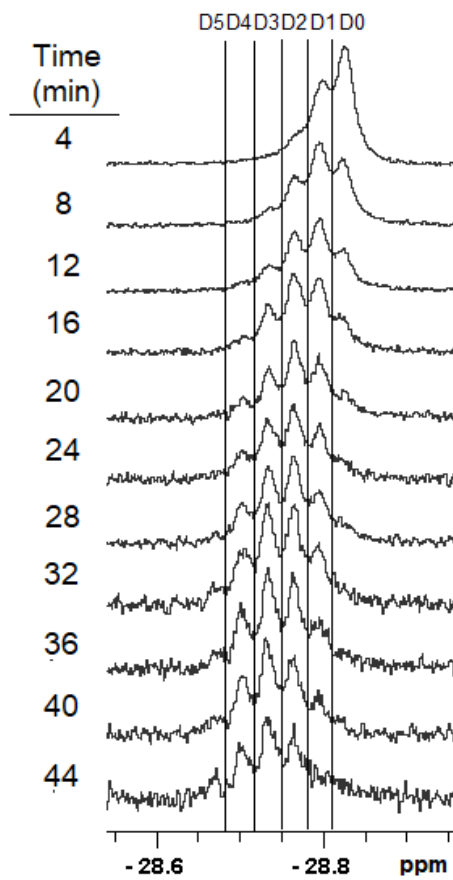


Figure 4.6 The H/D exchange of **3d** and C_6D_6 at 8 °C over a period of 44 minutes monitored by 1H NMR spectroscopy.

Same as complex **3a** and **3d** can also catalyze H/D exchange with deuterated solvents (**Scheme 4.8**). In this work, C_6D_6 was used as the deuterium source. The fully H/D exchange of complex **3a** and C_6D_6 was completed in 1.5 hours at 298 K, while it only took 10 minutes for **3d** to complete the exchange, demonstrating its much higher reactivity than **3a**. As shown in **Figure 4.6**, in order to record the stepwise conversion of **3d** in C_6D_6 with relatively slow decomposition of **3d**, we monitored the 1H NMR of the reaction at 8 °C. The resolution of $^{31}P\{^1H\}$ NMR spectrum was too low that the isotopologues were hard to be clarified in $^{31}P\{^1H\}$ NMR spectrum. The d_6 isotopologue is not observable in 1H NMR and the other five isotopologues were all observed. There is a difference of 0.3 ppm between each neighbouring isotopologue.

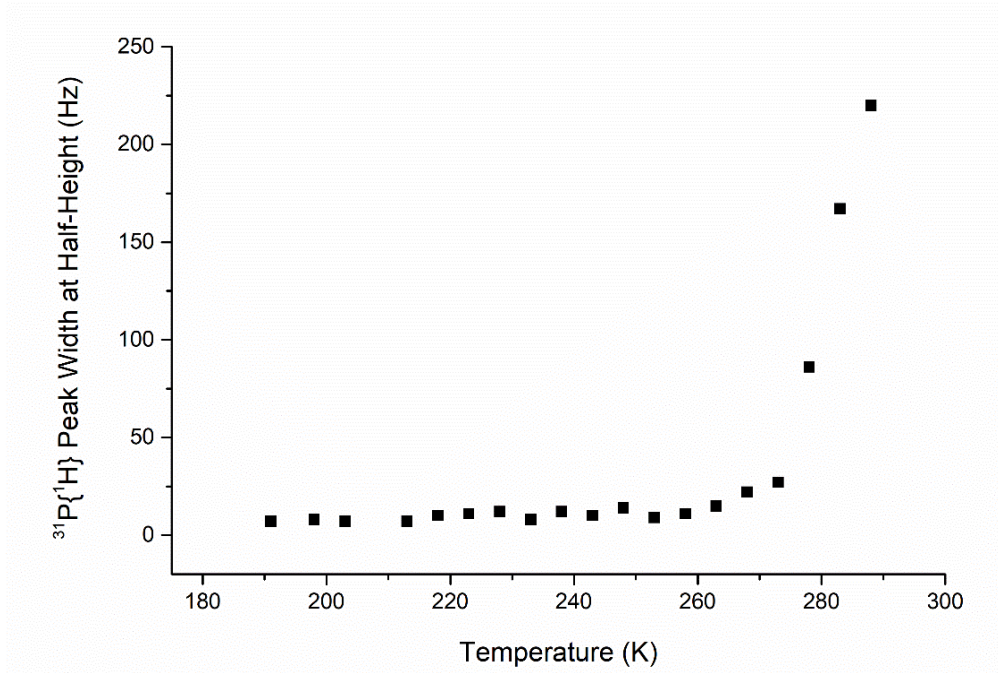


Figure 4.7 Plot of peak half height width in $^{31}\text{P}\{^1\text{H}\}$ NMR versus temperature for **3d**. The peak width is largely affected by temperature above $-10\text{ }^\circ\text{C}$.

To avoid the complexity caused by the H/D exchange reaction and the reactions with solvents, the NMR spectroscopically characterization was conducted in nondeuterated toluene at $-10\text{ }^\circ\text{C}$. In both ^1H and $^{31}\text{P}\{^1\text{H}\}$ NMR spectra, only one singlet peak was observed, indicating the fluxionality of hydride and phosphine ligands. As shown in **Figure 4.7**, in variable temperature NMR experiments (VT), the $^{31}\text{P}\{^1\text{H}\}$ peak width at half-height broadened from 8 Hz at $-80\text{ }^\circ\text{C}$ to 220 Hz at $20\text{ }^\circ\text{C}$, further proved the dynamic exchange of the hydride and phosphine ligands.

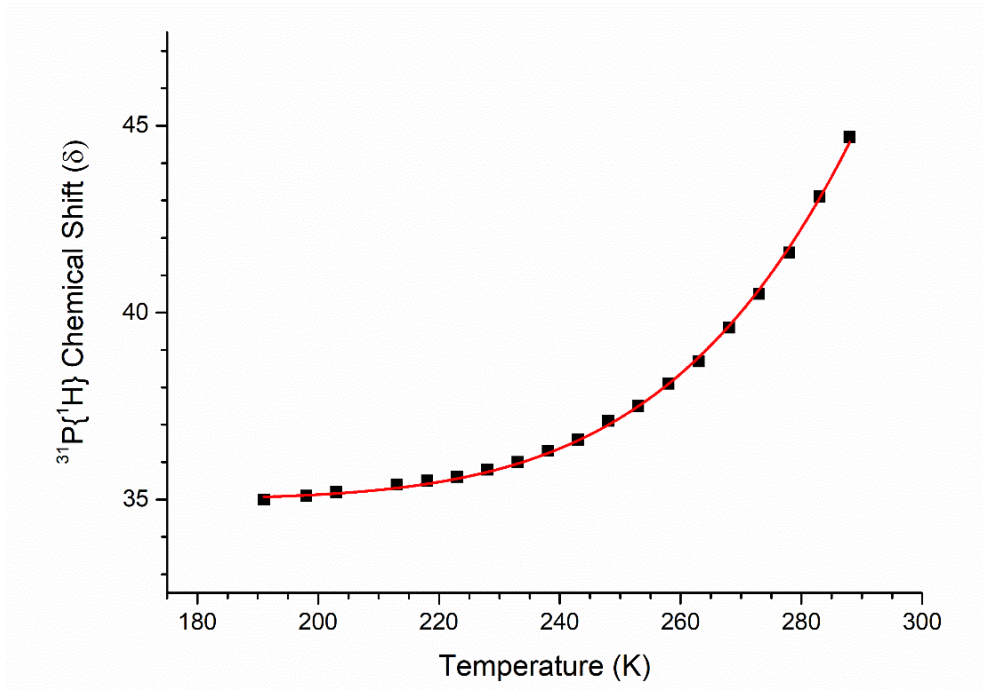
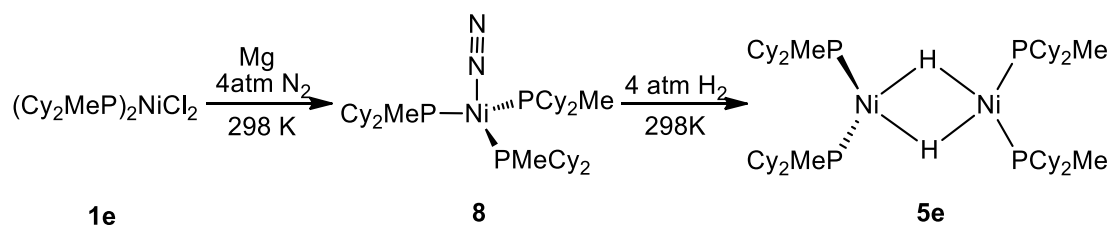


Figure 4.8 Plot of $^{31}\text{P}\{^1\text{H}\}$ NMR chemical shift versus temperature for **3d**. The red solid line is a fitted curve based on a model assuming that **3d** is a ground state singlet ($S = 0$) with a triplet state ($S = 1$) that is thermally accessible. According to the Boltzmann function, $2|J|$ from the Hamiltonian $H = -2JS_1S_2$ represents the energy difference between singlet ground state and triplet excited state. The chemical shift is influenced by a temperature-dependent magnetization $m(T)$ and follows the equation $\delta(T) = \delta_0 + \delta_p \cdot m(T)$, where δ_0 is the chemical shift for the diamagnetic ground state sample, which is δ 35 in this case, δ_p is a coefficient for the paramagnetic excited state. $m(T)$ is proportional to population difference of m_s and can be approximated by the equation $m(T) = \text{const} \cdot p(T)/T$, where $p(T)$ is the Boltzmann population at temperature T, $p(T) = e^{2J/KT}/(1 + 3e^{2J/KT})$. K is the Boltzmann constant 8.314 J/(K•mol).

In $^{31}\text{P}\{^1\text{H}\}$ VT NMR, we also found that the chemical shift was temperature dependent above the temperature of 190 K (**Figure 4.8**), moving towards higher field upon cooling down, which suggests the existence of a thermally accessible triplet state ($S = 1$) of the **3d**. The temperature dependent paramagnetic interaction caused the changes in chemical shift upon temperature. We adopted the same model for complex **3a** and fitted

the Hamiltonian $H = -2JS_1 \cdot S_2$ to the experimental data. The energy gap between the singlet state and the triplet state, $2J$, was determined to be 2125 cm^{-1} (6.1 kcal/mol). The energy difference is smaller than that of complex **3a** and the triplet state population of **3d** (0.01%) is much higher than **3a** (0.00025%) at 298 K.²³ This result may account for the higher reactivity of **3d** than **3a**. The chemical shift of **3d** in ^1H NMR was also influenced by temperature but not as largely as in $^{31}\text{P}\{^1\text{H}\}$ NMR, which suggests that the contact shift for hydride nuclei is smaller than phosphorus nuclei.

4.2.1.4 Dicyclohexylmethylphosphine



Scheme 4.9 The synthesis of $(\text{Cy}_2\text{Me})_3\text{P}(\mu\text{-N}_2)$ (**8**) from **1e** under 4 atm N_2 and the production of $[(\text{Cy}_2\text{MeP})_2\text{Ni}](\mu\text{-H})_2$ (**5e**) under 4 atm H_2 atmosphere.

As shown in **Table 4.1**, PCy_2Me (dicyclohexylmethylphosphine) has a much smaller cone angle than P^iPr_3 . The reduction of $(\text{Cy}_2\text{MeP})_2\text{NiCl}_2$ (**1e**) by activated Mg under 4 atm of nitrogen atmosphere produces a purple mononuclear Ni(0) complex $(\text{Cy}_2\text{MeP})_3\text{Ni}(\mu\text{-N}_2)$ (**7**) instead of an analogue of dinitrogen complex **2a** because the PCy_2Me is less bulky than P^iPr_3 (**Scheme 4.9**). The red solid was recrystallized from its saturated pentane solution at -40°C in a yield of 48.9%. Crystals suitable for single crystal X-ray diffraction was recrystallized from its saturated toluene solution by slow evaporation at 298 K.

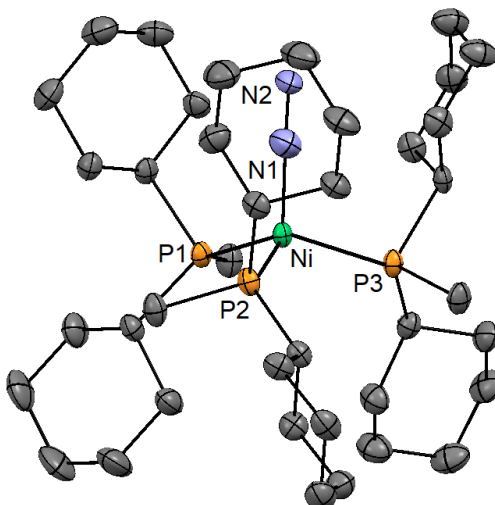
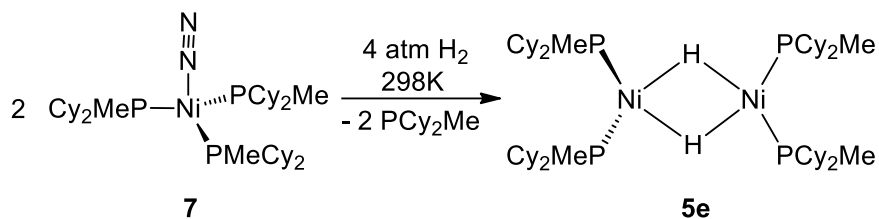
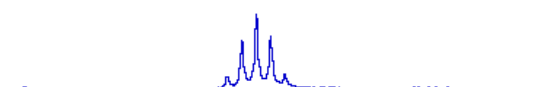


Figure 4.9 Solid state molecular structure of complex **7** was determined by single crystal X-ray diffraction. H atoms are omitted for clarity. Selected bond distances (unit: Å): Ni-N(1) = 1.718(2); Ni-P(1) = 2.1362(6); Ni-P(2) = 2.1432(7); Ni-P(3) = 2.1505(7); N(1)-N(2) = 1.17(2). Selective bond angles: N(2)-N(1)-Ni = 177.10(2)^o; P(1)-Ni-P(2) = 119.34(3)^o; P(1)-Ni-P(3) = 120.12(3)^o; P(2)-Ni-P(3) = 119.34(3)^o.

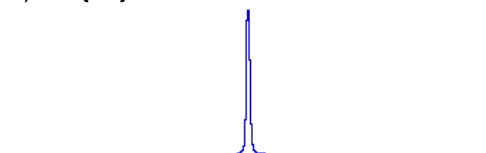
As shown in **Figure 4.9**, Ni atom is located slightly about the plane of the three P atoms and a N₂ moiety locates above the Ni atom. The Ni-N bond is perpendicular to the P plane, giving the structure an approximated C_{3v} symmetry. The Ni-N bond length is 1.718 Å, which is comparable to the Ni-N bond distances in **2a**, **2b** and **2d** (1.75-1.79 Å). The bond length between the two N atoms is 1.17 Å, which is longer than the gaseous N₂ molecule (1.09 Å) and comparable to **2a**, **2b** and **2d** (1.13-1.16 Å).^{33,31}



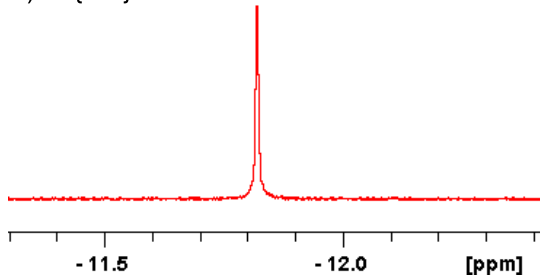
a) ^1H NMR of **5e**



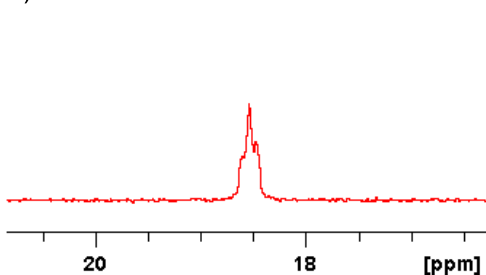
b) $^{31}\text{P}\{^1\text{H}\}$ NMR of **5e**



c) $^1\text{H}\{^{31}\text{P}\}$ NMR of **5e**



d) ^{31}P NMR of **5e**



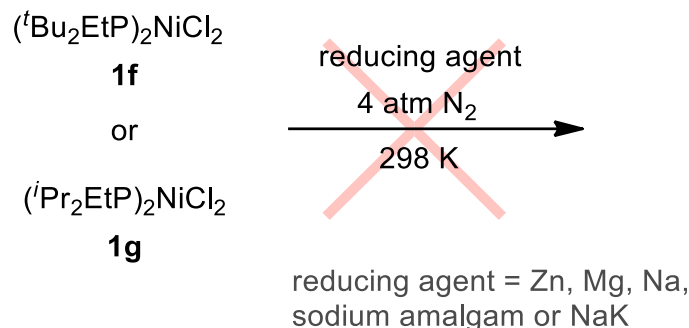
Scheme 4.10 The characterization of **5e** by NMR spectroscopy.

As shown in **Scheme 4.10**, when the THF solution of **7** was exposed to 4 atm H_2 environment, a new pentet was observed at $\delta -11.8$ in the ^1H NMR. In the $^1\text{H}\{^{31}\text{P}\}$ NMR, a singlet peak with the same chemical shift was observed. The corresponding peak in the $^{31}\text{P}\{^1\text{H}\}$ NMR was observed at $\delta 18.5$ and a triplet peak with the same chemical shift was observed in the ^{31}P NMR. The new resonance is probably $[(\text{Cy}_2\text{Me})_2\text{Ni}]_2(\mu\text{-H})_2$ (**5e**) a monophosphine analogue of $\text{L}_2\text{Ni}(\mu\text{-H})_2$ mentioned in the introduction. The coupling spin system of the bridging hydrides in **5e** is $\text{AA}'\text{X}_2\text{X}'_2$ because of the magnetic inequivalent phosphines. The bridging hydrides give a virtual pentet peak with $^2J_{\text{HP}} = 15.2$ Hz and the corresponding second-order peak in ^{31}P is a virtual triplet peak with $^2J_{\text{HP}} = 13.8$ Hz.

According to the $^{31}\text{P}\{^1\text{H}\}$ NMR, the reaction of **7** and H_2 was not completed. Only 50% of **7** was converted to **5e** even after gently heating at 45°C under 4 atm H_2 environment. The byproduct PCy_2Me generated during the reaction probably hinders the

completion of the reaction. The use of phosphine traps like NMO (see Chapter 2) may help the fully conversion of **7** to **5e**. Attempts to isolate and study of this complex are ongoing.

4.2.1.5 The Reduction of Di-*tert*-butylethylphosphine and Diisopropylethyl phosphine Supported Ni(II) Complexes



Scheme 4.11 The reduction of **1f** and **1g** led to the decomposition of the starting materials and produced Ni particles and the corresponding tertiary phosphines.

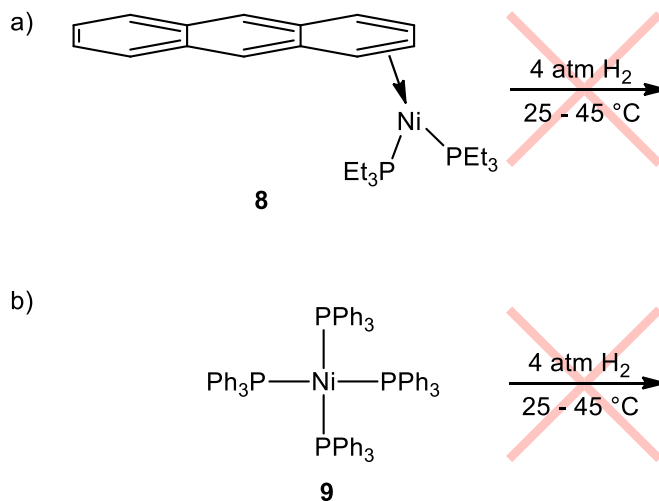
After testing the phosphines with high similarities to P^iPr_3 , we extended the scope to the phosphines with moderate differences from P^iPr_3 . Di-ethyl-*tert*-butylphosphine ($\text{P}^t\text{Bu}_2\text{Et}$), with a larger cone angle of 165° , and diisopropylethylphosphine ($\text{P}^i\text{Pr}_2\text{Et}$), with a smaller cone angle of 151° , were selected as examples.

Our strategy was to prepare the dinuclear nickel dinitrogen complex first from the reduction of L_2NiCl_2 (L = phosphine ligand). As shown in **Scheme 4.11**, We tried a variety of reducing agents, including Zn powder, activated Mg, sodium sand, sodium amalgam and NaK alloy, but only got nickel metal particles and free phosphine ligand as the reduction products. We also tried to reduce the **1f** and **1g** with the reductants mentioned above under 4 atmosphere H_2 gas environment, however, did not get any nickel hydride complex.

Although the preparation of dinitrogen complexes of $\text{P}^i\text{Pr}_2\text{Et}$ and P^tBuEt_2 failed, the possibility of preparing polynuclear complex supported by these two phosphines was

not ruled out. The reactions of different Ni(0)L_n (L = PⁱPr₂Et, PⁱBuEt₂) species with H₂ gas are ongoing now.

4.2.1.6 The Reactions of Triethylphosphine or Triphenylphosphine Supported Ni(0) species with H₂ gas



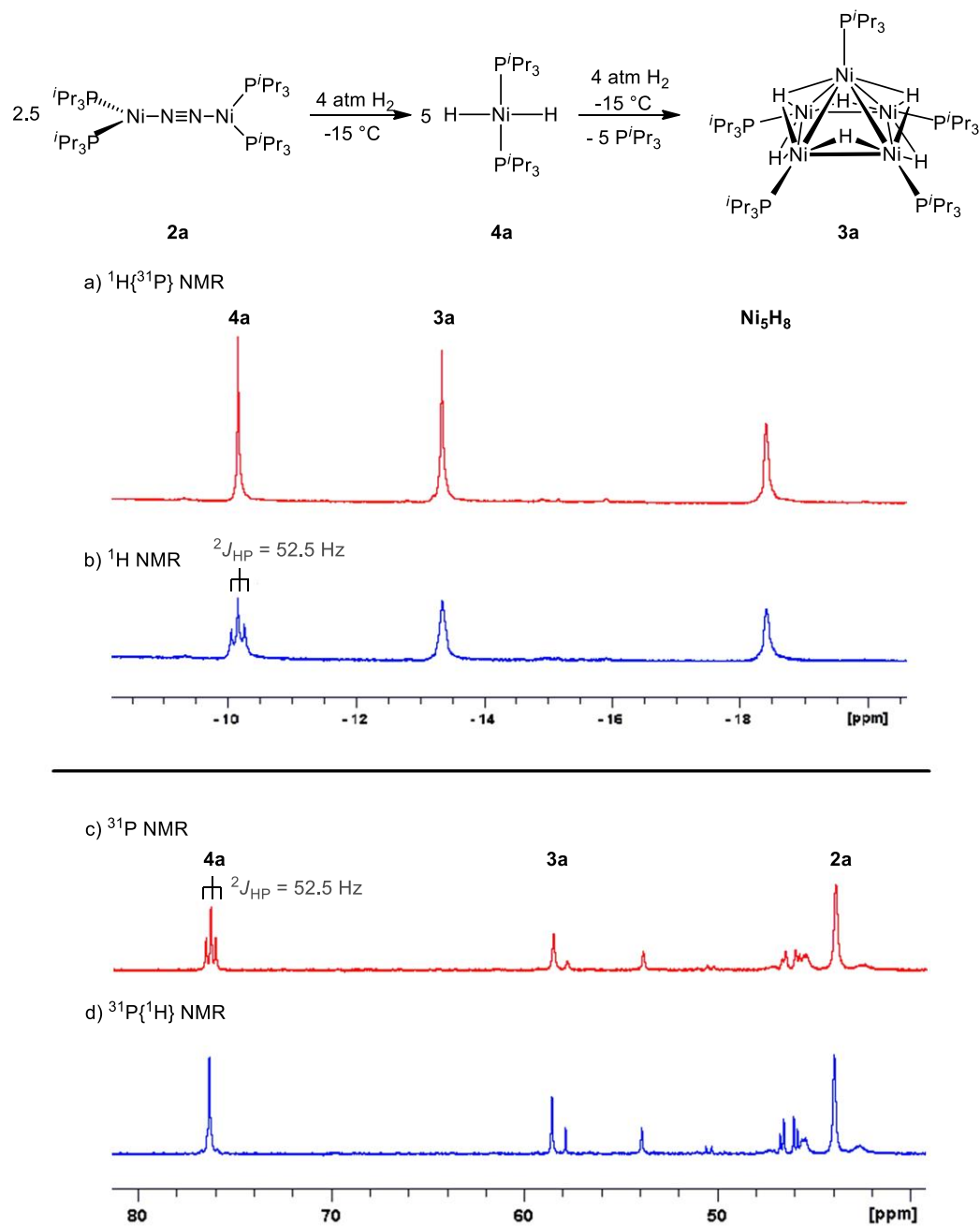
Scheme 4.12 No reaction observed by NMR spectroscopy when complex **8** and **9** were exposed to 4 atm of H₂ gas.

We also included phosphines with significant differences from PⁱPr₃ in this study. The cone angle of triethylphosphine is 132°, which is much smaller than PⁱPr₃. As shown in **Scheme 4.12a**, the L₂Ni(0) source we adopted here is (Et₃P)₂Ni(η²-anthracene) (**8**).³⁴ When the THF solution of **8** was exposed to 4 atm H₂ gas, no reaction was observed by NMR spectroscopy even after heating at 45 °C for 72 h.

All of the phosphines we examined so far have similar electronic parameters to PⁱPr₃. We were curious about what we could get from phosphines with significantly different electronic parameters. PPh₃ (triphenylphosphine) has a larger electronic parameter than other phosphines mentioned above, which means its electron donating ability is weaker. Ni(PPh₃)₄ (**9**), which is produced from the direct addition of PPh₃ to Ni(COD)₂, was used

as the Ni(0)L_n resource. There was no reaction when the pentane or THF solution of **9** was exposed to H₂ gas (shown in **Scheme 4.12b**).

4.2.2 Mechanistic Study of the Formation of Polynuclear Nickel Hydride Phosphine Complexes

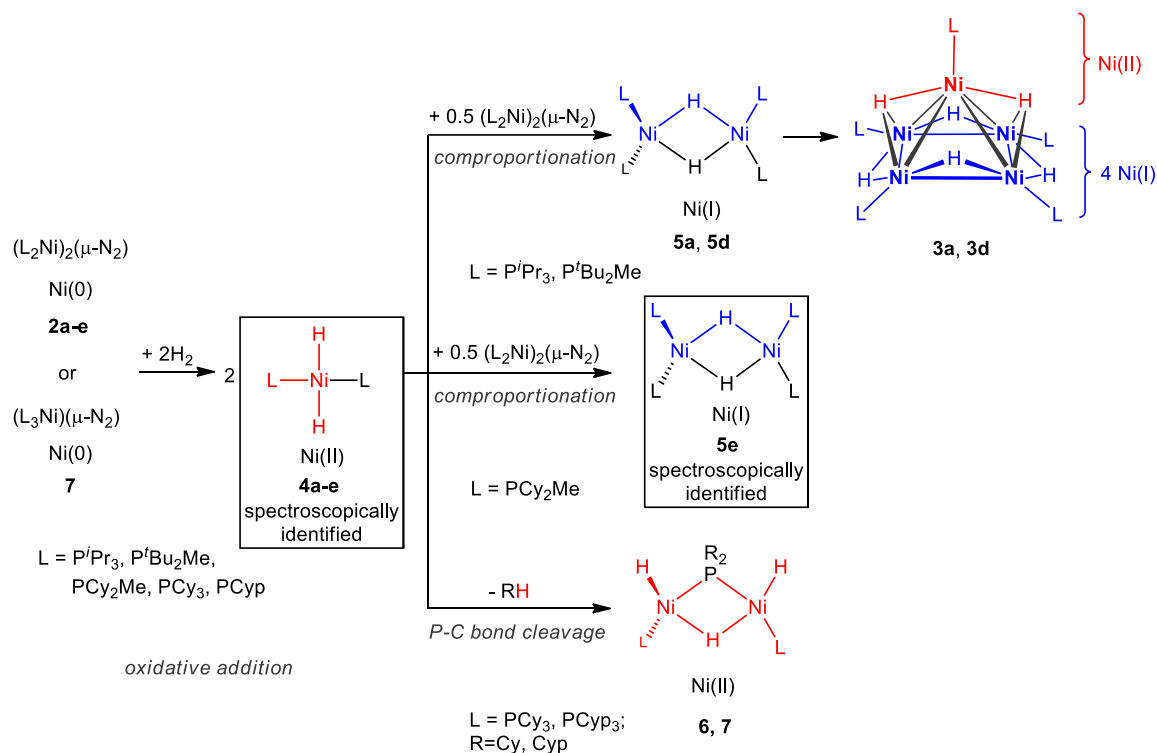


Scheme 4.13 NMR spectroscopically characterization of complex **4a**. The coupling constants of the triplets in ^1H and ^{31}P NMR spectra are both 52.5 Hz. The peak at δ 43.9 was proposed to be a Ni_5H_8 species.

In order to better understand how the polynuclear complexes formed, we used VT NMR to monitor the reactions. A sample of pentane solution of **2a** in a J. Young NMR tube was cooled to $-15\text{ }^{\circ}\text{C}$ under 4 atm pressure H_2 and both $^{31}\text{P}\{^1\text{H}\}$ and ^1H NMR were recorded every 15 minutes. In ^1H NMR, a species **4a** at $\delta -12.3$ appeared first, and as the integral of complex **3a** increased, the amount of species **4a** decreased. In $^{31}\text{P}\{^1\text{H}\}$, we also observed a singlet peak at $\delta 76.5$ and then disappeared, which was believed to be corresponding ^{31}P signal of species **4a**. The triplet proton peak and the singlet phosphorus peak suggested two phosphorus atoms with same chemical environment bound to a nickel centre and the species **4a** was probably a square-planar Ni(II) complex, *trans*-($^i\text{Pr}_3\text{P}$) $_2\text{NiH}_2$. To further prove our proposal, we monitored the reaction by $^1\text{H}\{^{31}\text{P}\}$ (phosphorous-decoupled proton NMR) and ^{31}P NMR (proton-coupled phosphorous NMR). As shown in **Scheme 4.13**, a singlet in $^1\text{H}\{^{31}\text{P}\}$ and a triplet peak in ^{31}P NMR were observed. Both peaks had the same chemical shifts to their corresponding peaks in ^1H and $^{31}\text{P}\{^1\text{H}\}$ NMR spectra, respectively. The coupling constants of the two triplets in ^1H and ^{31}P NMR spectra were both 52.5 Hz.

Next, we monitored the reaction of **2b** and **2c** with H_2 gas at $10\text{ }^{\circ}\text{C}$. Again, we observed the intermediates **4b** and **4c** by NMR spectroscopy. For **4b**, the chemical shifts in ^1H and ^{31}P are $\delta -9.92$ and $\delta 62.1$, respectively, and the coupling constant is $^2J_{\text{HP}} = 53.5$ Hz. For **4c**, ^1H and ^{31}P chemical shifts were observed respectively at $\delta -9.21$ and $\delta 67.9$, with a coupling constant of $^2J_{\text{HP}} = 52.2$ Hz.

In the case of **3d**, however, we did not observed the L_2NiH_2 type intermediate because of the extremely high reaction rate. Even if the NMR spectrometer was cooled to $-45\text{ }^{\circ}\text{C}$ and the reaction tube was frozen in liquid N_2 before being loaded into the NMR machine, we still failed to observe an intermediate because the reaction to **3d** was completed when we waited the solution thawed. But based on the detection and characterization of **4a-c**, we can reasonably presume that ($^i\text{Bu}_2\text{MeP}$) $_2\text{NiH}_2$ (**4d**) is also one of the intermediates to the production of **2d**.



Scheme 4.14 The reaction of $(L_2Ni)(\mu-N_2)$ (**2a-d**) or **2e** and H_2 gas. The Ni(II) intermediate L_2NiH_2 (**4a-e**) was observed and characterized by NMR spectroscopy.

The characterization of complex $L_2Ni(II)H_2$ (**4a-e**) strongly supported the plausible mechanism we raised before. As shown in **Scheme 4.14**, Complex $L_2Ni(II)H_2$ is generated through direct oxidative addition of H_2 to Ni(0) centre of complex $(L_2Ni)_2(\mu-N_2)$ (**2a-e**). For P^iPr_3 and P^tBu_2Me , one equivalent of $L_2Ni(II)H_2$ and one equivalence of $L_2Ni(0)$ generated from $(L_2Ni)_2(\mu-N_2)$ solution produces the next intermediate, $(L_2Ni)_2(\eta-H)_2$ (**4a-e**), through comproportionation reactions. Two $(L_2Ni)_2(\eta-H)_2$ form the basal frame, which replaces one of the phosphine ligand on NiH_2L_2 to build up the cluster. In the case of PCy_3 and $PCyp_3$, instead of forming the Ni(I) intermediate, two equivalence of $L_2Ni(II)H_2$ produce the Ni(II) complex, $(LHNi)_2(\eta-H)(\eta-PCy_2)$, through P–C bond cleavage. One of the cyclopentyl/cyclohexyl group departures from the phosphine ligand together with a hydride ligand, which produces cyclopentane/cyclohexane byproduct. The byproducts were characterized by $^{13}C\{^1H\}$ NMR.

However, we came across some problems when we tried to isolate L_2NiH_2 from the reaction solutions. Complex **4a-c** and **4e** are too kinetically unstable. They take part into the formation of cluster as soon as they were generated. In the case of $PCyp_3$, **2d** was dissolved in pentane and stirred for 30 minutes at $-15\text{ }^\circ\text{C}$ under 4 atm H_2 environment. The reaction solution was cooled down to $-80\text{ }^\circ\text{C}$ in a dry ice/acetone bath for 8 hours, however, no crystal precipitated because of the high solubility.

We also tried to synthesize the intermediate $(Cy_3P)_2NiH_2$ through the reaction of $(Cy_3P)_2Ni(H)Cl$ with hydride sources such as NaH and $NaBH_4$. However, neither of the hydride sources gave out the complex we expected.

4.3 Conclusions and Future Work

In this chapter, we studied the behavior of a set of tertiary phosphines in the preparation of polynuclear nickel hydride complexes. Among all of the phosphines we tried, we found that only those phosphines with a Tolman cone angle very close to 160° (P^iPr_3 , P^iBu_2Me , PCy_3 , $PCyp_3$) can produce the Ni(0) precursor, $(L_2Ni)_2(\mu-N_2)$. We successfully synthesized and fully characterized the P^iBu_2Me derivative of cluster **3a** and **3d**. The use of other Ni(0) complexes, including $(Et_3P)_2Ni(\eta^2\text{-anthracene})$, $(PPh_3)_4Ni$ and $LNi(\eta^6-C_7H_8)$ as the starting materials to prepare clusters failed. Complex **3a** and **3d** are rare examples of electron deficient phosphine supported late first row metal hydride cluster. Previous work of our group demonstrated the versatile reactivities of complex **2a** in cooperative catalysis of inert bond activation. In this work, it has been proved that complex **3d** is even more active and has a higher reactivity in H/D exchange reaction. Therefore, it is reasonable to expect powerful catalytic capabilities of **3d** in various types of reactions in our future work. For PCy_2Me , which has a much smaller Tolman cone angle than 160° , the reduction of $(Cy_2MeP)_2NiCl_2$ produces $(Cy_2MeP)_3Ni(\mu-N_2)$ instead of $(L_2Ni)_2(\mu-N_2)$. The reaction of **7** and H_2 produces a dinuclear complex $[(Cy_2MeP)_2Ni]_2(\mu-H)_2$ (**5e**). Complex **5e** is potentially reactive a wide range of organic chemicals because of the two bridging hydrides. The study about inert bond activation mediated by **5e** will probably show

interesting results in the future. The reaction of **2b** or **2c** and H₂ gas produces a different complex, **6** or **7**. They are dinuclear nickel complexes stable at room temperature under N₂ atmosphere.

In order to figure out the reaction mechanism of L_nNi(0) and H₂ gas, we monitored the reactions by NMR spectroscopy. All of the analogues of (L₂Ni)₂(μ-N₂) (**2a-d**) share the first intermediate, L₂Ni(II)H₂ (**4a-d**), which is generated from the oxidative addition of H₂ to the nickel centre of (L₂Ni)₂(μ-N₂). Complex (L₂Ni)₂(μ-N₂) is more reactive to H₂ gas than LNi(η⁶-C₇H₈), suggesting that the oxidative addition to L₂Ni(0) species features a lower energy barrier than LNi(η⁶-C₇H₈) species. The introduction of bulkier phosphine ligand may be helpful to the isolation of L₂Ni(II)H₂ by increasing its solubility. The isolation of the intermediates will support a solid experimental evidence to the mechanism of the formation of the pentanuclear cluster.

For PⁱPr₃ and P^tBu₂Me, we proposed that a second intermediate, (L₂Ni)₂(η-H)₂ (**5a**, **5d**), is generated from the comproportionation reaction of L₂NiH₂ and (L₂Ni)₂(μ-N₂). Two (L₂Ni)₂(μ-H)₂ and one L₂NiH₂ then finally comprise the cluster on losing three phosphine ligands. In the case of PCy₃ and PCyp₃, P–C bond cleavage happens prior to the comproportionation reaction and produced (LHNi)₂(μ-H)(μ-PR₂) (R = Cy, Cyp).

The study about the PCy₂Me supported nickel complex demonstrated the preparation of a different nickel dinitrogen complex, (Cy₂MeP)₃Ni(μ-N₂) (**8**). The lesser steric hindrance of PCy₂Me favours more phosphines bound to the Ni centre. The reaction of complex **8** and 4 atm H₂ gas produces a dinuclear complex [(Cy₂MeP)₂Ni](μ-H)₂ (**5e**). The NMR spectroscopic characterization of **5e** offers more evidence to our proposal that L₂NiH₂ and (L₂Ni)₂(η-H)₂ are the two major intermediates in the preparation of the pentanuclear clusters.

In this chapter, it has been showed that reactive L_nNi(0) species are good starting point to synthesize polynuclear nickel hydride complexes. In this study, dinitrogen complexes are reactive enough H₂ gas. Steric parameter may be one of the factors that decide the production of the reduction reaction of L₂NiCl₂ and the production of the

reaction of $L_nNi(0)$ with H_2 gas. Phosphines with approximate 160° cone angles like P^iPr_3 may be able to form $(L_2Ni)_2(\mu-N_2)$ type dinitrogen complex, while smaller PCy_2Me (cone angle is 146°) has the potential to form a $L_3Ni(\mu-N_2)$ type dinitrogen complex. Phosphines with cone angles smaller than 146° are too small to support a $L_3Ni(\mu-N_2)$ type complex. Phosphines with cone angles between 160° and 146° such as P^iPr_2Et (cone angle is 151°) are too big to form a $L_3Ni(\mu-N_2)$ type complex either type of dinitrogen complex. Phosphines with cone angles larger than 160° such as P^tBu_2Et (cone angle is 165°) are too big to form a $(L_2Ni)_2(\mu-N_2)$ type complex. The reaction of **2a** or **2d** and H_2 produces a pentanuclear cluster, while the reaction of **2b** or **2c** and H_2 produces **6** or **7**. The production of **6** and **7** demonstrates the possibility that the intermediate **4** favours the P–C bond cleavage pathway than $(L_2Ni)(\mu-H)_2$. DFT calculation of the energies could help avoid phosphines that may undergo P–C bond cleavage. The reaction of **7** and H_2 gas does not produce a pentanuclear complex as we expected but ceased at the formation of **5e**. This is probably caused by the small steric hindrance of the PCy_2Me . Smaller phosphine ligands are harder to leave from $(L_2Ni)(\mu-H)_2$ than larger phosphine ligands and make $(L_2Ni)(\mu-H)_2$ relatively stable.

In conclusion, reactive $L_nNi(0)$ resources are vital to the preparation of polynuclear nickel hydride clusters. Phosphines with cone angles close to 160° are good choices to prepare pentanuclear clusters and phosphine with cone angles close to 146° have the potential to form dinuclear hydride complexes. The isolation and fully characterization of the intermediates help us further understand the mechanism of the production of polynuclear nickel hydride complexes. With better understanding of the mechanism, we could be able to select suitable phosphines we need and design and synthesize polynuclear complexes, which will accelerated the progress in cooperatively catalyzed inert bond activations.

4.4 Experimental Section

4.4.1 General Procedures

All experiments were performed under an N₂ atmosphere using either standard Schlenk techniques or a glovebox. Dry, oxygen-free solvents were employed throughout. Anhydrous pentane, toluene, benzene and tetrahydrofuran (THF) were purchased from Sigma Aldrich and used as received. ¹H, ³¹P{¹H}, and ¹³C{¹H} NMR spectra were recorded on a Bruker AMX spectrometer operating at 500 MHz. All chemical shifts are recorded in parts per million, and all coupling constants are reported in hertz. ¹H NMR spectra were referenced to solvent resonances ((Me₃Si)₂O, δ 0.0065³⁵⁻³⁷; benzene-*d*₆, δ 7.16; toluene-*d*₈, δ 2.08) with respect to tetramethylsilane at δ 0.00. ³¹P{¹H} NMR spectra were referenced to external 85% H₃PO₄ at δ 0.00. ¹³C{¹H} NMR spectra were referenced to solvent resonances ((Me₃Si)₂O, δ 1.94; benzene-*d*₆, δ 128.05; toluene-*d*₈, δ 20.43) with respect to tetramethylsilane at δ 0.00. Elemental analyses were performed by the Center for Catalysis and Materials Research, Windsor, Ontario. Phosphorus trichloride, nickel(II) chloride and hydrogen gas were purchased from Sigma Aldrich. Tricyclohexylphosphine (PCy₃) was purchased from Oakwood Products, Inc. All of the solid compounds mentioned above were deoxygenated under vacuum before use. P^{*i*}Bu₂Me (di-*tert*-butylmethylphosphine), P^{*i*}BuEt₂ (*tert*-butyldiethylphosphine), PCy₃ (tricyclohexylphosphine), PCyp₃ (tricyclopentylphosphine), P^{*i*}Pr₂Et (*diisopropylethylphosphine*) and PCy₂Me (dicyclohexylmethylphosphine) were prepared from PCl₃ and the corresponding Grignard reagents and purified by recrystallization or fractional distillation. [(Cy₃P)₂Ni]₂(μ-N₂) was prepared according to the method of Aresta⁵. (L₂Ni)₂(μ-N₂) (L = P^{*i*}Pr₃, P^{*i*}Bu₂Me, PCyp₃) were prepared according to the method of Beck published in 2013²¹.

4.4.2 Synthesis and Characterization of Complexes

Synthesis and Characterization of NiCl₂(P^{*i*}BuEt₂)₂ (1f) 2 g of P^{*i*}BuEt₂ (13.7 mmol) and 0.98 g NiCl₂ (7.6 mmol) was stirred for 2 d at room temperature in toluene. The

solvent was evaporated under vacuum and $\text{NiCl}_2(\text{P}^i\text{BuEt}_2)_2$ was extracted by pentane. The solution was cooled to $-40\text{ }^\circ\text{C}$ for 16 h and dark red powder precipitated was collected and dried under vacuum. The yield is 1.62 g (66.4%). Single crystal X-ray diffraction quality crystals was recrystallized from HMDSO by slow evaporation of the solvent at room temperature. ^1H NMR (C_6D_6 , 500 MHz, 298 K): δ 1.07 (s, 2H, CH_2), 1.26 (s, 6H, Et- CH_3), 1.37 (s, 9H, $^i\text{Bu-CH}_3$), 1.95 (s, 2H, CH_2). $^{31}\text{P}\{^1\text{H}\}$ NMR (C_6D_6 , 202.5 MHz, 298 K): δ 20.4 (s, $^{13}\text{C}\{^1\text{H}\}$ (C_6D_6 , 125.8 MHz, 298 K): δ 9.6 (s, Et- CH_3), 12.0 (s, CH_2), 29.0 ($^i\text{Bu-CH}_3$), 32.5 (s, CCH_3). Anal. Calcd for $\text{C}_{16}\text{H}_{38}\text{Cl}_2\text{NiP}_2$ (MW 422.02): C, 45.54; H, 9.08. Found: C, 45.12; H, 8.95.

Synthesis and Characterization of $\text{NiCl}_2(\text{P}^i\text{Pr}_2\text{Et})_2$ (1g) 1.5 g of $\text{P}^i\text{Pr}_2\text{Et}$ (10.3 mmol) and 0.69 g NiCl_2 (5.3 mmol) was stirred in 20 mL toluene at room temperature for 3 d. The excess NiCl_2 was filtered off and toluene was evaporated under vacuum. Extracted the solid residue by 15 mL pentane and decreased the volume of pentane to 5 mL. Cooled down the solution $-40\text{ }^\circ\text{C}$ for 16 h. 1.69 g cubic dark red crystals suitable for single crystal X-ray diffraction precipitated and were collected by filtration. Yield is 78.2%. ^1H NMR (C_6D_6 , 500 MHz, 298 K): δ 1.21 (s, 12H, $i\text{Pr-CH}_3$), 1.33 (s, 6H, Et- CH_3), 1.43 (s, 4H, CH), 1.52 (s, 12H, $i\text{Pr-CH}_3$), 2.05 (s, 4H, CH_2). $^{31}\text{P}\{^1\text{H}\}$ NMR (C_6D_6 , 202.5 MHz, 298 K): δ 19.0 (br). $^{13}\text{C}\{^1\text{H}\}$ (C_6D_6 , 125.8 MHz, 298 K): δ 9.7 (s, Et- CH_3), 11.3 (s, CH_2), 18.2 (s, $i\text{Pr-CH}_3$), 19.6 (s, $i\text{Pr-CH}_3$), 22.7 (s, CH). Anal. Calcd for $\text{C}_{16}\text{H}_{38}\text{Cl}_2\text{NiP}_2$ (MW 422.02): C, 45.54; H, 9.08. Found: C, 45.69; H, 8.79.

Synthesis and Characterization of $\text{NiCl}_2(\text{PCyp}_3)_2$ (1c) A mixture of 2 g PCyp_3 (8.4 mmol) and 0.54 g NiCl_2 (4.2 mmol) in 40 mL toluene was gently refluxed for 3 h with good stirring. Filtered off the unreacted NiCl_2 , decreased the volume to 25 ml and cooled it to $-40\text{ }^\circ\text{C}$ for 16 h. Dark red crystals suitable for single crystal X-ray diffraction precipitated and was collected by filtration. Yield is 67.7% (1.72 g). ^1H NMR (C_6D_6 , 500 MHz, 298 K): δ 1.48 (s, 12H, CHCH_2CH_2), 1.79 (s, 12H, CHCH_2CH_2), 2.02 (s, 12H, CHCH_2), 2.32 (s, 18H, CH and CHCH_2). $^{31}\text{P}\{^1\text{H}\}$ NMR (C_6D_6 , 202.5 MHz, 298 K): δ 35.7 (br). $^{13}\text{C}\{^1\text{H}\}$ (C_6D_6 , 125.8 MHz, 298 K): δ 26.7 (s, CHCH_2CH_2 , 12H), 30.2 (s, CHCH_2 ,

12H), 35.1 (s, CH, 6H). Anal. Calcd for C₃₀H₅₄Cl₂NiP₂ (MW 606.29): C, 59.43; H, 8.98. Found: C, 59.11; H, 9.32.

Synthesis and Characterization of (Cy₂MeP)₃Ni(μ-N₂) (7) The heterogeneous mixture of 4.9 g PCy₂Me (23 mmol) and 2.94 g NiCl₂ (13.8 mmol) in 30 mL toluene was stirred vigorously at 298 K for 72 h. Filtered off the excess NiCl₂ and evaporated the solvent under vacuum. (Cy₂MeP)NiCl₂ was got as a purple solid and used in the next reaction step without further purification. A high-pressure Schlenk flask was charged with 5.2 g (Cy₂MeP)NiCl₂, 4.5 g freshly activated Mg (0.19 mol) and 40 mL THF. The mixture was stirred for 3.5 h under 4 atm H₂. The colour of the reaction solution turned from purple to dark red. Volatiles were evaporated under vacuum and the residue was extracted by pentane. Filtered the pentane extraction through Celite and decreased the volume of the filtrate to 10 mL. 1.9 g red solid was recrystallized from the pentane solution at -40 °C and collected by filtration. The total yield of the reactions is 39.5%. Single crystal X-ray diffraction quality crystals were recrystallized from the saturated toluene solution by slow evaporation at 298 K. ¹H NMR (C₆D₆, 500 MHz, 298 K): δ 1.22 (s, 9H, Me-CH₃), 1.22-1.44 (m, 24H, PCHCH₂), 1.46-1.54 (m, 6H, PCH), 1.64-1.74 (m, 12H, PCHCH₂CH₂), 1.81-1.92 (m, 18H, PCHCH₂CH₂CH₂), 2.13-2.19 (m, 6H, PCHCH₂CH₂CH₂). ³¹P{¹H} NMR (C₆D₆, 202.5 MHz, 298 K): δ 6.3. ¹³C{¹H} (C₆D₆, 125.8 MHz, 298 K): δ 11.8 (m, Me-CH₃), 27.3 (s, PCHCH₂CH₂CH₂), 28.0 (m, PCHCH₂CH₂), 28.2 (m, PCHCH₂CH₂), 29.3 (s, PCH₂CH₂), 30.5 (m, PCH₂CH₂), 38.9 (m, PCH). Anal. Calcd for C₃₉H₇₅N₂NiP₃ (MW 692.66): C, 64.73; H, 10.45; N, 3.87. Found: C, 64.32; H, 10.23; N, 4.07.

Synthesis and Characterization of [(^tBu₂MeP)₂Ni]₂(μ-N₂) (2d) 2.4 g NiCl₂ (18.5 mmol) was added to the toluene solution of 5.5 g ^tBu₂Me (34.3 mmol) and stirred at room temperature for 2 d. Evaporated the solvent under vacuum and extracted the (^tBu₂Me)₂NiCl₂ by pentane. The saturated solution was cooled to -40 °C for 2 d. 4.4 g (10.2 mmol) dark red microcrystalline precipitated was collected and was dissolved in 35 ml THF in a high-pressure Schlenk flask. 1.23g (51.1 mmol) Mg turning activated by grinder was added to the flask. The flask was then cooled in a liquid N₂ bath under N₂ gas flow and warmed up to room temperature with good stirring. The colour of the solution

turned to dark red from violet in 1 h. Stirred the reaction solution for another 1 h after the colour changed. Fully evaporated all of the solvent under vacuum, extracted the residue by pentane, decreased the volume of pentane to 15 mL and cooled the solution in a $-40\text{ }^{\circ}\text{C}$ freezer. 0.46 g dark red powder precipitated after 24 h and was collected and dried under vacuum. Yield is 23.5 %. Red crystals qualified for single crystal X-ray diffraction was recrystallized from pentane at $-40\text{ }^{\circ}\text{C}$. ^1H NMR ($(\text{Me}_3\text{Si})_2\text{O}$, 500 MHz, 298 K): δ 0.96 (s, 12H, Me- CH_3), 1.19 (d, $^3J_{\text{H-P}} = 11.8\text{ Hz}$, 72H, $^t\text{Bu-CH}_3$). $^{31}\text{P}\{^1\text{H}\}$ NMR ($(\text{Me}_3\text{Si})_2\text{O}$, 202.5 MHz, 298 K): δ 37.3. $^{13}\text{C}\{^1\text{H}\}$ ($(\text{Me}_3\text{Si})_2\text{O}$, 125.8 MHz, 298 K): δ 29.7 (vt, $^1J_{\text{C-P}} + ^3J_{\text{C-P}} = 4.6$, 72H, $^t\text{Bu-CH}_3$), 33.9 (vt, $^1J_{\text{C-P}} + ^3J_{\text{C-P}} = 6.6$, 12H, Me- CH_3). Anal. Calcd for $\text{C}_{36}\text{H}_{84}\text{Ni}_2\text{N}_2\text{P}_4$ (MW 786.34): C, 54.99; H, 10.77; N, 3.56. Found: C, 50.26; H, 10.93; N, 3.83. Low carbon may be due to the formation of Ni carbide.

Synthesis and characterization of $[(\text{Cy}_3\text{P})\text{NiH}]_2(\mu\text{-H})(\mu\text{-PCy}_2)$ (6) 2.0 g of $[\text{Ni}(\text{PCy}_3)_2]_2(\mu\text{-N}_2)$ and 50 mL of THF was added to a 200 mL high pressure Schlenk flask. Degassed the flask by freeze-pump-thaw three times and refilled it with H_2 gas at $-197\text{ }^{\circ}\text{C}$. Warmed it up to room temperature, stirred vigorously for 8 h at room temperature and evaporated the solvent under vacuum. The product was extracted by pentane, filtered through Celite and cooled to $-40\text{ }^{\circ}\text{C}$ for 16 h. Orange microcrystalline precipitated and was filtered off and dried under vacuum. Yield is 0.46 g (35.4%). Crystals suitable for single crystal X-ray diffraction was recrystallized from a saturated solution of benzene/HMDSO (1: 1) at room temperature. ^1H NMR (C_6D_6 , 500 MHz, 298 K): δ -12.94 to -12.76 (m, 1H, bridging hydride), -9.28 to -9.09 (m, 2H, terminal hydride), 1.24–1.38 (m, 30H, terminal PCHCH_2), 1.62–1.74 (m, 24H, terminal $\text{PCHCH}_2\text{CH}_2$), 1.81–1.83 (m, 12H, terminal $\text{PCHCH}_2\text{CH}_2\text{CH}_2$), 2.03–2.09 (m, 4H, bridging $\text{PCHCH}_2\text{CH}_2\text{CH}_2$), 2.14–2.16 (m, 16H, bridging $\text{PCHCH}_2\text{CH}_2$), 2.50–2.57 (m, 2H, bridging PCH). $^{31}\text{P}\{^1\text{H}\}$ NMR (C_6D_6 , 202.5 MHz, 298 K): δ 90.8 (d, 2P, terminal P, $^2J_{\text{P-P}} = 156\text{ Hz}$), 155.8 (t, bridging P, $^2J_{\text{P-P}} = 156\text{ Hz}$). $^{13}\text{C}\{^1\text{H}\}$ (C_6D_6 , 125.8 MHz, 298 K): δ 27.06 (s, 12C, terminal $\text{PCHCH}_2\text{CH}_2$), 27.29 (s, 6C, terminal $\text{PCHCH}_2\text{CH}_2\text{CH}_2$), 27.63 (d, 6C, terminal PCH , $^2J_{\text{C-P}} = 11.0\text{ Hz}$), 28.20 (d, 12C, terminal, PCHCH_2 , $^1J_{\text{C-P}} = 10.1\text{ Hz}$), 33.94 (s, 4C, bridging $\text{PCHCH}_2\text{CH}_2$), 33.44 (s, 2C, bridging $\text{PCHCH}_2\text{CH}_2\text{CH}_2$), 35.77 (d, 2C, bridging PCH , $^2J_{\text{C-P}} = 24.7\text{ Hz}$), 36.28 (d,

4C, bridging, PCHCH₂, ¹J_{C-P} = 14.9 Hz). Anal. Calcd for C₄₈H₉₁Ni₂P₃ (MW 847.57): C, 68.02; H, 10.82. Found: C, 67.53; H, 10.79.

We simulated the hydride region ¹H NMR spectrum of the [(Cy₃P)NiH]₂(μ-H)(μ-PCy₂) on the software program TopSpin 4.0.6. The peak of H_a was observed at δ -12.85. J_{HaHb} = J_{HaHb'} = 10.9 Hz; J_{HaPa} = 32.2 Hz; J_{HaPb} = J_{HaPb'} = 16.8 Hz. The peak of H_b and H_{b'} is a second order multiplet, observed at δ -9.18. J_{HbPb} = J_{Hb'Pb'} = 28.5 Hz; J_{HbPb'} = J_{Hb'Pb} = 8.0 Hz; J_{HbPa} = J_{Hb'Pa} = 41 Hz. The linewidth is 3.3 Hz.

Synthesis and characterization of [(Cyp₃P)NiH]₂(μ-H)(μ-PCyp₂) (7) 0.5 g of [Ni(PCy₃)₂]₂(μ-N₂) and 50 mL of THF was added to a 200 mL high pressure Schlenk flask. Degassed the flask by freeze-pump-thaw three times and refilled it with H₂ gas at -197 °C. Warmed it up to room temperature, stirred vigorously for 12 h at room temperature and evaporated the solvent under vacuum. The residue was extracted by pentane, filtered through Celite and the filtrate was cooled to -40 °C for 5 d. Dark yellow cubic crystals suitable for single crystal X-ray diffraction precipitated. Filtered the solution and collected 0.078 g product with a yield of 21.1%. ¹H NMR (C₆D₆, 500 MHz, 298 K): δ -12.22 to -12.04 (m, 1H, bridging hydride), -8.80 to -8.62 (m, 2H, terminal hydride), 1.42–1.78 (m, 32H, terminal and bridging PCH₂CH₂CH₂), 1.78–1.96 (m, 32H, terminal and bridging PCHCH₂), 1.96–2.17 (m, 8H, terminal and bridging PCH₂). ³¹P{¹H} NMR (C₆D₆, 202.5 MHz, 298 K): δ 51.2 (d, 2P, ²J_{P-P} = 160.0 Hz, terminal P), 162.0 (t, bridging P, ²J_{P-P} = 160.0 Hz). ¹³C{¹H} (C₆D₆, 125.8 MHz, 298 K): δ 26.63 (d, ²J_{C-P} = 8.1 Hz, terminal PCHCH₂CH₂), 26.94 (d, ²J_{C-P} = 7.5 Hz, bridging PCHCH₂CH₂), 31.00 (d, ²J_{C-P} = 5.6 Hz, terminal PCHCH₂), 34.15 (s, bridging PCHCH₂), 37.88 (d, ²J_{C-P} = 25.8 Hz, bridging PCH), 38.06 (d, ²J_{C-P} = 18.6 Hz, terminal PCH). Anal. Calcd for C₄₈H₉₁Ni₂P₂ (MW 847.57): C, 68.02; H, 10.82. Found: C, 67.53; H, 10.79.

We simulated the hydride region ¹H NMR spectrum of the [(Cy₃P)NiH]₂(μ-H)(μ-PCy₂) on the software program TopSpin 4.0.6. The peak of terminal H (H1, H2) and bridging H (H3) were observed at δ -8.71 and -12.13, respectively. The terminal H peak is second-order. J_{H3H1} = J_{H3H2} = 11.1 Hz; J_{H3P3} = 33.3 Hz; J_{H3P1} = J_{H3P2} = 17.8 Hz; J_{HbPb} = J_{Hb'Pb'} = 29.0 Hz; J_{HbPb'} = J_{Hb'Pb} = 8.8 Hz; J_{HbPa} = J_{Hb'Pa} = 39.5 Hz.

Synthesis and characterization of [(^tBu₂MeP)Ni]₅H₆ (3d**)** 1.0 g of [Ni(P^tBu₂Me)₂]₂(μ-N₂) was dissolved in 30 mL of pentane in a 100 mL high pressure Schlenk flask. Degassed the flask on a Schlenk line by freeze-pump-thaw three times. Refilled the flask at -197 °C and stirred vigorously at 0 °C for 4h. Filtered the reaction solution quickly through Celite at room temperature, cooled the filtrate down to -40 °C for 3 days. Filtered the mixture through frit and collected 0.255 g (yield 45.8 %) dark red crystals suitable for single crystal X-ray diffraction. The NMR data was collected at low temperature in toluene to decrease the decomposition of the cluster. ¹H NMR (toluene, 500 MHz, 263 K): δ -29.18 (s, 6H, hydride), 1.16 (s, 15H, PCH₃), 1.43 (s, 90H, PCC₂H₅). ³¹P{¹H} NMR (toluene, 202.5 MHz, 263 K): δ 38.7 (s). ¹³C{¹H} (toluene, 125.8 MHz, 263 K): δ 28.9 (s, ^tBu-CH₃), 31.5 (s, Me-CH₃). Anal. Calcd for C₄₅H₁₁₀Ni₅P₅ (MW 1099.69): C, 49.15; H, 10.08. Found: C, 48.67; H, 10.10.

4.4.3 The Decomposition of Complex 3d in Pentane, Benzene and Toluene

15 mg (0.014 mmol) of **3d** was dissolved in pentane, benzene and toluene, separately. The ³¹P{¹H} NMR were monitored at room temperature. After 2 h, the reactions finished and produced the same production. ³¹P{¹H}(202.5 MHz): δ 44.5 (d, J_{pp} = 22.6 Hz), 44.7 (s), 56.0 (dd, J_{pp} = 48 Hz, J_{pp} = 16 Hz), 62.0 (d, J_{pp} = 14.0 Hz), 62.5 (d, J_{pp} = 16.3 Hz), 236.4 (m).

4.4.4 NMR Spectroscopically Characterization of [(Cy₂Me)Ni]₂(μ-H)₂ (**5e**)

A J. Young NMR tube was charged 20 mg (Cy₂MeP)₃Ni(μ-N₂) (0.02 mmol) was dissolved in 0.6 mL THF. N₂ gas was removed from the tube by freeze-pump-thaw three times. H₂ gas was filled into the tube at -197 °C in a liquid N₂ bath. NMR spectra were recorded at 298 K. ¹H NMR (THF, 500 MHz): δ -10.15 (virtual pentet, ²J_{H-P} = 15.2 Hz, 2H, hydride). ¹H{³¹P}NMR (THF, 500 MHz): δ -10.15 (s, 2H, hydride). ³¹P NMR (THF, 202.5 MHz): δ 18.5 (vt, ²J_{P-H} = 13.8 Hz). ³¹P{¹H} NMR (THF, 202.5 MHz): δ 18.5 (s).

4.4.5 NMR Spectroscopically Characterization of L_2NiH_2 (4a-c)

We monitored the reaction of $(L_2Ni)_2(\mu-N_2)$ with H_2 gas by variable temperature NMR spectroscopy. All of the NMR samples were prepared in the method described as follows: A J. Young NMR tube was charged with 0.6 ml THF and 10 mg of complex **2** or its derivatives. Then N_2 gas was evaporated from the tube on a Schlenk line by freeze-pump-thaw three times. Cooled down the tube to $-197\text{ }^\circ\text{C}$ in a liquid nitrogen bath and refilled the tube with H_2 gas. Kept the tube in the liquid nitrogen bath until the NMR spectrometer was adjusted to the target temperature.

Characterization of $(P^iPr_3)_2NiH_2$ (4a) 1H NMR (pentane, 500 MHz, 273 K): δ -10.15 (t, $^2J_{H-P} = 52.5$ Hz, 2H, hydride). $^1H\{^{31}P\}$ NMR (pentane, 500 MHz, 253 K): δ -10.15 (s, 2H, hydride). ^{31}P NMR (pentane, 202.5 MHz, 273 K): δ 76.5 (t, $^2J_{P-H} = 52.5$ Hz). $^{31}P\{^1H\}$ NMR (pentane, 202.5 MHz, 253 K): δ 76.5 (s).

Characterization of $(Cy_3P)_2NiH_2$ (4b) 1H NMR (pentane, 500 MHz, 283 K): δ -9.92 (t, $^2J_{HP} = 53.5$ Hz, 2H, hydride). $^1H\{^{31}P\}$ NMR (pentane, 500 MHz, 283 K): δ -9.92 (s, 2H, hydride). ^{31}P NMR (pentane, 202.5 MHz, 283 K): δ 62.1 (t, $^2J_{P-H} = 53.5$ Hz). $^{31}P\{^1H\}$ NMR (pentane, 202.5 MHz, 283 K): δ 62.1 (s).

Characterization of $(Cyp_3P)_2NiH_2$ (4c) 1H NMR (pentane, 500 MHz, 283 K): δ -9.21 (t, $^2J_{H-P} = 52.2$ Hz, 2H, hydride). $^1H\{^{31}P\}$ NMR (pentane, 500 MHz, 283 K): δ -9.21 (s, 2H, hydride). ^{31}P NMR (pentane, 202.5 MHz, 283 K): δ 67.9 (t, $^2J_{P-H} = 52.2$ Hz). $^{31}P\{^1H\}$ NMR (pentane, 202.5 MHz, 283 K): δ 67.9 (s).

4.5 X-ray Crystallography

Table 4.2 Crystallographic Data for Complex **2d**, **3d**, **6** and **7**

Compound	2d	3d	6	7
Chemical Formula	C ₃₆ H ₈₄ Ni ₂ N ₂ P ₂	C ₄₅ H ₁₁₁ Ni ₅ P ₅	C ₄₈ H ₉₁ Ni ₂ P ₃	C ₃₉ H ₇₅ N ₂ NiP ₃
Formula Weight	786.34	1100.73	847.57	723.64
Temp	170 K	170 K	170 K	170 K
Crystal system	Triclinic	Triclinic	Triclinic	Orthorhombic
Space group	P -1	P -1	P -1	P 21/c
a/ Å	11.383(8)	12.6004(7)	10.4087(8)	17.1346(15)
b/ Å	16.8439(15)	13.1101(9)	10.6488(8)	11.0504(10)
c/ Å	24.744(2)	19.8895(14)	23.3005(18)	21.5955(19)
α/ °	82.726(4)	79.509(3)	78.284(2)	90
β/ °	87.128(2)	83.262(3)	79.894(2)	94.278(3)
γ/ °	88.911(3)	66.497(3)	84.165(2)	90
V/ Å ³	4699.8(7)	2959.0(3)	2483.7(3)	4077.6
Z	4	2	2	4
D _{calc} /g cm ⁻³	1.111	1.235	1.227	1.139
μ(Mo-Kα) / mm ⁻¹	0.961	1.723	917.59	0.618
F(000)	1720.0	1192.0	1002.0	1535.0
Reflection collected	185569	73771	121379	160472
Independent reflections	27543	10411	15811	9362

R(int)	7.80	5.84	4.06	6.36
R1 ($I > 2\sigma(I)$)	4.88	3.87	2.97	3.80
wR2(all)	12.13	9.89	7.66	8.42
GOF	1.008	1.036	1.204	1.088

R1: also known as the R-value, represents the agreement between calculated and observed models.

wR2: similar to R1, but refers to squared F-values.

GOF: goodness of fit parameter.

4.6 References

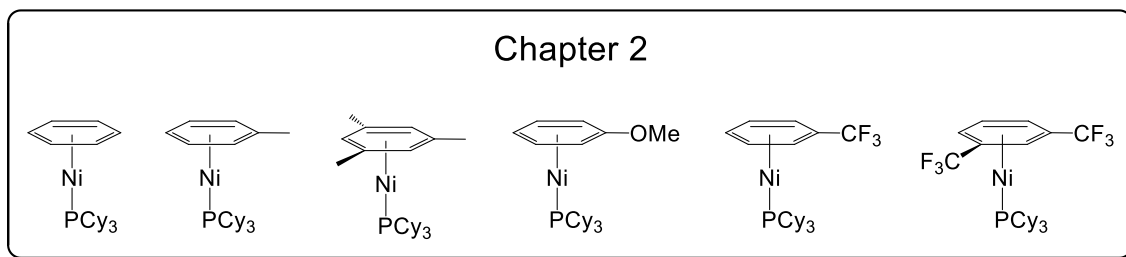
1. E. O. Fisher, *Chem. Ber.*, 1979, **112**, XXI-XXXIX.
2. G. G. Hlatky and R. H. Crabtree, *Coordin. Chem. Rev.*, 1985, **65**, 1-48.
3. A. Humphries and H. Kaesz, *Prog. Inorg. Chem.*, 1979, 145-222.
4. H. D. Kaesz and R.-B. Saillant, *Chem. Rev.*, 1972, **72**, 231-281.
5. C. F. N. M. Aresta, A. Sacco, *Inorganica Chim. Acta*, 1975, **12**, 167-178.
6. D. Moore and S. Robinson, *Chem. Soc. Rev.*, 1983, **12**, 415-452.
7. K. H. Whitmire, *J. Coord. Chem.*, 1988, **17**, 095-203.
8. H. Suzuki, *Eur. J. Inorg. Chem.*, 2002, **2002**, 1009-1023.
9. J. P. Fackler Jr, *Metal-Metal Bonds and Clusters in Chemistry and Catalysis*, Springer Science & Business Media, 2013.
10. B. Thimmappa, *Coordin. Chem. Rev.*, 1995, **143**, 1-34.
11. J. I. van der Vlugt, *Eur. J. Inorg. Chem.*, 2012, **2012**, 363-375.
12. M. D. Curtis, *J. Clust. Sci.*, 1996, **7**, 247-262.
13. S.-i. Kabashima, S. Kuwata and M. Hidai, *J. Am. Chem. Soc.*, 1999, **121**, 7837-7845.
14. P. Lemoine, *Coordin. Chem. Rev.*, 1988, **83**, 169-197.
15. E. Rosenberg, M. J. Abedin, D. Rokhsana, D. Osella, L. Milone, C. Nervi and J. Fiedler, *Inorganica Chim. Acta*, 2000, **300**, 769-777.
16. K. Herbst, P. Zanello, M. Corsini, N. D'Amelio, L. Dahlenburg and M. Brorson, *Inorg. Chem.*, 2003, **42**, 974-981.
17. A. Kaldor, D. M. Cox and M. R. Zakin, *Molecular surface chemistry: Reactions of gas-phase metal clusters*, Wiley: New York, 1988.
18. O. K. Farha, I. Eryazici, N. C. Jeong, B. G. Hauser, C. E. Wilmer, A. A. Sarjeant, R. Q. Snurr, S. T. Nguyen, A. O. z. r. Yazaydın and J. T. Hupp, *J. Am. Chem. Soc.*, 2012, **134**, 15016-15021.

19. E.-L. Muetterties, T. Rhodin, E. Band, C. Brucker and W. Pretzer, *Chem. Rev.*, 1979, **79**, 91-137.
20. F. Zaera, *Chem. Rev.*, 1995, **95**, 2651-2693.
21. R. Beck, M. Shoshani, J. Krasinkiewicz, J. A. Hatnean and S. A. Johnson, *Dalton Trans*, 2013, **42**, 1461-1475.
22. R. Beck and S. A. Johnson, *Organometallics*, 2012, **31**, 3599-3609.
23. R. Beck, M. Shoshani and S. A. Johnson, *Angew. Chem. Int. ed.*, 2012, **51**, 11753-11756.
24. M. M. Shoshani and S. A. Johnson, *Nat. Chem.*, 2017, **9**, 1282.
25. M. M. Shoshani, V. Semeniuchenko and S. A. Johnson, *Chem.: Eur. J.*, 2018, **24**, 14282-14289.
26. M. M. Shoshani and S. A. Johnson, *Inorg. Chem.*, 2015, **54**, 11977-11985.
27. B. L. Barnett, C. Krüger, Y. H. Tsay, R. H. Summerville and R. Hoffmann, *Chem. Ber.*, 1977, **110**, 3900-3909.
28. J. A. Bilbrey, A. H. Kazez, J. Locklin and W. D. Allen, *J. Comput. Chem.*, 2013, **34**, 1189-1197.
29. H. Clavier and S. P. Nolan, *Chem. Commun.*, 2010, **46**, 841-861.
30. C. A. Tolman, *Chem. Rev.*, 1977, **77**, 313-348.
31. P. W. Jolly, K. Jonas, C. Kruger and Y. H. Tsay, *J. Organomet. Chem.*, 1971, **33**, 109.
32. S. Zhu, M. M. Shoshani and S. A. Johnson, *Chem. Commun.*, 2017, **53**, 13176-13179.
33. R. Beck, M. Shoshani, J. Krasinkiewicz, J. A. Hatnean and S. A. Johnson, *Dalton T*, 2013, **42**, 1461-1475.
34. A. Stanger and R. Boese, *J. Organomet. Chem.*, 1992, **430**, 235-243.
35. M. A. Farag, A. Porzel, E. A. Mahrous, M. M. El-Massry and L. A. Wessjohann, *Anal. Bioanal. Chem.*, 2015, **407**, 1937-1949.
36. S. Losio, G. Leone, F. Bertini, G. Ricci, M. C. Sacchi and A. C. Boccia, *Polym. Chem.*, 2014, **5**, 2065-2075.
37. K. H. Tatsuki Kitayama, Springer Laboratory, 2013.

Chapter 5 Summary and Future Work

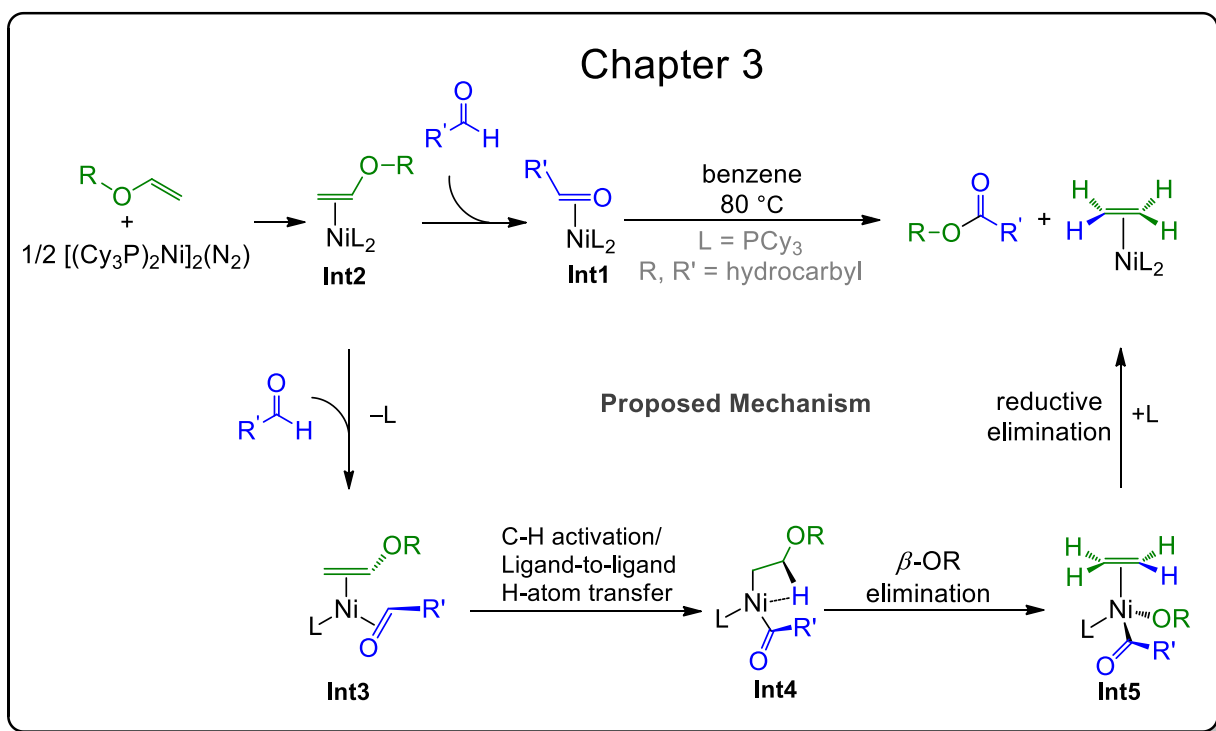
5.1 Summary

This dissertation started with the interest to the mechanistic study of nickel mediated aromatic C–O activation. Most of the published mechanistic studies about aromatic C–O activation are computational studies, whereas experimental studies are quite rare. Those computational studies proposed diverse pathways of nickel mediated C–O activation. One of the ambiguities of those proposals is the number of supporting ligand involved in each step of the catalysis cycle.¹⁻⁶ As shown in **Figure 5.1**, In order to experimentally study the mechanism of C–O activation, we successfully synthesized and fully characterized the first synthetically available LNi(0) species, (Cy₃P)Ni(η⁶-arene).

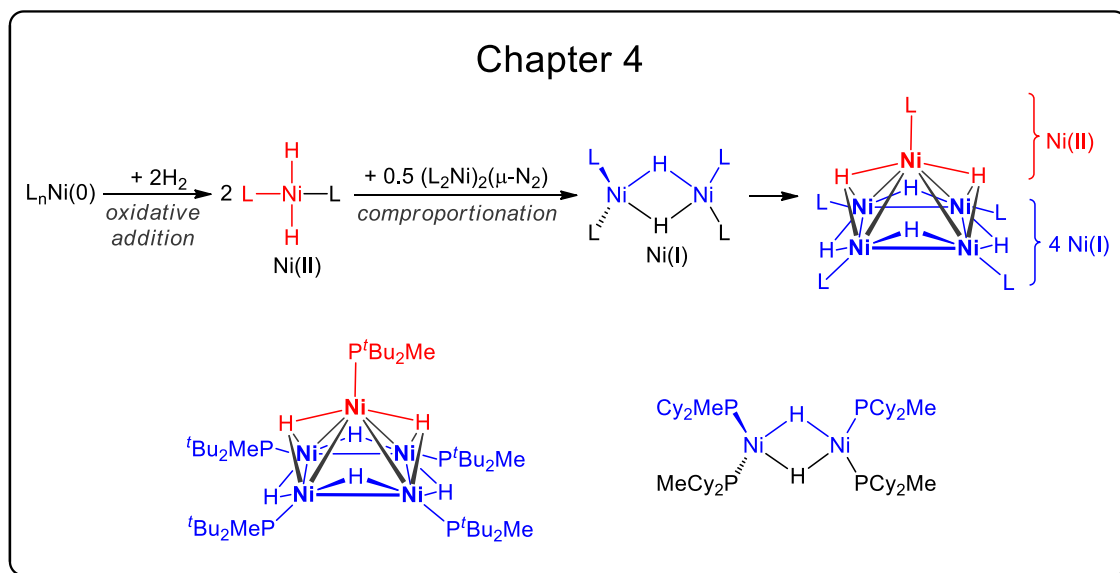


Both (Cy₃P)Ni(η⁶-PhMe) (**1**) and [(Cy₃P)₂Ni]₂(μ-N₂) (**2**) were applied as the LNi(0) and L₂Ni(0) source in the mechanistic study of alkenyl ether C(sp²)–O bond activation.

The reaction of **1** or **2** with vinyl ethers at 298 K generates the same products $(\text{Cy}_3\text{P})_2\text{Ni}(\eta^2\text{-ROCH=CH}_2)$. $(\text{Cy}_3\text{P})_2\text{Ni}(\eta^2\text{-}^t\text{BuOCH=CH}_2)$ was isolated and fully characterized. The reaction of vinyl ethers with more than one β -H and complex **2** firstly produces aldehydes and $(\text{Cy}_3\text{P})_2\text{Ni}(\eta^2\text{-CH=CH}_2)$; aldehydes then couple with the vinyl ethers to produce esters as the final product. The reaction of vinyl ethers with no more than one β -H and acetaldehyde in the presence of complex **2** could also produce esters. Based on our experimental and DFT calculation study, we proposed a mechanism where the vital steps of the coupling of aldehyde and vinyl ether is the formation of a β -H agostic Ni(II) intermediate and the following β -OR elimination. Our study also sets a solid foundation to the development of an aliphatic esters preparation methodology without selectivity difficulties like Tishchenko style reactions.⁷



With C–O activation in mind, we were also interested in electron deficient nickel clusters. Electron deficient transition metal clusters have proved to be highly reactive and are able to trigger the activation and functionalization of inert bonds through cooperative interaction with substrates. Our previous work about the pentanuclear cluster $[(^i\text{Pr}_3\text{P})\text{Ni}]_5\text{H}_6$ has showed that such electron deficient hydride clusters could smoothly activate inert C–O bonds.^{8, 9} The design and synthesis of electron deficient polynuclear complexes will offer more interesting pathways to inert C–O activation that require relatively mild reaction conditions. Both $\text{LNi}(0)$ and $\text{L}_2\text{Ni}(0)$ were attempted as starting materials to prepare Ni hydride complexes, but only $\text{L}_2\text{Ni}(0)$ is reactive to H_2 gas. We investigated the behavior of a series of tertiary phosphine ligands with different steric parameters in the preparation of polynuclear nickel hydride complexes. Phosphines with a Tolman cone angle close to 160° has the potential to form a pentanuclear $(\text{LNi})_5\text{H}_6$. Phosphines with a cone angle close to 146° close could potentially form a dinuclear complex $(\text{L}_2\text{Ni})_2(\mu\text{-H})_2$. Intermediates of the reactions were spectroscopically characterized and a mechanism was raised based on the experimental study.



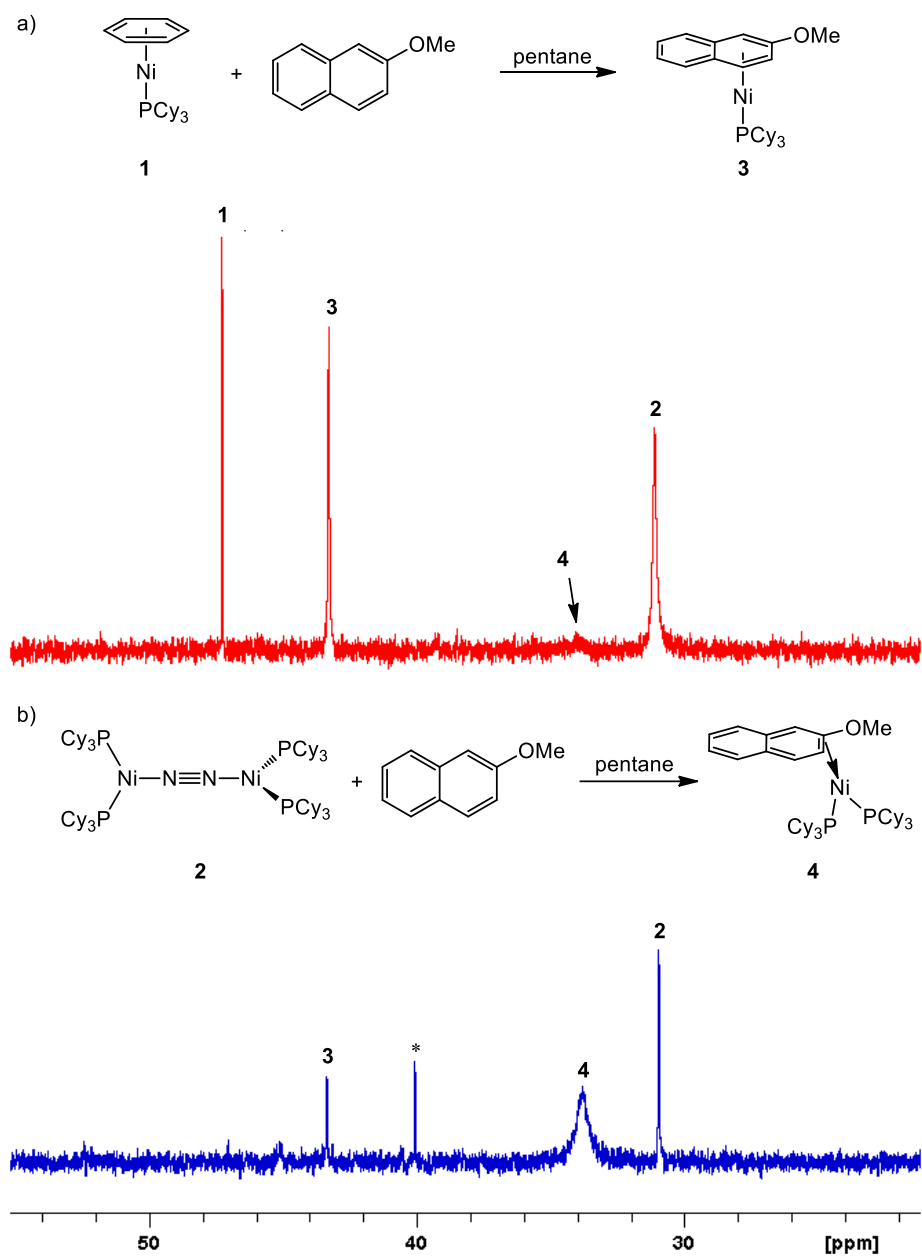
5.1 Preliminary Results and Future Work

5.1.1 Mechanistic Studies of C–O Activation

This thesis has previously examined alkenyl C(sp²)–O activation and proposed a mechanism that includes ligand-to-ligand hydrogen atom transfer and β -OR elimination steps. Apart from alkenyl C(sp²)–O activation, we are also interested in the activation of other types of C–O bonds activation mediated by Ni complexes.

Reaction of 2-methoxynaphthalene with L_nNi(0) sources. According to the “naphthalene problem”, naphthyl ethers are much easier to be activated than phenyl ethers. We are interested in the differences of the activations of these two type of substrates. Mechanistic studies about them may reveal the reason why phenyl ethers are harder to be activated and help people design catalysts especially for phenyl ether activation and functionalization. In the case of anisole, the reactions with (Cy₃P)Ni(η^6 -PhMe) (**1**) or [(Cy₃P)₂Ni]₂(μ -N₂) (**2**) with LNi(0) produce the same complex (Cy₃P)Ni(η^6 -PhOMe). In contrast, the reactions of **1** or **2** with 2-methoxynaphthalene, as we expected, produce different products. As shown in **Scheme 5.1a**, when (Cy₃P)Ni(η^6 -PhMe) (**1**) and an equivalent of 2-methoxynaphthalene were dissolved in pentane, a sharp singlet resonance was observed at δ 43.4, comparable to the chemical shifts of other (Cy₃P)Ni(η^6 -arene) complexes, which is probably the monophosphine adduction (Cy₃P)Ni(η^6 -2-methoxynaphthalene) (**3**). As shown in **Scheme 5.1b**, when [(Cy₃P)₂Ni]₂(μ -N₂) (**2**) and 6 equivalents of 2-methoxynaphthalene were dissolved in pentane, a new broad singlet was observed at δ 33.4 in the ³¹P{¹H} NMR spectrum. Upon cooling, the broad singlet decoalesces to give two broad peaks at the low temperature limits as shown in **Figure 5.1**. The preliminary NMR data of the reaction solution supports the assignment of this species as a (Cy₃P)₂Ni adduct of 2-methoxynaphthalene (Cy₃P)₂Ni(η^2 -2-methoxynaphthalene) (**4**). Although complex **2** could be converted to complex **4** in a quantitative yield by ³¹P{¹H} NMR, the isolation is still a problem. Excess 2-methoxynaphthalene is required to complete the reaction. Only trace amount of 2-

methoxynaphthalene was recrystallized at a temperature as low as $-80\text{ }^{\circ}\text{C}$. The addition of NMO as the phosphine trap did not help complete the conversion to **4** with stoichiometric amount of 2-methoxynaphthalene. Bulkier phosphines or substituent groups on naphthyl ether may help increase the solubility and thus the isolation of the intermediates.



Scheme 5.1 The $^{31}\text{P}\{^1\text{H}\}$ NMR spectra of: a) **1** reacted with 2-methoxynaphthalene to give predominantly a product tentatively assigned as $(\text{Cy}_3\text{P})\text{Ni}(\eta^6\text{-2-methoxynaphthalene})$ (**3**); b) **2** reacted with two equivalents of 2-methoxynaphthalene to give a product tentatively assigned as $(\text{Cy}_3\text{P})_2\text{Ni}(\eta^2\text{-2-methoxynaphthalene})$ (**4**). * is a trace unknown byproduct.

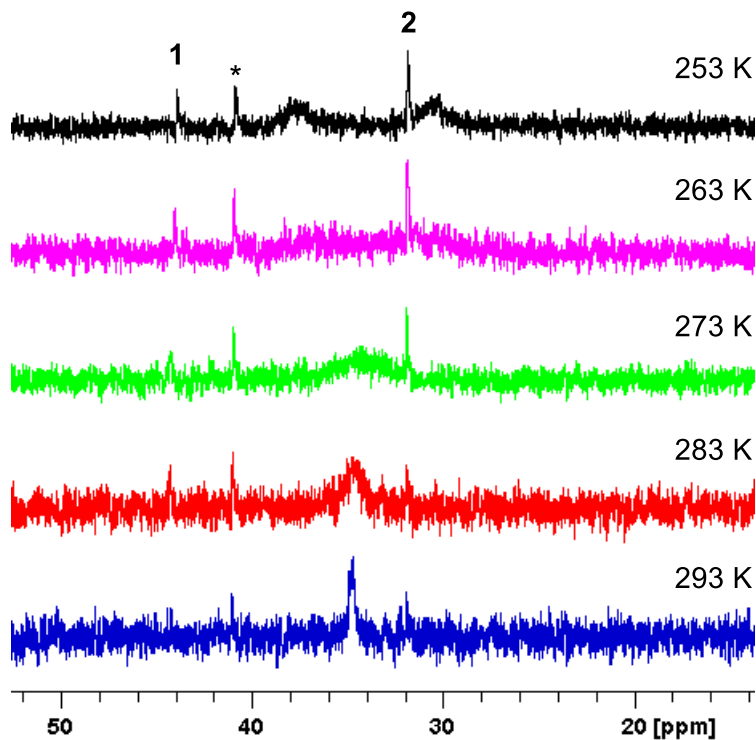
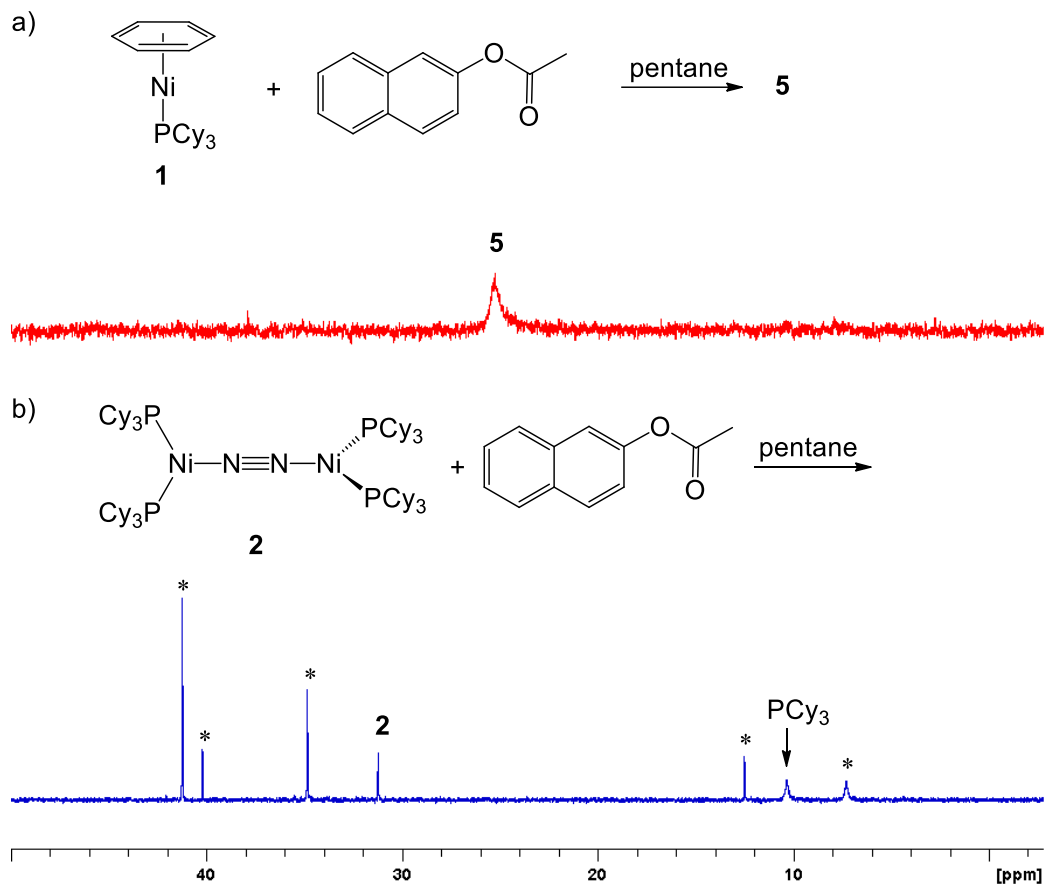


Figure 5.1 Variable-temperature $^{31}\text{P}\{^1\text{H}\}$ NMR of $(\text{Cy}_3\text{P})_2\text{Ni}(\eta^2\text{-2-methoxynaphthalene})$ (**4**) in pentane. The singlet peak at δ 33.8 decoalesces into two broad singlets at 253 K. * is a trace unidentified byproduct.

Reaction of 2-naphthyl acetate and $\text{L}_n\text{Ni}(0)$ and $\text{L}_n\text{Ni}(0)$ sources. Naphthyl acetate also contains aromatic $\text{C}(\text{sp}^2)\text{-O}$ bond and could serve as an alternative to naphthyl ether in the study related to the “naphthalene problem”. As mentioned in Chapter 1, the reaction of naphthyl pivalate with $[(\text{Cy}_3\text{P})_2\text{Ni}]_2(\mu\text{-N}_2)$ (**2**) in toluene, i.e. complex **1** and one equiv of PCy_3 , produces a dinuclear complex with one phosphine ligand bound to each Ni atom.¹ The reaction solution turn to dark green with the reaction completes. This novel dinuclear $\text{LNi}(\text{I})$ complex was isolated as a bright olive-green colour solid and is sparingly soluble in pentane and toluene.



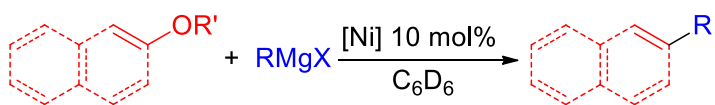
Scheme 5.2 The $^{31}\text{P}\{^1\text{H}\}$ NMR spectra of: a) **1** reacted with 2-naphthyl acetate in a ratio of 1:3, producing a product at δ 25.2. b) **2** reacts with 2-methoxynaphthalene in a ratio of 1:2, producing multiple products. * represents unknown species.

In the case of 2-naphthyl acetate, the addition of one equiv of **1** to a pentane solution of 3 equiv of 2-naphthyl acetate, only one product complex **5** was generated according to the $^{31}\text{P}\{^1\text{H}\}$ NMR (**Scheme 5.2a**). A broad singlet resonance was observed at δ 25.2, which is comparable to the dinuclear LNi(I) complexes (δ 23.3-26.8). However, the colour of the solution is red instead of green. Also, the solubility of the **5** is high in pentane. No solid precipitated from its saturated pentane solution after cooling down to -80 °C for 8 h. As shown in **Scheme 5.2b**, the mixture of $[(\text{Cy}_3\text{P})_2\text{Ni}]_2(\mu\text{-N}_2)$ and 2-naphthyl acetate in a ratio of 1: 2 in pentane produces multiple productions. Heating the reaction solution in a 40 °C bath leads to the decomposition to Ni metal particle and PCy_3 . The difference between the

reaction of $\text{LNi}(0)$ with naphthyl acetate and naphthyl pivalate reveals again the complexity of Ni catalyzed C–O activation. Even different substituents on substrates may lead to different mechanism or reactions. Experimental studies of as much as diverse substrates are desired to figure out the similarities and differences between these substrates and offer solid evidence to verify or falsify the proposed mechanisms. Only with further understanding of the mechanisms could we design more powerful catalysis and increase the efficiency of reactions in the future.

*5.1.2 The Application of $(\text{Cy}_3\text{P})\text{Ni}(\eta^6\text{-PhMe})$ (**1**) as a Catalyst in $\text{C}(\text{sp}^2)\text{-O}$ Activation*

Although the monophosphine complex $(\text{Cy}_3\text{P})\text{Ni}(\eta^6\text{-PhMe})$ (**1**) was firstly designed to assist the mechanistic study of C–O activation, we are also curious about its behavior as a catalyst in C–O activation. As shown in **Table 5.1**, we monitored the Kumada-type cross-coupling of aryl ethers with catalytic amount of complex **1** by NMR spectroscopy with mesitylene as the internal standard to calculate yields. It is found that complex **1** catalyzed the functionalization of methoxynaphthalene smoothly at room temperature and the activation of anisole with gentle heating. In contrast, other known Ni catalysts need harsher reaction conditions¹⁰⁻¹⁸.

Table 5.1 Kumada-type Coupling Catalyzed by $(\text{C}_3\text{P})\text{Ni}(\eta^6\text{-PhMe})$ (**1**)

Substrates	Grignard Reagents	Conditions	Products	Yield (%)
	MeMgBr	RT, 2h		90
		RT, 4h		84
		RT, 12h		49
		RT, 8h		84
	MeMgBr	RT, 4h		80
		RT, 12h		74
	MeMgBr	RT, 6h		77
	MeMgBr	80 °C, 12h		80
	MeMgBr	RT, 12h		86
	MeMgBr	80 °C, 12h		77
	MeMgBr	80 °C, 12h		86

The cross-coupling of 2,3-dimethoxynaphthalene and MeMgBr using complex **1** as the catalyst was done on a gram scale, and the isolation yield of the product, 2,3-

dimethylnaphthalene, was 82%. The monophosphine complex has the potential to be applied as a versatile catalyst in C–O activation in larger scale synthesis in the future.

In addition, we also want to test complex **1** in other types of reactions such as Suzuki-Miyaura and Heck cross-coupling. It would be beneficial to expand the scope of nucleophiles in these coupling reactions to include less reactive non-metal organics.

5.1.3 The Preparation of $(LNi)_5H_6$ ($L =$ Phosphine Ligand) Cluster and Reactivity Study

As discussed in Chapter 4, we tried a series of phosphines various in steric and electric properties in the preparation of polynuclear Ni hydride complexes. Our continuous interest in how phosphine ligand impacts the geometry and chemical properties of polynuclear Ni complex provokes us to examine more phosphines.

As shown in Chapter 4, $[(^tBuMe_2P)Ni]_5H_6$ is less stable but also more reactive than its iPr_3P analogue. Previous work in our group demonstrated the powerful reactivity of $[(^iPr_3P)Ni]_5H_6$ in the cooperative activation of diverse substrates. It is reasonable to believe that the more reactive $[(^tBuMe_2P)Ni]_5H_6$ is probably able to promote the activation of even more inert bonds and unique substrates. It is also interesting if the solid state cluster can interact with gaseous molecules such as H_2 , CO , CO_2 , C_2H_4 , etc., which suggests that our cluster has the potential to be applied as a gas storage and heterogeneous catalyst.

We are also curious about the dinuclear nickel hydride complex $[(Cy_2MeP)Ni]_2(\mu-H)_2$. Previous work of our group shows that its P^iBu_3 analogue is able to catalyze H/D exchange facilely. However, $[(^iBu_3P)Ni]_2(\mu-H)_2$ is not synthetically available because P–C bond cleavage caused the decomposition of it. $[(Cy_2MeP)Ni]_2(\mu-H)_2$ is stable at 298 K in solution without the problem of P–C bond cleavage. Meanwhile, the active bridging hydrides endow the complex the potential to catalyze H/D exchange and other bond activations. We are curious about its interactions with inert C–O bond as well as other inert bonds.

The purpose of the mechanistic studies of C–O activation is better understand the reaction pathways so that new catalysts can be designed. Both a better understanding of current catalysts and the discovery of new bond activation mechanisms is needed to access the full synthetic potential accessible via the large range of available ether starting materials. Although computational studies currently play a significant role in mechanistic studies, experimental studies are always necessary to offer solid evidence and verify mechanisms proposed base on theoretical studies. $L_nNi(0)$ (L = tertiary phosphine or NHC ligands) species are often used in experimental mechanistic studies of nickel catalyzed reactions, especially in the synthesis of intermediates, though the experimental synthesis of these species is often hampered by a lack of suitable starting materials. With $(Cy_3P)Ni(\eta^6\text{-arene})$ complexes, these complexes can be prepared efficiently. Furthermore, the application of $(Cy_3P)Ni(\eta^6\text{-arene})$ is not limited to the mechanistic study of C–O bond activations, but could also extend to the mechanistic study of any other Ni-phosphine mediated or catalyzed reactions.

Polynuclear catalysts provide an alternative approach to inert bond activation chemistry. With many metals that can act cooperatively in bond activation there is the potential for catalysis to occur under relatively mild reaction conditions. We have previously shown $[(^iPr_3P)Ni]_5H_6$ to engage in a number of remarkable inert bond activation reactions under ambient conditions, and it would be desirable to develop these stoichiometric transformations into catalytic functionalization reactions. However, the thermal sensitivity $[(^iPr_3P)Ni]_5H_6$ limits its prospects for catalysis at this point. The metal-metal bonds in transition metal clusters resemble the metal-metal bonds in transition metal heterogeneous catalysts. We could also better understand heterogeneous catalytic systems based on mechanistic studies of transition metal cluster catalyzed reactions.

5.3 Experimental Section

5.3.1 General Procedures

All experiments were performed under an N₂ atmosphere using either standard Schlenk techniques or a glovebox. Dry, oxygen-free solvents were employed throughout. Anhydrous pentane were purchased from Alfa Aesar and used as received. ¹H and ³¹P{¹H}, ¹³C{¹H} NMR spectra were recorded on a Bruker AMX spectrometer operating at 500 MHz. All chemical shifts are recorded in parts per million, and all coupling constants are reported in hertz. ¹H NMR spectra were referenced to solvent resonances (benzene-*d*₆, δ 7.16; chloroform-*d*, 7.26) with respect to tetramethylsilane at δ 0.00. ³¹P{¹H} NMR spectra were referenced to external 85% H₃PO₄ at δ 0.00. ¹³C{¹H} NMR spectra were referenced to solvent resonances (benzene-*d*₆, δ 128.05; chloroform-*d*, δ 77.16). [(Cy₃P)₂Ni]₂(N₂) (**1**)¹⁹ and (Cy₃P)Ni(η⁶-C₇H₈)²⁰ was prepared according to published method.

5.3.2 Reaction of L_nNi(0) and 2-methoxynaphthalene

NMR scale reaction of (Cy₃P)Ni(η⁶-PhMe) and 2-methoxynaphthalene
(Cy₃P)Ni(η⁶-C₇H₈) (11 mg, 0.025 mmol) and 2-methoxynaphthalene (4 mg, 0.025 mmol) were dissolved in 6 ml pentane and mixed well. After 1 h, ³¹P{¹H} was recorded and featured a resonance at δ 43.4. A tiny new broad singlet showed up at δ 33.8.

NMR scale reaction of [(Cy₃P)₂Ni]₂(μ-N₂) and 2-methoxynaphthalene
[(Cy₃P)₂Ni]₂(μ-N₂) (12 mg, 0.019 mmol) and 2-methoxynaphthalene (3 mg, 0.038 mmol) were dissolved in 6 ml pentane and mixed well. After 0.5 h, ³¹P{¹H} was recorded. A broad new peak at δ 43.4 (W_{1/2} = 100 Hz) and a tiny singlet at δ 33.8 were observed.

Variable-temperature NMR of (Cy₃P)₂Ni(η²-2-methoxynaphthalene) (4**)**
[(Cy₃P)₂Ni]₂(μ-N₂) (12 mg, 0.019 mmol) and 2-methoxynaphthalene (3 mg, 0.038 mmol) were dissolved in 6 ml pentane and transferred to a J. Young NMR tube. ³¹P{¹H} was

recorded at 293 K, 283 K, 273 K, 263 K and 253 K. The broad peak split into 2 doublets coupling to each other with a constant of ${}^2J_{PP} = 52$ Hz.

NMR scale reaction of $(\text{Cy}_3\text{P})\text{Ni}(\eta^6\text{-PhMe})$ and 2-naphthyl acetate
 $(\text{Cy}_3\text{P})\text{Ni}(\eta^6\text{-PhMe})$ (17 mg, 0.039 mmol) and 2-naphthyl acetate (16 mg, 0.12 mmol) were dissolved in 7 ml pentane and mixed well. After 1 h, ${}^{31}\text{P}\{^1\text{H}\}$ was recorded and featured a broad resonance at δ 25.2 ($W_{1/2} = 117$ Hz).

NMR scale reaction of $[(\text{Cy}_3\text{P})_2\text{Ni}]_2(\mu\text{-N}_2)$ and 2-naphthyl acetate
 $[(\text{Cy}_3\text{P})_2\text{Ni}]_2(\mu\text{-N}_2)$ (10 mg, 0.008 mmol) and 2-naphthyl acetate (2 mg, 0.015 mmol) were dissolved in 7 ml pentane and mixed well. After 1 h, ${}^{31}\text{P}\{^1\text{H}\}$ was recorded. Five new sharp singlet peaks were accorded at δ 7.3, δ 12.5, δ 34.8, δ 40.2 and δ 41.2, respectively.

5.3.3 $(\text{Cy}_3\text{P})\text{Ni}(\eta^6\text{-PhMe})$ Catalyzed Kumada-type Cross-coupling Reactions of aryl ethers

General procedure $(\text{Cy}_3\text{P})\text{Ni}(\eta^6\text{-PhMe})$ (4 mg, 0.009 mmol), 0.092 mmol aryl ether and mesitylene (6 mg, 0.050 mmol) were dissolved in 0.6 mL C_6D_6 . Grignard reagent (0.10 mmol) was then added to the solution. Monitor the reaction by ${}^1\text{H}$ NMR. When the new peaks of product stopped increasing, calculated the conversion yield according to the integrals of CH_3/CH_2 group on the product and the CH_3 group on mesitylene.

Synthesis and characterization of 2,3-dimethylnaphthalene 2 g of 2,3-dimethoxynaphthalene (0.011 mol) and 0.45 g $(\text{Cy}_3\text{P})\text{Ni}(\eta^6\text{-PhMe})$ (0.001 mol) were fully dissolved in 20 ml toluene in a 50 mL 2-neck round bottom equipped with a condenser. Diethyl ether solution of methyl magnesium bromide (3 M, 4 mL, 0.012 mol) was needle transferred to the reaction flask dropwise over 15 min at room temperature. Heat up the reaction solution to 80 °C for 12 h. Evaporated volatiles, extracted the residue by 60 mL ethyl acetate, filtered through celite and rinsed by 3×10 mL ethyl acetate. Concentrated the filtrate and purified the product by flash chromatography on silica gel (eluent: toluene). 1.36 g 2,3-dimethylnaphthalene was got (yield is 82 %). ${}^1\text{H}$ NMR (CDCl_3 , 500 MHz, 298

K): δ 2.42 (s, 6H, CH_3), 7.27-7.92 (m, 6H, naphthyl-*H*). $^{13}C\{^1H\}$ ($CDCl_3$, 125.8 MHz, 298
K): δ 22.01 (s, CH_3), 124.1, 126.9, 127.3, 132.2, 134.6.

5.4 References

1. R. J. Somerville, L. V. A. Hale, E. Gomez-Bengoa, J. Bures and R. Martin, *J. Am. Chem. Soc.*, 2018, **140**, 8771-8780.
2. Z. Li, S. L. Zhang, Y. Fu, Q. X. Guo and L. Liu, *J. Am. Chem. Soc.*, 2009, **131**, 8815-8823.
3. T. Wititsuwannakul, Y. Tantirungrotechai and P. Surawatanawong, *ACS Catal.*, 2016, **6**, 1477-1486.
4. H. Ogawa, H. Minami, T. Ozaki, S. Komagawa, C. Wang and M. Uchiyama, *Chem. Eur. J.*, 2015, **21**, 13904-13908.
5. J. Cornella, E. Gomez-Bengoa and R. Martin, *J. Am. Chem. Soc.*, 2013, **135**, 1997-2009.
6. X. Hong, Y. Liang and K. N. Houk, *J. Am. Chem. Soc.*, 2014, **136**, 2017-2025.
7. V. E. Tishchenko, *Journal of the Russian Physico-Chemical Society*, 1906, **38**, 355-418.
8. M. M. Shoshani, V. Semeniuchenko and S. A. Johnson, *Chem. Eur. J.*, 2018, **24**, 14282-14289.
9. M. M. Shoshani and S. A. Johnson, *Nat. Chem.*, 2017, **9**, 1282-1285.
10. J. W. Dankwardt, *Angew. Chem. Int. Ed.*, 2004, **43**, 2428-2432.
11. L. Guo, C. C. Hsiao, H. F. Yue, X. Q. Liu and M. Rueping, *ACS Catal.*, 2016, **6**, 4438-4442.
12. L. Guo, X. Q. Liu, C. Baumann and M. Rueping, *Angew. Chem. Int. Ed.*, 2016, **55**, 15415-15419.

13. T. Morioka, A. Nishizawa, K. Nakamura, M. Tobisu and N. Chatani, *Chem. Lett.*, 2015, **44**, 1729-1731.
14. B. M. Rosen, K. W. Quasdorf, D. A. Wilson, N. Zhang, A. M. Resmerita, N. K. Garg and V. Percec, *Chem. Rev.*, 2011, **111**, 1346-1416.
15. B. Su, Z. C. Cao and Z. J. Shi, *Acc. Chem. Res.*, 2015, **48**, 886-896.
16. M. Tobisu, T. Shimasaki and N. Chatani, *Angew. Chem. Int. Ed.*, 2008, **47**, 4866-4869.
17. M. Tobisu, T. Takahira, A. Ohtsuki and N. Chatani, *Org. Lett.*, 2015, **17**, 680-683.
18. L. G. Xie and Z. X. Wang, *Chem. Eur. J.*, 2011, **17**, 4972-4975.
19. M. Aresta, C. F. Nobile and A. Sacco, *Inorg. Chim. Acta*, 1975, **12**, 167-178.
20. S. Zhu, M. M. Shoshani and S. A. Johnson, *Chem. Commun.*, 2017, **53**, 13176-13179.

APPENDIX

Copyright Permission for joint publication entitled: “Versatile (η^6 -arene)Ni(PCy₃) nickel monophosphine precursors” *Chem. Commun.*, 2017, **53**, 13176-13179

I, Manar M. Shoshani, give Sha Zhu permission to use the results and ideas published in the paper entitle “Versatile (η^6 -arene)Ni(PCy₃) nickel monophosphine precursors” in her doctoral dissertation. We were the principle investigators on this joint paper, under the supervision of Dr. Samuel A. Johnson.

Manar Shoshani

August 18, 2019

VITA AUCTORIS

NAME: Sha Zhu

PLACE OF BIRTH: Tianjin, China

YEAR OF BIRTH: 1989

EDUCATION: University of Windsor, PhD Chemistry
Windsor, ON, 2012

Nankai Univeristy, B.Sc. Chemistry,
Tianjin, China, 2008

Yaohua High School, Windsor, ON,
2006

PUBLICATIONS: 1) **S. Zhu**, M. M. Shoshani and S. A. Johnson, *Chem. Commun.*, 2017, **53**, 13176-13179.

2) M. Elsbey, J. Liu, **S. Zhu**, L. Hu, G. Huang and S. A. Johnson, *Organometallics*, 2019, **38**, 436-450.